On the Role of 25-Hydroxycholesterol in Astrocytoma Growth

Dissertation

of

Gerald Markus Eibinger

performed at the

Institute of Medical Biochemistry and Molecular Biology

Medical University of Graz

Supervisor:

Prof. Dr. Wolfgang Sattler

2014

Declaration

I hereby declare that this thesis is my own original work and that all individuals and organisations that have contributed were fully acknowledged. Within the current thesis I have followed the guidelines of good scientific practise, no unallowed aids were used, and animal experiments followed the guidelines of the Austrian animal experimental law.

Graz, June 2014 …….....

Abstract

The first part of the present work deals with production and effects of 25-hydroxycholesterol (25-OHC) in glioblastoma multiforme (GBM). GBM is the most common malignant primary brain tumor and is invariably fatal to affected patients. Oxysterols belong to a class of bioactive lipids that are implicated in neurological diseases and are associated with various types of cancer. We investigated expression and transcriptional regulation of cholesterol-25-hydroxylase (CH25H) in human A172, U87MG and GM133 glioblastoma cell lines.

Transcription and translation of CH25H was upregulated in response to TNFα and IL1β. To determine whether 25-OHC acts as chemoattractant for tumor-associated macrophages the human THP-1 monoblastic leukemia line was treated with varying amounts of the oxysterol. Experiments revealed that 25-OHC and lipid extracts isolated from GM133-conditioned medium induce chemotactic migration of THP-1 cells. In response to exogenously added 25-OHC, THP-1 cells reorganize intermediate filament-associated vimentin to more cortical and polarized structures. Using RNA interference, it could be demonstrated that G protein-coupled receptor 183 (EBI2) contributes to 25-OHC-mediated chemotactic migration of THP-1 cells. These *in vitro* data indicate that GBM-derived and secreted 25-OHC may be involved in the recruitment of immune-competent cells to a tumor via EBI2.

The second part of the work revealed *in vivo* effects of lipopolysaccharide (LPS) on lipid composition with respect to fatty acids and oxysterols in plasma and brain of C57/Bl6 mice. Endotoxemia resulting in increased serum triglyceride levels could be detected (accompanied by increased linoleic acid in serum), as well as increased total serum cholesterol and oxysterol levels. All observed effects were less pronounced in the brain. Nevertheless an approx. 20% increase of 24S-OHC, 25-OHC and 27-OHC could be detected in murine brain in response to peripheral LPS.

Kurzfassung

Der erste Teil der vorliegenden Arbeit beschäftigt sich mit der Biosynthese und den Effekten von 25-Hydroxycholesterin (25-OHC) im Glioblastom (GBM). Das Glioblastom ist der häufigste primäre maligne Tumor des Gehirns mit infauster Prognose. Oxysterole sind durch ihre chemische Struktur in der Lage, durch Zellmembranen zu diffundieren. Diese bioaktiven Lipide sind in neurologische Erkrankungen ebenso wie in verschiedene Krebsarten involviert. In dieser Arbeit wurde Expression und transkriptionelle Regulation der Cholesterin 25-Hydroxylase (CH25H) in humanen A172, U87MG und GM133 Zellen untersucht. Transkription und Translation von CH25H konnte durch TNFα und IL1β Behandlung gesteigert werden. Um chemoattraktive Eigenschaften von 25-OHC untersuchen zu können, wurde die humane monoblastäre Zelllinie THP-1 mit 25-OHC behandelt. Die Experimente zeigten, dass 25-OHC und Lipidextrakte von GM-133 konditioniertem Medium die chemotaktische Migration von THP-1 Zellen fördern und die Struktur ihrer Intermediärfilamente verändern. Durch RNA-Interferenz wurde schließlich gezeigt, dass der G-Protein Rezeptor 183 (EBI2) zur 25-OHC-induzierten Migration der THP-1 Zellen beiträgt. Diese Daten legen den Schluss nahe, dass von Tumorzellen gebildetes 25-OHC zur Einwanderung immunkompetenter Zellen in den Tumor beitragen könnte.

Der zweite Teil der Arbeit beschäftigt sich mit *in vivo* Effekten von Lipopolysaccharid (LPS) auf den Lipidmetabolismus von C57/Bl6 Mäusen in Plasma und Hirn. Dabei zeigte sich, dass LPS zu erhöhtem Totalcholesterin und Triglyceriden (darunter erhöhte Linolsäure) sowie stark erhöhten Oxysterolen im Plasma führt. Im Gehirn waren alle Effekte weniger ausgeprägt, 24S-OHC, 25-OHC und 27-OHC waren dennoch im Vergleich zu den Kontrollwerten um ca. 20% erhöht.

Acknowledgement

I wish to acknowledge my supervisor, Wolfgang Sattler for giving me the possibility to perform my PhD thesis at the institute of biochemistry and molecular biology, for being patient with all problems, and for teaching me the principles of science and of a good scientist. I further want to acknowledge my working group for their discussions and their help and technical assistance: Andreas Üllen, Christoph Nußhold, Eva Bernhart, Andrea Wintersperger, Sabine Waltl, Sabine Damm, and our technician Helga Reicher. Very special thanks to Christoph Nußhold for reading the manuscript and his helpful suggestions. Furthermore, I want to thank Günter Fauler for instructing and teaching of GC-MS analysis. Special thanks also to Sasa Frank for instructing the formation of recombinant adenoviruses. Thanks also to Dagmar Kratky and her technician Anton Ibovnik for discussions and technical assistance and to Ernst Malle for reading the manuscript of the publication and helpful discussions. Last but not least, I want to acknowledge my parents for all their support during my education and my friends Zita and Patrick for reading the manuscript.

Table of contents

1 Introduction

1.1 On astrocytes and astrocytoma

1.1.1 Central nervous system (CNS)

The nervous system is probably the most fascinating part of the human body, as besides coordinating our basal vital functions it is responsible for our consciousness, memory, and language and the origin and the centre of our thoughts and feelings, in short the central place of our whole experience (1). From an evolutionary perspective, a nervous system increases the chance that an individual animal will survive and reproduce, thereby increasing the chances for survival of the species (2).

It was a long way from sponges, which are the only animals without any nervous system, over simple invertebrate animals with a diffusely organized nervous system (nerve net), like cnidarians, until it became concentrated at the rostral end in flatworms, which is termed cephalisation. This centralized nervous structure grew and evoluted from invertebrates to vertebrates and the localization of the nerve cord changed from the ventral to the dorsal side (2). Among mammals, whales have the largest brain weight (up to 10 kg) and in some rodents the brain weight comprises 10% of total body weight, while in humans it is about 2% (3). The adult human brain has a mass of approx. 1500 g and contains in the order of 10^{11} neurons, which are interconnected by about 10^{14} synapses (4).

Anatomically, the human nervous system can be divided into the peripheral nervous system (PNS) which consists of the peripheral nerves and ganglia and the central nervous system (CNS) consisting of brain and spinal cord (5). As a third part the

autonomic nervous system (ANS) consists of enteric, sympathetic, and parasympathetic system, which has central and peripheral components and is innervating internal and glandular organs (6).

Within the CNS, the largest volume proportion is the neocortex with 77%, followed by the cerebellum (10%), basal ganglia (4%), diencephalon (4%), midbrain (1%), hindbrain (2%) and the spinal cord (2%) (4).

Histologically, brain and spinal cord consist of grey and white matter. The grey matter contains the cell bodies of the neurons and is located at the outer layer of the cerebral cortex and in the inner part of the spinal cord. The white matter is located below the grey matter of the cortex and it forms the outer layer of the spinal cord. It contains all the myelinated axons of the CNS including all ascending and descending pathways, cerebral interconnections, connections from the cortex to the basal ganglia, the cerebellum, and the spinal cord (6).

There are two major classes of cells in the CNS, the neurons, which make up 20% of the total cell population, and the neuroglial cells. The neurons are responsible for excitation and nerve impulse conduction and communicate with each other via the synapses. The neuroglial cells can be divided into astrocytes, oligodendrocytes, microglia, and ependymal cells. Astrocytes are small stellate cells, which are found throughout the CNS and fulfil many important functions, which will be discussed in the next subchapter. Oligodendrocytes are responsible for the myelination of CNS neurons and can be found in large numbers in the white matter. Microglia are found throughout the white and the grey matter of the CNS. They are able to phagocytose and are important in mediating immune responses. Ependymal cells form the barrier that separates the ventricles and the central canal of the spinal cord from the neuronal environment and facilitate the movement of the cerebrospinal fluid (1, 6).

The brain is enclosed by three protective layers within the cranium. These layers also enclose the spinal cord. The first is the dura mater, which is a tough thick membrane lying close to the cranium and vertebrae. The second is the adjacent arachnoidea mater, a thin membrane with processes into the subarachnoid space, which makes contact with the delicate third membrane, the pia mater, which envelopes the contours of the brain and even dips into the sulci (6).

The space between the arachnoidea and the pia mater and also the complex system of lacunae within the brain are filled with liquor cerebospinalis (cerebrospinal fluid, CSF), a serous fluid, which is produced by the plexus choroidalis in the first and second ventricle, with a total volume of about 160 ml and a daily production of about 500 to 600 ml (7, 8). The CSF reduces the physical effective brain weight from 1500 g to 50 g (1), but besides these mechanical functions, it also plays an important role in regulating ion homeostasis of the brain extracellular milieu, and it is able to remove potentially harmful substances (8). Recent investigations report that healthy CSF contains ~150,000 leukocytes per ml, most of which are memory T cells participating in higher brain functions (e.g. memory and learning) via IL-4 release, thus indicating one more important role for CSF (9).

1.1.2 Astrocytes

The term neuroglia (“Nervenkitt”) was first introduced by the famous German pathologist Rudolf Virchow in the 1850’s. Virchow talked about small round-shaped cells that fill the extracellular shape around the nerve cells (which were defined as cells comprising over an axon). With the advances of staining methods, different neuroglial cells (astrocytes, oligodendrocytes and microglia) could be distinguished morphologically (10).

To date, our knowledge about the diversity and specific functions of neuroglial cells has markedly increased and changed. The classical picture of an astrocyte was that of a star-shaped intermediate filament (glial fibrils) containing cell with numerous processes surrounding neurons and blood vessels (11). However, the definition of an astrocyte is much more complex, because astrocytes cannot be considered as a homogenous cell population (12).

According to Kimelberg (13), astroglia can be identified by the expression of glial fibrillary acidic protein (GFAP) and S100 (a calcium binding) protein. Commonly astroglia are divided into four groups, namely protoplasmic, interlaminar, polarized, and fibrous astrocytes.

The protoplasmic astrocyte is the most prevalent type of astrocyte. It is located in the deeper layers of the cortex and the majority of the GFAP-positive processes do barely overlap (14, 15). Human protoplasmic astrocytes are much larger than those of rodents. Although the body of a human protoplasmic astrocyte is only 10 µm in diameter, their processes span 100-200 µm (**Fig. 1**). It is further estimated that one single astrocyte can modulate the function of about 2,000,000 synapses (12).

Interlaminar astrocytes only occur in primates and only in the first cortex layer. They extend long, frequently unbranched processes, which terminate in cortex layer 3 or 4. Although these astrocytes comprise one of the most striking differences between the cortices of primates and those of other species, their function remains unknown (12).

The third type of human astrocyte is the polarized astrocyte, which is an essentially unipolar cell residing in deep layers of the cortex, extending one or two GFAP-positive processes into less deeper layers of the grey matter. They have only sparse synaptic contact, and although their function is unknown, they are supposed to play a role as an alternative pathway for long distance communication across cortical layers (16).

Fibrous astrocytes, which occur only in the white matter, are the fourth and least distinguished class of astrocytes between primates and non-primate animals. They are less complex than protoplasmic astrocytes and have fewer, overlapping processes. Their simple morphology and relative uniformity suggests that their function might be confined to metabolic support (12).

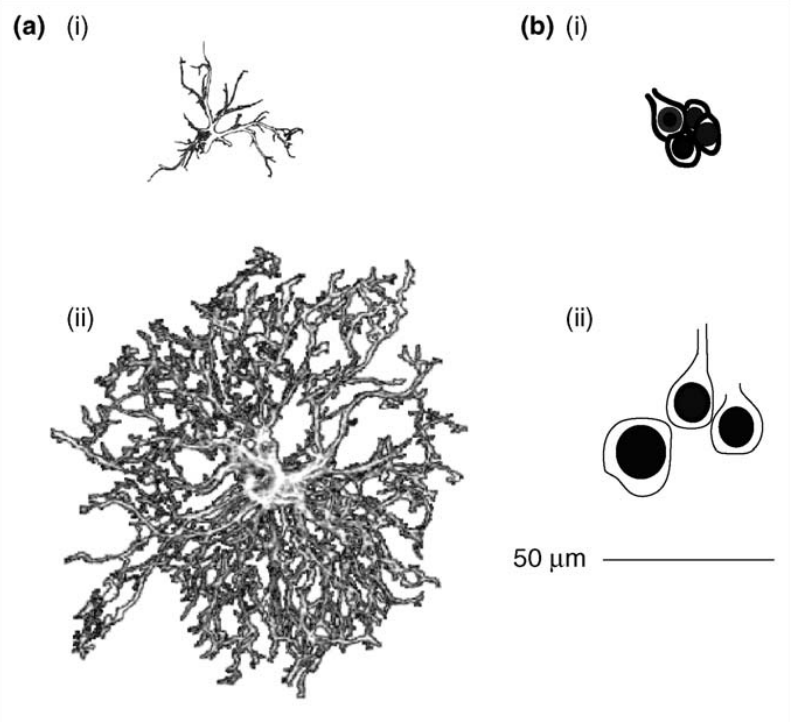

Figure 1: Comparison between human and mouse astrocytes

Although the relative brain mass is comparable between mouse and human (about 2% of total body mass), there are huge differences in complexity. This is also reflected by astrocyte morphology. **(a)** Graphical representation of mouse (i) and human (ii) cortical astrocytes. **(b)** Graphical representation of mouse (i) and human (ii) cortical neurons. The increase in complexity and size of astrocytes from mouse to human is disproportionate to the evolution of neural structure (12).

During the last years, several studies have shown that astrocytes have a much wider range of functions than previously expected (17). It becomes more and more obvious that astrocytes are multifunctional cells regulating a multitude of different processes in the CNS, besides essential neuron supporting functions (18).

These historically well-recognized functions comprise i) the contribution to the blood brain barrier (BBB) function (membrana limitans gliae perivascularis), which is important for uptake of nutrients, ii) supplying (self-synthesized) cholesterol to neurons via ApoE-containig vesicles, iii) uptake of metabolic products from the neurons, and iv) regulating the brain interstitial electrolyte balance (12, 18, 19).

In addition to these “classic” functions, they are also involved in controlling BBB permeability via secretion of ATP, endothelin-1, glutamate, IL-6, tumor necrosis factor α (TNFα), MIP-2, and nitric oxide, thereby controlling blood flow, vascular tone, providing energy for neurons and supplying building blocks of neurotransmitters that fuel synapse activity (20). One of the most interesting questions in current astrocyte research is, whether astrocytes share information processing functions inside the CNS. This issue was reviewed by Kimelberg (21), who concluded a rather only neuron supportive than information processing role for astrocytes. However, taking into account the fact that they can modulate synaptic signalling under the influence of TNFα (22), it seems likely that there is a smooth transition from supporting neurons to information processing.

1.1.3 Astrocytoma

Although in adults primary brain tumors comprise only 2% of all cancers, they are of high social dimension due to their early onset, with the peak incidence between the 3rd and 5th life decade, and their dismal prognosis (23, 24). Astrocytomas can be divided into 4 different grades. Grade I is called pilocytic astrocytoma (occurring mostly in childhood) and is the only astrocytic tumor with a good prognosis after complete surgical resection (23, 25). Grade II comprises the low-grade fibrillary astrocytoma and the more benign pleomorphic xanthoastrocytoma (24). Grade III (**Fig. 2**) comprises the anaplastic astrocytoma and grade IV is called glioblastoma multiforme

(**Fig. 3**), which is not only the most malign primary brain tumor, but also the most common one (23, 25).

Figure 2: **Grade III anaplastic astrocytoma (25)**

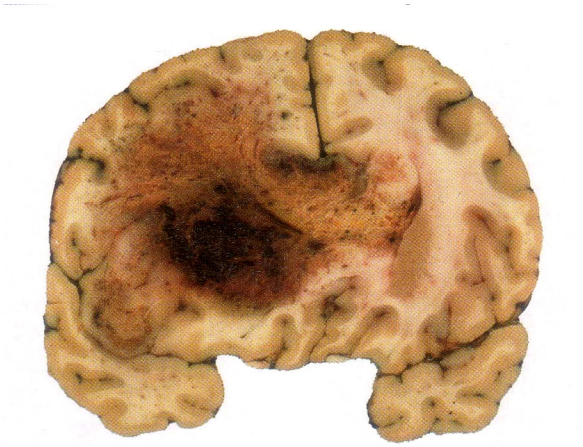

Figure 3: **Glioblastoma multiforme (grade IV) (25)**

To understand the mechanisms of gliomagenesis and its resistance to treatment it is important to gain knowledge about the gene expression profiles of different grades of glioma. It is also important to mention that glioblastoma can arise by at least two different pathways: by progression from a previous lower grade astrocytoma (secondary GBM) in ca. 5-10% of the cases and mostly occurring in younger patients (below 45 years) or *de novo* from precursor cells (primary GBM), which is the case in 90-95% of all GBM cases and occurring in older patients (26, 27). The most frequent

genetic alterations found in GBM are loss of heterozygosity (LOH) on chromosome 10q, mutations of the gene for tumor suppressor protein 53 (TP53), epidermal growth factor receptor (EGFR) amplification, phosphatase and tensin homolog (PTEN) mutation, and cyclin-dependent kinase inhibitor 2A ($p16^{INK4a}$) deletion (27). These mutations (except LOH 10q) do not occur at similar frequencies in primary and secondary GBM. Although both types are histologically indistinguishable, the genetic alterations can allow to differentiate between the two types (**Fig. 4**).

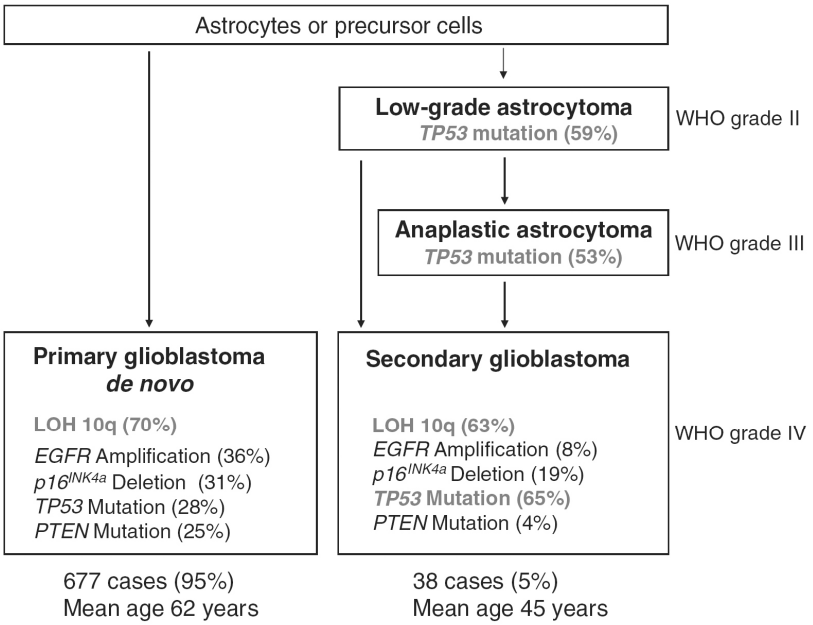

Figure 4: Most frequent genetic alterations found in primary and secondary GBM

The LOH 10q mutation occurs at almost similar frequencies in primary and secondary GBMs. TP53 mutations occur at higher frequency in secondary GBMs, whereas EGFR amplifications and PTEN mutations were detected nearly exclusively in primary GBMs (27).

1.1.3.1 Deregulated Pathways

Although genetic and molecular alterations may differ, almost all of them lead to changes in the same set of key signalling pathways that result in brain tumor growth and progression (28). Growth and survival promoting activation of receptor tyrosine kinases (RTKs) can occur via various mechanisms, including overexpression, gene amplification, activating mutations, deletions, or overexpression of their ligands (**Fig. 5**). Similarly, the inactivation of p53 and pRB pathways can occur directly by mutations, deletions, or promoter methylations at the TP53 and RB loci, as well as indirectly by inactivation of tumor suppressors, like $p16^{INK4a}$ (26).

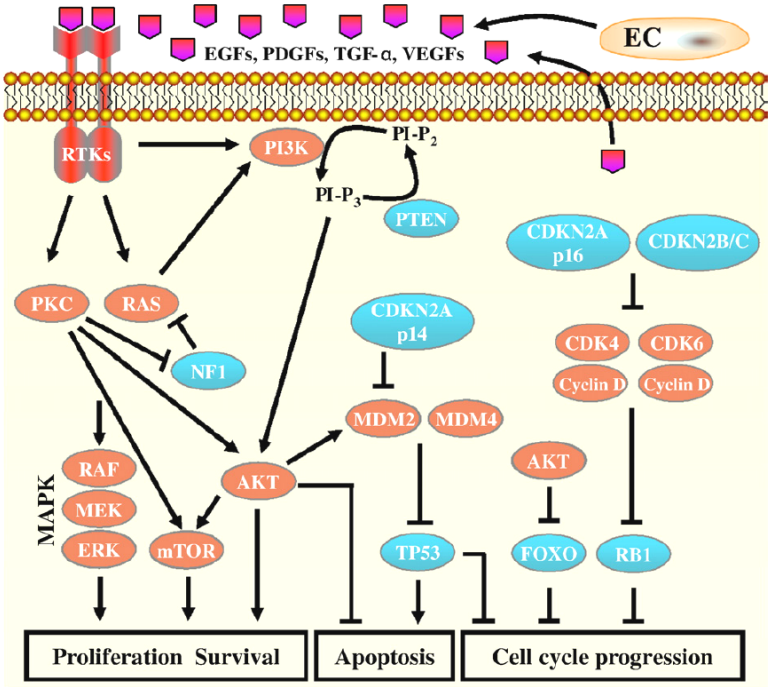

Figure 5: Key deregulated pathways in human glioma

Growth and survival promoting activation of receptor tyrosine kinases (RTKs), but also the inactivation of cell cycle arrest and pro-apoptotic pathways can be induced via different mechanisms, like overexpression, gene amplification, activating mutations, deletions, promoter methylations, overexpression of receptor ligands, inactivation or constitutive activation of positive or negative regulators. Interestingly, a variety of different genetic and molecular alterations lead to modifications of the same major intracellular signalling pathways in glioma cells (26).

Due to the lack of cell cycle guardians, which could prevent improper cell division, glioma cells accumulate mutations that, together with hyperactivated mitogenic pathways, promote glioma cell proliferation and survival and support further genetic instability (26).

Receptor tyrosine kinases

RTKs are a group of membrane receptors, which are frequently hyperactivated in tumors. They activate several signalling pathways involved in cellular growth and survival as well as upregulation of genes promoting angiogenesis and invasion. EGFR gene amplification is very common (50% of the cases), and many GBM patients express a truncated constitutively active EGFR isoform lacking the extracellular binding domain (29). A mutant EGFR lacking exons 2-7 (EGFRvIII) is expressed in approximately 20-30% of GBM patients resulting in ligand-independent tyrosine kinase activity that stimulates downstream survival and growth pathways (30, 31). Gliomas can also release EGFR ligands like epidermal growth factor (EGF) itself or transforming growth factor (TGF)-α, thereby supporting EGFR activation in an autocrine manner (32).

Platelet-derived growth factor receptor (PDGFR) and its ligands can also lead to a relevant induction of RTKs in malignant gliomas via autocrine as well as paracrine pathways, as platelet derived growth factors (PDGFs) are also expressed in high grade brain tumors, as well as in proliferating endothelial cells (33-35).

Other reasons for hyperactivated RTK signalling can be ascribed to ERBB2/HER2 mutations and MET amplifications, which have been reported by the Cancer Genome Atlas project in 8% and 4% of analysed GBMs, respectively (28).

Activated RTKs and their downstream phosphatidylinositol 3-kinase (PI3K)/AKT pathway do not only stimulate growth but also contribute to augmentation of anti-

apoptotic properties of glioblastoma cells. For example, overexpression of the anti-apoptotic protein B cell lymphoma protein 2 (BCL-2) leads to increased resistance to apoptosis during tumorigenesis, which is also reflected by the correlation between BCL-2 expression and tumor grade (36, 37).

Hypoxia is also a key phenomenon in glioblastoma, as the tumor in many cases expands faster than neovascularisation can proceed. Lack of oxygen leads to stabilisation of hypoxia-inducible factor 1 (HIF-1)-α, which induces production of vascular endothelial growth factor (VEGF), which in turn induces blood vessel formation and neovascularisation via the VEGF receptor (VEGFR) (38, 39). Other RTK ligands like EGF, PDGF-BB, and basic fibroblast growth factor (bFGF) increase expression and secretion of VEGFs, which not only leads to increased angiogenesis, but also directly supports glioma growth, as VEGFR signals via different intracellular signalling cascades, among them PTEN/PI3/AKT, MAPK/ERK, and NO (40-42).

Mutation of an enzyme of the citric acid cycle, namely isocitrate dehydrogenase (IDH)-1, which is found in over 70% of grade II or III astrocytomas or of IDH2, which is often found in tumors lacking IDH1 mutations, leads to increased HIF-1α production suggesting that normal unmutated IDH1 may act as a tumor suppressor repressing HIF and VEGF activated pathways (43-45).

RAS activation

After RTK signalling activation, the most important effect is possibly an increase in active RAS-GTP. This triggers the activation of various downstream factors including RAF and mitogen-activated protein kinase (MAPK) pathways (46). Mutated RAFs are found in a large variety of human cancers and also high grade astrocytomas contain high amounts of activated RAS (47).

Neurofibromin-1 (NF1), a protein, which negatively regulates RAS by stimulating GTP hydrolysis has been shown to be inactivated by mutations in 18% of GBM patients (28). However, NF1 loss can also be caused by increased proteasomal degradation caused by hyperactivation of protein kinase C (PKC) (48).

PI3K/AKT pathways

PI3Ks are activated via activation of RTKs. The catalytic subunit p110 of PI3K induces the conversion of phosphatidylinositol(4,5)diphosphate (PIP2) to phosphatidylinositol(3,4,5)triphosphate (PIP3), a second messenger molecule activating protein kinase B/AKT (49). This leads to cell proliferation and inactivation of pro-apoptotic proteins. PI3K can also be constitutively active, which is the case in 18% of human GBM due to mutations (28). Further enhancement of PI3K/AKT activation can be caused by loss of the tumor suppressive phosphatase and tensin homolog (PTEN) gene, which encodes PIP3 3-phosphatase, an enzyme that antagonises the activity of PI3K (50).

Phosphorylation of AKT induces phosphorylation and activation of mTOR kinase, NFκB, and mouse double minute 2 homolog (MDM2) E3 ubiquitin ligase, and the inactivation and degradation of the pro-apoptotic proteins p53, BAD, BAX, caspase-3, or FOXO1, thereby leading to increased cell proliferation and survival (51). Activation of NFκB leads to autocrine cytokine secretion (i.e. TNFα or IL-1β), increased resistance to apoptosis, and tumor cell invasion and its constitutive activation contributes to progression of diffuse gliomas (52, 53).

PKC signalling

Another pathway, which can be turned on via RTK activation, is the PKC signalling pathway, consisting of a family of 14 serine-threonine kinases. Increased PKC signal-

ling can be found in many malignant CNS tumors with increased stimulation of the downstream RAF/MEK/ERK growth promoting pathway and inhibition of the anti-apoptotic protein BCL-2 (54). Moreover, PKC is also able to activate AKT and mTOR (55) and increases the expression of matrix metalloprotease (MMP) 1 and 2, thereby leading to increased degradation of extracellular matrix and enhanced tumor invasiveness (54).

Inhibition of apoptosis and activation of cell cycle progression

The gene TP53 encodes for the important tumor suppressive transcription factor p53 controlling cell cycle progression and apoptosis in response to a large variety of stress signals. In the presence of DNA damaging cell toxins, p53 is stabilized and induces the expression of effector genes, like p21, an important cell cycle checkpoint protein, which inhibits cell cycle transition from the G1 to the DNA replicative S phase (56). Inactivation of TP53 by mutation (which favours improper cell cycle progression and cell division) is very common in GBM, especially in secondary GBM (27). Inactivation of p53 can also occur via overexpression or amplification of the MDM2 and MDM4 genes, which are negative regulators of p53. While MDM2 leads to increased proteasomal p53 degradation, MDM4 inhibits p53 transcription and enhances activity of MDM2 (57-59).

Another cell cycle guardian is the retinoblastoma protein RB, controlling the transition from G1 into S phase via binding to the elongation factor E2F. After phosphorylation and inactivation of RB (by a CDK4/cyclin D1 complex, which in term can be inhibited by $p16^{INK4a}$ under stress conditions, see also Fig. 5), E2F becomes released and activates genes involved into the G1 to S transition (27, 60). Among the most common growth promoting events in GBM are $p16^{INK4a}$ deletions, amplification of CDK4 or cy-

clin D, RB deletion, promoter methylation, or RB inactivation by phosphorylation (27, 28, 61-63).

1.1.3.2 Tumor microenvironment

The old, reductionistic view, which considered a tumor as a homogenous mass of clonally expanding cells has turned out to be fragmentary. Our way of understanding tumors has changed in a way that nowadays we regard tumors as complex tissues, in which mutant cells have conscripted and subverted normal cell types (even normally anti-tumoral immune cells) to serve as active collaborators in their neoplastic agenda (64). Brain tumors are highly heterogenous and harbour multiple cell types, some of which have stem cell like properties. However, there is also a considerable amount of nontransformed cells in the tumor parenchyma like vascular cells, microglia, peripheral immune cells, and neuronal precursor cells (65).

Macrophages/microglia

The presence of tumor associated macrophages in glioma was first observed by Penfield in 1925 (66), and, in fact, the majority of nontransformed cells in gliomas are tumor-associated macrophages (67, 68). These cells are CD45 positive like peripheral monocytes, whereas brain microglia are CD45 negative indicating that tumor-associated macrophages in glioma are invading from the blood (69). Known chemoattractants for tumor-associated macrophages are monocyte chemotactic protein-3 (MCP3), colony-stimulating factor 1 (CSF-1), or granulocyte-colony stimulatory factor (G-CSF) (70-72). Monocyte chemotactic protein-1 (MCP-1) even increased aggressiveness of gliomas (73). Glioma cells produce anti-inflammatory cytokines

like interleukin (IL)-10, IL-4, IL-6, and transforming growth factor (TGF)-β (65). Some of those cytokines are potent suppressors of microglia activation and proliferation (74). However, microglia were shown to exert pro-tumoral effects in many experimental settings. They promoted migration of GL261 mouse glioma cells (75) and glioma cell invasion was reduced in microglia-depleted brain slices (76). Depletion of microglia in mice led to an 80% reduction of glioma volume *in vivo* (77).

Lymphocytes

Lymphocyte infiltration was predominantly discovered in brain tumors with high malignancy and CD8-positive cells were found in a higher proportion than in peripheral blood (78). In this study, the leukocyte density of high grade tumors was higher than in low grade tumors. However, the correlation between lymphocyte infiltration and prognosis is controversial (79). Of clinical importance could be the population of regulatory T cells (Tregs), which is increased in human, as well as in mouse gliomas (80, 81). Stimulation of Toll-like receptor (TLR)9 decreased the number of infiltrating Tregs and prolonged survival indicating a pro-tumorigenic role for Tregs and an important regulatory role for TLRs (82).

Neuronal precursor cells

Glioblastomas can also interact with neuronal precursor cells (NPCs), which has been overlooked for many years. These cells show directed migration towards primary brain tumors over long distances and can track down even single, scattered glioblastoma cells (83). In mouse glioblastoma models, implantation of NPCs improved survival, which could also explain why glioma growth is attenuated in younger animals, which have a larger number of more motile NPCs (84, 85).

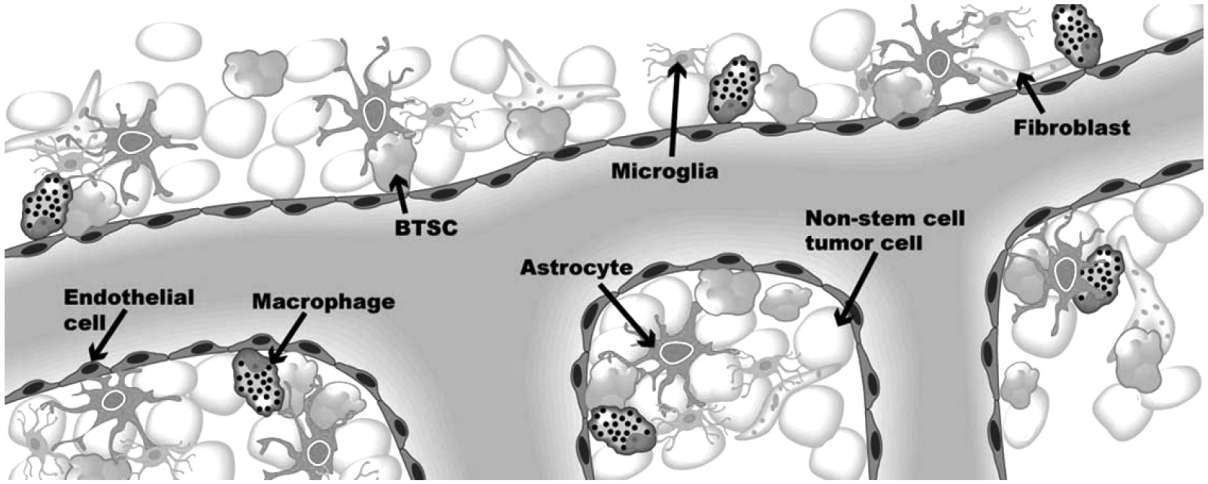

Figure 6: Brain tumor microenvironment

The brain tumor microenvironment consists of tumor cells and several non malignant stromal cells, which are thought to contribute to tumor progression and invasion (65).

BTSC = brain tumor stem-like cell

Endothelial and perivascular cells

Gliomas are highly vascularized tumors and there is increasing evidence that endothelial cells, pericytes, and astrocytes form a neurovascular unit, which supports tumor progression (65). The so called perivascular niche (PVN) has attracted much attention, as it has been shown that endothelial cells interact closely with self-renewing brain tumor cells and even secrete factors that maintain these cells in a stem cell-like state. Accordingly, depletion of blood vessels from xenografts led to decreased amounts of self-renewing brain tumor cells and arrested growth (86). Endothelial cells are critical participants in the progression of brain tumors, due to their contribution to tumor neovascularisation (87, 88). Surrounding pericytes were shown to be recruitable by tumor-secreted factors like HIF-1α as well (89). Reactive astrocytes are frequently associated with glioma cells and have been implicated in the progression of brain tumors by mediating glioblastoma cell invasion via activation of proMMP2 (90). Finally, even fibroblasts were shown to be active tumor collaborators

by producing and activating MMP2 and its activators membrane-type 1-MMP and membrane-type 2-MMP (91), which are all involved in glioma progression (92-94).

Brain tumor stem-like cells

Brain tumor stem-like cells (BTSCs) are neoplastic cells, which populate the PVN. BTSCs are expressing nestin and CD133, associate with the tumor endothelium and are present in several brain tumor subtypes with a strong correlation between the number of vessel-associated BTSCs and increasing tumor grade (86). Endothelium-derived factors were not only shown to accelerate tumorsphere formation of glioma cells (95), but they also increase the tumorigenic capacities of BTSCs (86). One important niche-derived factor is NO. It activates notch signalling in BTSCs, thereby enhancing their self-renewal characteristics *in vitro* and their tumorigenic capacities *in vivo* (96).

1.1.4 Therapy and prognosis of glioblastoma (astrocytoma IV)

Until 2005, glioblastoma therapy consisted of gross surgical resection followed by field radiotherapy up to a maximal dose of 60 Gy, whereupon the extent of surgical excision was associated with longer survival and better neurologic function (97-100). Although complete surgical resection of a tumor offers probably the best outcome for patients, the majority of high grade tumors cannot be resected completely, because of their rapid and highly infiltrative growth, the relative lack of specific early symptoms and the high density of critical structures inside the brain (24, 25).

Although radiation therapy is an effective nonsurgical therapy for glioblastoma, early diagnosis and treatment with radiotherapy only did not improve survival, but caused severe side effects, like fatigue, malaise, insomnia, and poor emotional functioning,

especially at higher doses (101, 102). Postoperative radiation therapy prolonged the progression free survival, but had no effect on the overall survival (103).

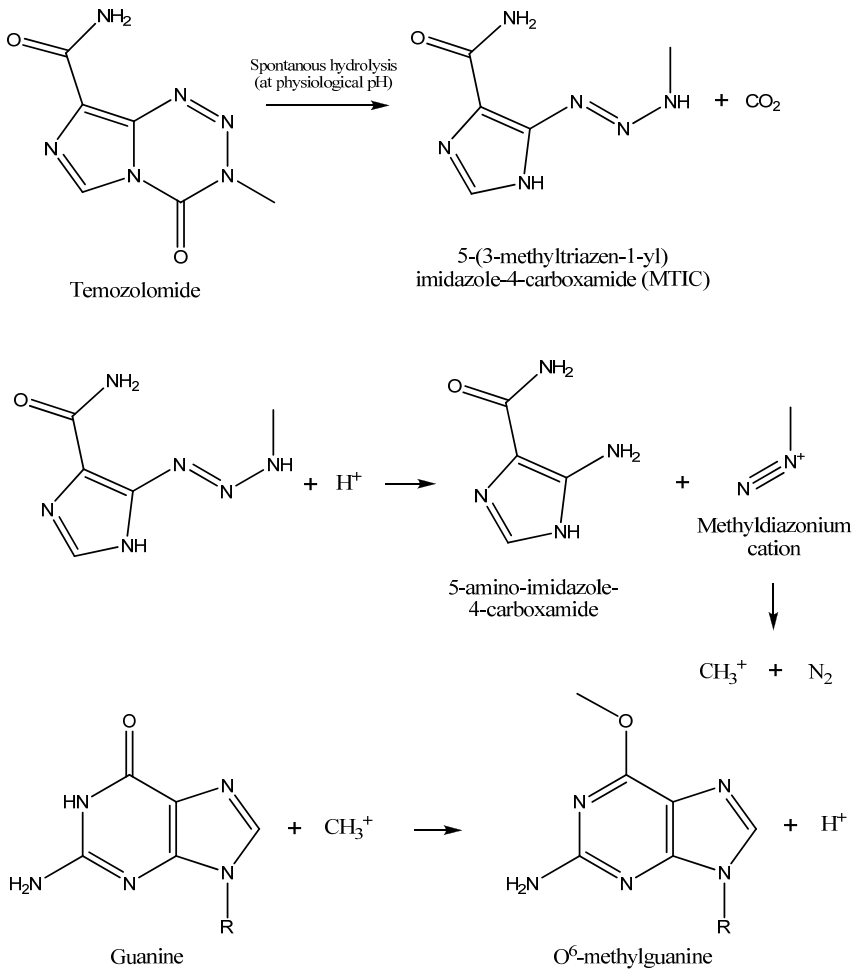

Figure 7: Temozolomide and its active metabolite, 5-(3-methyltriazen-1-yl)imidazole-4-carboxamide (MTIC)

Temozolomide is a so-called prodrug, which has excellent oral bioavailbility and can also penetrate into the brain, due to its lipophilic properties. There it converts spontaneously into its active metabolite, MTIC, which has affinity to the DNA major groove. There it alkylates preferentially the middle residue of a GGG sequence, which leads to mismatches, with normal corresponding base, cytosin, being replaced by thymin. However, tumor cells are able to acquire resistance against this agent, for example via increased production of the enzyme O^6-alkylguanine transferase (23).

In 2005, it was shown that the combination of temozolomide with radiotherapy as initial treatment prolongs the survival of glioblastoma patients, which has remained state of the art therapy until today (104). Temozolomide, originally developed in the 1980s, is rapidly and completely absorbed after oral administration, has excellent penetration into all body tissues (including the brain), and spontaneously hydrolyses into its active metabolite 5-(3-methyltriazen-1-yl)imidazole-4-carboxamide (MTIC) (**Fig. 7**), which acts as a major groove-directed DNA alkylating agent, thereby being base selective and preferentially alkylating the middle guanine residue of a GGG sequence (23).

However, despite these therapeutic efforts, glioblastoma prognosis remains extremely bad with a mean survival of 14.6 months and a two year survival of 26% (**Fig. 8**) (105). Although the 2-year survival rates are better for younger (<50 years) than for older patients (106, 107), there is still a need for new and better therapeutic strategies. One of those could aim to manipulate cerebral cholesterol metabolism, as the brain has some specifics, which shall be described in the next chapter.

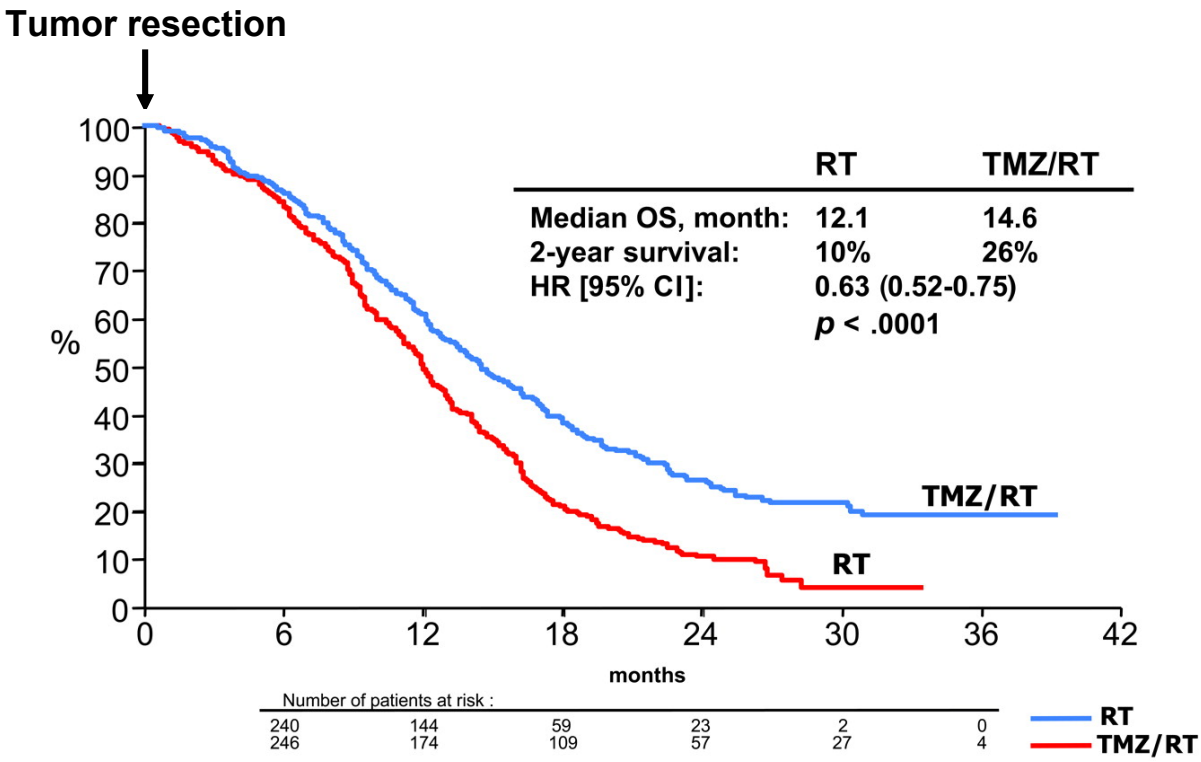

Figure 8: Glioblastoma prognosis

After tumor resection, combined temozolomide, and radiotherapy increases the two year survival from 10% to 26% (modified from (105)).

1.2 Brain cholesterol metabolism

1.2.1 Sources and functions of brain cholesterol

In the brain cholesterol is highly enriched in comparison to other tissues. Although in humans, the brain has only less than 2% of total body mass, it contains about 25% of total body cholesterol (108). The majority of CNS cholesterol is believed to reside in two different pools: one represented by the plasma and intracellular membranes of astrocytes and neurons and the other by the myelin sheaths (formed by oligodendroglia), containing about 70% lipids and 30% protein (dry weight), which is opposite from the situation found in most other cell membranes (109) (**Fig. 10**). Also neurons need high amounts of cholesterol, as they have a huge membrane area due to the large amounts of dendrites and synapses. For example, a purkinje cell has a surface of about 150,000 µm² (110), whereas a myocyte reaches only 5000 µm² (111).

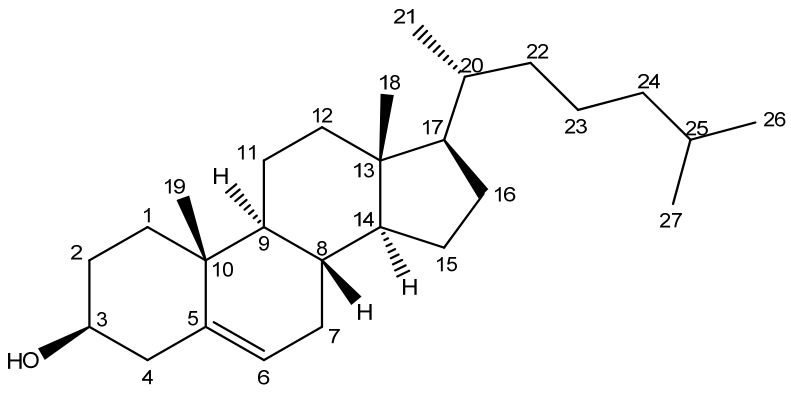

Figure 9: Chemical structure of cholesterol

Brain sterols are present predominantly (99%) in the form of unesterified cholesterol with small amounts of cholesterol precursors (108). As it is known that lipoproteins in mouse, rat, and human do not cross the BBB, and also peripherally-administered

labelled cholesterol cannot be found in the CNS of mammals, it is obvious that CNS cholesterol has to be derived from *de novo* synthesis (112, 113).

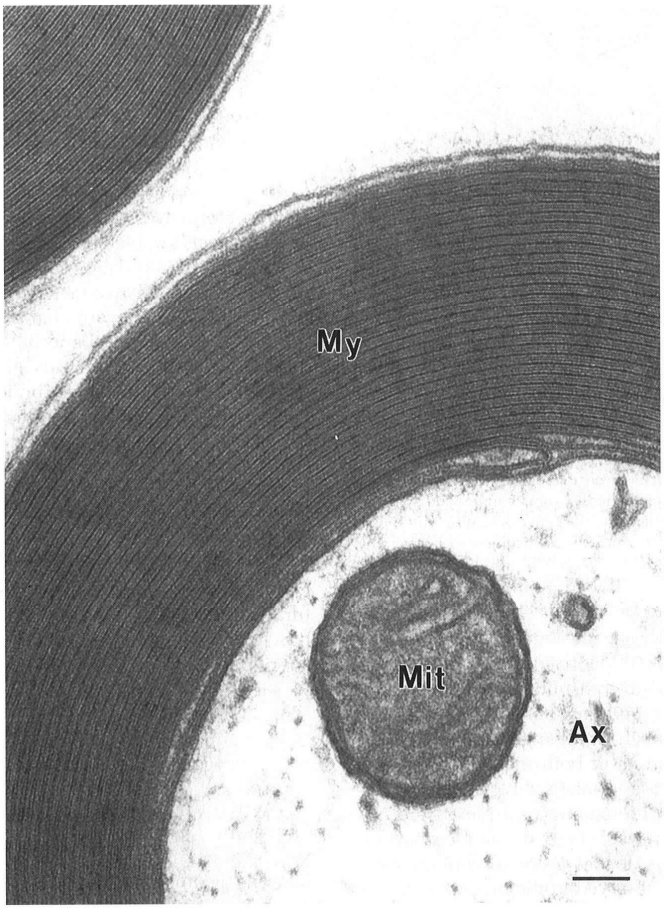

Figure 10: Myelinated axon

The electron micrograph shows a transverse section through a myelinated axon of a rat sciatic nerve. Although this picture demonstrates a nerve from the PNS (where the myelin is built up by a Schwann cell), it shows the high membrane demand for the construction of a myelin sheath, which in the CNS is made up by the oligodendrocytes. (My) myelin sheath, (Ax) axon, (Mit) mitochondrium. The scale bar indicates 75 nm. (2)

The majority of CNS cholesterol is produced by oligodendrocytes during the myelination process taking place shortly after birth (108). After myelination, cholesterol synthesis continues at a very low level and occurs mainly in astrocytes (108, 109, 114, 115). Not surprisingly, CNS cholesterol has a long half-life between two and six months (116, 117). Lipoproteins inside the CNS consist of ApoE containing high den-

sity lipoprotein (HDL)-like particles and are secreted from the glia (mainly astrocytes and microglia), but also from neurons under some specific conditions (118-123).

Cholesterol biosynthesis (**Fig. 11**) is an energetically expensive and complex pathway requiring many enzymatic reactions distributed in different organelles (124). It involves a complex set of around 30 enzymatic reactions to build up the 27 carbon atom-containing cholesterol molecule out of C_2 components (125, 126). The first step, the generation of HMG-CoA out of Acetyl-CoA, takes place in the cytosol, catalyzed by the enzyme 3-hydroxy-3-methylglutaryl-coenzyme-A synthase (HMGCS). The next step is the formation of mevalonate, which takes place in the ER, as the enzyme 3-hydroxy-3-methylglutaryl-coenzyme-A reductase (HMGCR) is an integral ER membrane enzyme (125). This is also the major rate limiting step in the cholesterol synthesis pathway (124). The conversion of mevalonate into farnesyl–pyrophosphate, which is accomplished by the enzyme farnesyl-diphosphate-sythase (FDS), is exclusively peroxisomal. The remaining reactions take place in the ER with membrane-bound enzymes (125, 127).

The rate of cholesterol biosynthesis is lower in neurons as compared to glial cells (128). In neurons, cholesterol synthesis is restricted to the neuronal somata and does not occur in axons (116). Although there is evidence for cholesterol transport from the soma to the axon (129), neuronal axons have to rely on external cholesterol delivered from astrocytes (128). Astrocytes secrete cholesterol via ATP-binding cassette transporter (ABC)A1 and pack it into ApoE containing lipoprotein particles (114, 130, 131).

These ApoE coated particles are taken up by neurons via a low density lipoprotein (LDL) receptor subtype (132-135) and promote axonal extension (136). ApoE deficient mice develop impairment in learning and memory (137-139) and deficiency of ApoE causes neurodegeneration in the CNS during aging (140).

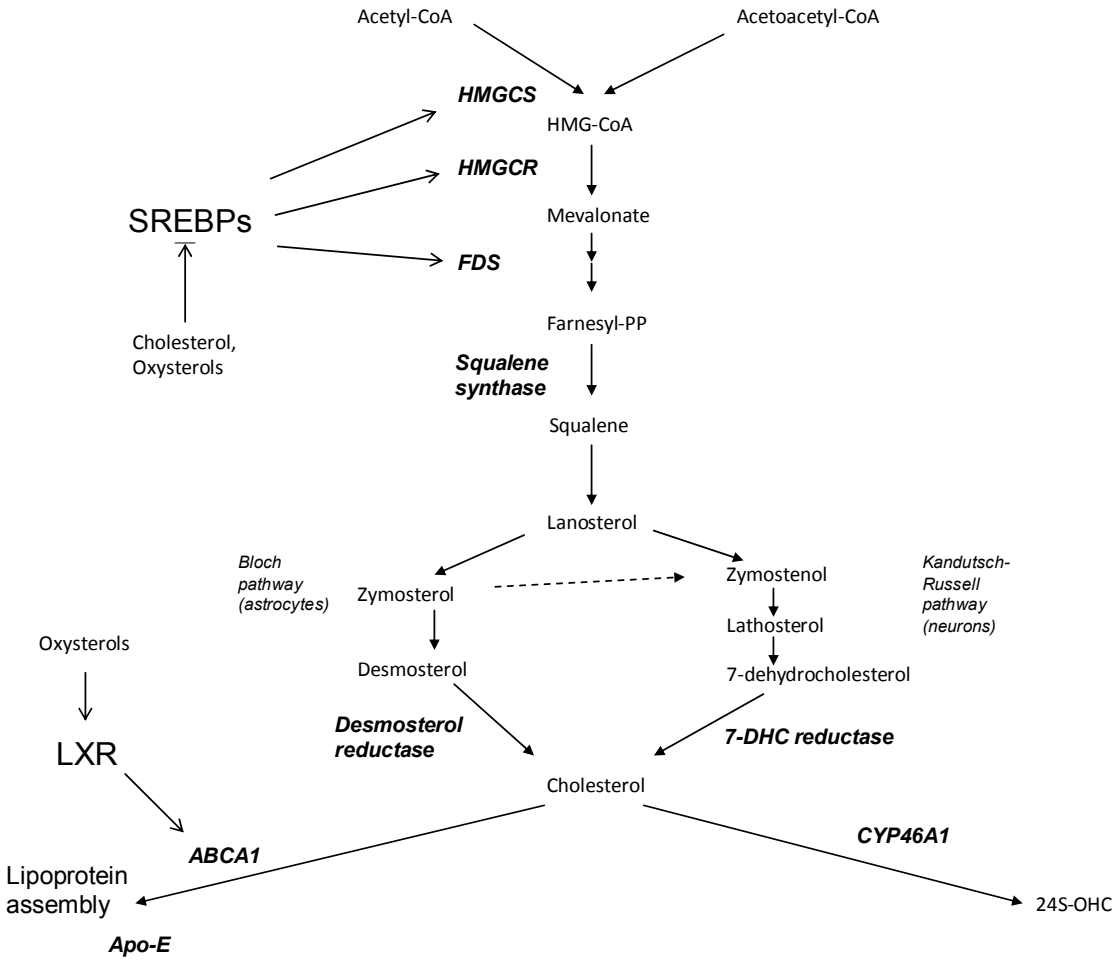

Figure 11: Schematic presentation of the cholesterol biosynthetic pathways in the brain

Overview over the most important steps in cholesterol biosynthesis showing the key enzymes and the transcription factors responsible for their regulation. (Modified from (141, 142).)

1.2.2 Regulation of the cholesterol biosynthesis

The complex system of cholesterol biosynthesis needs to be regulated tightly. Among the major regulators are the members of the sterol regulatory element binding protein (SREBP) family SREBP1a, SREBP1c, and SREBP2 (143). SREBPs are synthesized as large inactive precursor proteins and inserted into the ER (144). The C-terminus interacts with the SREBP cleavage activating protein (SCAP) (145). SCAP is the

sensor for cholesterol and interacts with the insulin-induced gene (INSIG) anchor proteins, which occur in two isoforms, INSIG-1 and INSIG-2 and are the receptors for oxysterols (146). When cholesterol is highly abundant, it binds to SCAP, which undergoes conformational changes, thereby stabilizing its complex with INSIG and SREBP, which is being retained to the ER (147). Similarly, oxysterols also stabilize the SREBP, SCAP, INSIG complex, but via binding to INSIG (148). In case of sterol depletion, SCAP changes its conformation and binding to INSIG is disrupted and the SREBP/SCAP complex is transported via COPII-coated vesicles into the Golgi, where two proteases, site 1 and site 2 protease, release the N-terminal transcription factor domain of SREBP from the membrane (149). This protein dimerizes and is imported into the nucleus by importin β, where it acts as a transcription factor upregulating genes important for synthesis and uptake of cholesterol, like HMGCR and the LDL-receptor (150).

Another key regulator of (brain) cholesterol metabolism is the nuclear receptor liver-X receptor (LXR). LXR is activated by oxysterols (151, 152) and induces the expression of ApoE and ABCA1 and reduces the expression of HMGCR (153-155).

1.2.3 Excretion of brain cholesterol

The brain has to get rid of excess cholesterol, although it is thought that only neurons need to deal with cholesterol overload, because they import the component (142). In contrast to cholesterol, 24S-hydroxycholesterol (24S-OHC) and other side chain oxidized cholesterols can pass membranes easily (156, 157). The enzyme cholesterol 24-hydroxylase (CYP46A1) is expressed mainly in neurons of the cerebral cortex, hippocampus, dentate gyrus, amygdale, putamen, and thalamus (158). There is little, if any expression of CYP46A1 in glial cells (159). This enzyme is not maximally ex-

pressed until myelination is completed. In humans, 24S-OHC is the major hydroxylated sterol excreted from the CNS. 6-8 mg cholesterol leave the CNS as 24S-OHC into the circulation per day (160). In contrast, only 1-2 mg cholesterol per 24 h are exported from the brain via the CSF in ApoE-containing lipoproteins (108, 161).

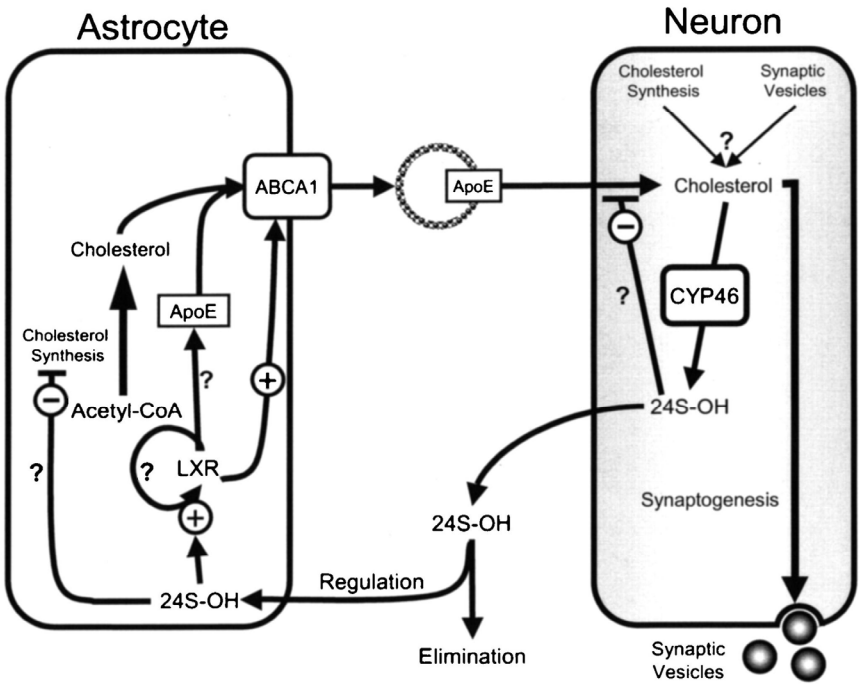

Figure 12: Model of astrocyte-neuron interactions in cholesterol homeostasis

Neurons have a high cholesterol demand, but although they are capable of synthesizing cholesterol themselves, they rely on supply from nearby astrocytes. It is suggested that this kind of outsourcing could help neurons to save energy for generation and transmission of electrical activity. 24S-hydroxycholesterol, the neuronal “excretion form” of cholesterol, could possibly stimulate efflux of cholesterol from astrocytes, because it is a strong LXR activator (109).

1.3 Important oxysterols and their physiological role

This subchapter will provide an overview over the most important oxysterols, whereas the next subchapter deals with the most important known receptors for oxysterol signalling. Oxysterols are generated by enzymatic hydroxylation of cholesterol and play important roles in lipid metabolism and, as signalling-active and mutagenic compounds, received considerable attention in tumor biology (162). The tumor specific functions of oxysterols, especially of 25-hydroxycholesterol (25-OHC) will be briefly summarized below.

1.3.1 7α-hydroxycholesterol

Oxidation of cholesterol to 7α-hydroxycholesterol (7α-OHC) is accomplished by the P450 enzyme CYP7A1, which is located in the ER and is more or less liver specific (163). This is the first step in the classical bile acid biochemical pathway, by which about 400 to 600 mg cholesterol are eliminated daily (164). Small amounts of CYP7A1 have also been detected in kidney, heart, and lung (165). Humans with mutations in the CYP7A1 gene have a markedly decreased bile acid excretion, elevated levels of total and LDL cholesterol, and accumulate cholesterol in the liver (166). However, formation of 7-oxygenated sterols from cholesterol has also been reported upon incubation of cholesterol and horseradish peroxidase or soybean lipoxygenase in the presence of ethyl linoleate via a hydroperoxide intermediate indicating that 7α-OHC, 7β-OHC, and 7-ketocholesterol can also be formed via unspecific autoxidation (167).

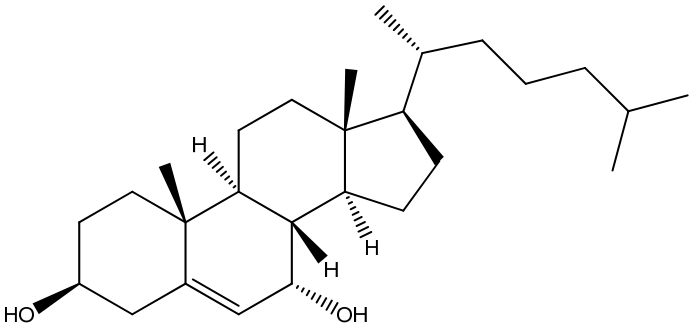

Figure 13: 7α-hydroxycholesterol

Regarding the regulation of the CYP7A1 gene, it is known that it is negatively regulated by bile acids (168-170). Lipopolysaccharide (LPS) administration leads to rapid downregulation of CYP7A1, occurring within 90 min and being sustained for at least 16 h (171). Interestingly, low food intake leads to upregulation of CYP7A1 in the rat (172).

1.3.2 24S-hydroxycholesterol

24S-OHC is formed out of cholesterol by the ER-located cytochrome P450 enzyme CYP46A1, which is predominantly expressed in the brain, whereas other tissues only contain trace amounts (158). As already mentioned, 24S-OHC is the cholesterol metabolite, which has its greatest importance in the excretion of brain excess cholesterol, because it can cross the BBB passively and enters into the circulation, where it is transported in association with lipoproteins before metabolized in the liver (109). Although this metabolic route is of great importance for the brain to maintain cholesterol homeostasis, only 6 to 8 mg of cholesterol is metabolized to 24S-OHC per day in the human body, which is indicative for the brain's rather slow cholesterol turnover (173).

24S-OHC plays a dual role: besides being the secreted metabolite of brain cholesterol, it is also a strong LXRα and β agonist (151) and regulates transcription of several enzymes involved in cholesterol homeostasis (174).

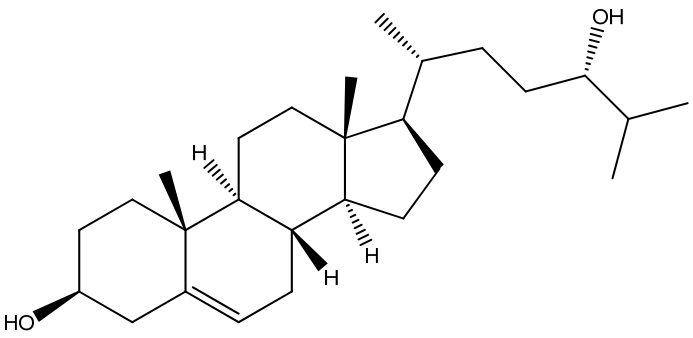

Figure 14: 24S-hydroxycholesterol

Although there is only limited knowledge on the regulation of the cholesterol 24-hydroxylase until now, the CYP46A1 gene has been shown to underlie positive regulation via Sp1, Sp3 and Sp4 transcription factors and can also be induced by the histone deacetylase (HDAC) inhibitor trichostatin A (175, 176).

1.3.3 25-hydroxycholesterol

According to Diczfalusy (177), 25-OHC can be generated as by-product of other enzymes like the CYP27 and CYP46 enzymes and the enzyme CYP3A4. The most important pathway, however, is via a non-cytochrome P-enzyme with a diiron cofactor, which was discovered in 1998 and was called cholesterol 25-hydroxylase (CH25H) (178). This enzyme, which is expressed in several human tissues at very low levels, was shown to be ER- or Golgi-located.

25-OHC is a potent regulator of LXR-mediated pathways that impact on brain lipid homeostasis (179). This oxysterol affects expression of the cholesterol efflux pumps

ABCA1 and ABCG1, and expression of ApoE (180). 25-OHC is able to stimulate LXR-independent oligodendrocyte apoptosis and suppresses myelin gene expression in peripheral nerves via LXR/Wnt/β-catenin-mediated pathways (181). 25-OHC can further act as a negative regulator of SREBP-dependent pathways by binding to INSIG1 and -2 thereby inhibiting proteolytic activation of SREBPs (145).

However, as 25-OHC is produced at rather low concentrations, it is less clear, if the concentrations needed to regulate LXR- or SREBP-dependent pathways can be reached *in vivo* (177). Recent studies have demonstrated that 25-OHC regulates cell migration and proliferation at nanomolar concentrations that are also present *in vivo*. These aspects will be covered below.

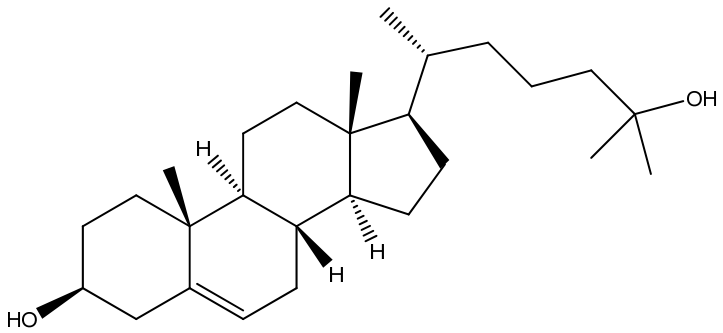

Figure 15: 25-hydroxycholesterol

Regarding the regulation of CH25H, it is known that CH25H is induced by interferons (IFNs) (182) and that 25-OHC concentrations are elevated in humans exposed to endotoxin treatment (183). It has also been reported that 25-hydroxy-vitamin D_3 and 1,25-dihydroxy-vitamin D_3 induced CH25H at high, for humans possibly toxic, doses (10 nM and 500 nM, respectively) (184).

1.3.4 27-hydroxycholesterol

27-hydroxycholesterol (27-OHC) is formed by the mitochondrial P450 enzyme CYP27A1, which is ubiquitously expressed throughout the whole body (185, 186).
27-hydroxylation of cholesterol offers an alternative (acidic) pathway for bile acid biosynthesis and CYP27A1 is mutated in individuals suffering from cerebrotendinous xanthomatosis (166). In normal subjects, about 18-20 mg cholesterol per day are converted via 27-hydroxylation (187). It is estimated that about 4% of normal bile acid synthesis is accomplished by extrahepatic 27-hydroxylation of cholesterol (186).

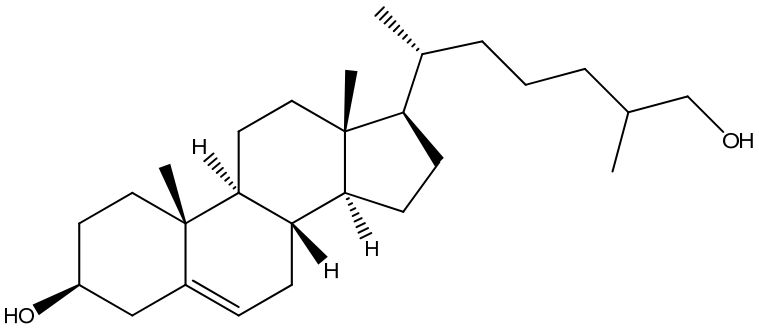

Figure 16: 27-hydroxycholesterol

This metabolic pathway does not only facilitate cholesterol excretion of bradytrophic tissues (i.e. the tendons), but it has also been shown to play a major role in lung alveolar macrophages, which accumulate high cholesterol amounts, if CYP27A1 is blocked pharmacologically (186, 188).
Besides its role as cholesterol metabolite and bile acid precursor, 27-OHC can also become involved into major metabolic regulatory mechanisms, as it binds to and activates both, LXRα and LXRβ (189, 190).

1.4 Oxysterol receptors

1.4.1 Liver X receptors

The LXR family consists of two isoforms of a nuclear receptor, LXRα, which is found in tissues with high metabolic activity, primarily in the liver (where also the name liver X receptor is derived, as LXRα was the first isotype to be cloned (191, 192)), and LXRβ, which is expressed ubiquitously (168). Oxysterols and some other cholesterol derivatives are the natural activators of LXRs (152). There are also synthetic activators of LXR like T0901317 and GW3965. As LXR forms a heterodimer with retinoid-X receptor RXR before binding to the DNA, LXR-dependent genes can also be upregulated by RXR activators, such as retinoic acid (192).

Mice lacking LXRs have a rather mild phenotype as long as they are kept on chow diet without cholesterol. However, during aging they accumulate cholesterol in macrophages and some of them develop autoimmunity (193). Among the best-studied effects of LXR is the promotion of reverse cholesterol transport, the delivery of cholesterol from the periphery to the liver for excretion. Peripheral cells secrete excess cholesterol into HDL particles via the cholesterol transporter ABCA1, which was one of the earliest identified LXR target genes and also one of the most highly regulated ones (194). LXR activation leads to markedly increased ABCA1 expression in macrophages and many other tissues like the intestine (195). Other important LXR targets are the cholesterol transporters ABCG1, ABCG5, and ABCG8 (196, 197) and a cluster of apolipoprotein genes including APOE, APOC1, APOC2, and APOC4 (180, 198). Moreover, LXR activation has been shown to increase expression of the gene for the glucose transporter GLUT4, thereby promoting glucose uptake in white and brown adipose tissue, which is also consistent with the finding that LXR can be

activated by glucose itself thereby ameliorating glucose tolerance through coordinate regulation of glucose metabolism in liver and adipose tissue (199-202).

1.4.2 Sterol regulatory element binding protein

LXR and SREBP transcriptional pathways work in a coordinated and reciprocal fashion for maintaining cellular and systemic cholesterol homeostasis. SREBPs become activated in response to low cholesterol levels, whereas LXRs are sensors for elevated cholesterol levels (193). The three mammalian SREBP isoforms SREBP-1a, SREBP-1c, and SREBP-2 are encoded by two genes, sterol regulatory element binding transcription factor (SREBF)1 and SREBF2. SREBP-1a activates fatty acid and cholesterol synthesis, SREBP-1c activates fatty acid synthesis, whereas SREBP-2 enhances cholesterol synthesis and uptake (145). Newly synthesized SREBPs are inserted into the ER membrane as inactive precursors (203). The transcriptionally active protein bHLH-LZ, which is the N-terminal domain of SREBP, is released by the sequential activation of two proteases, which are called site-1 and site-2 protease and are located in the Golgi complex (203). However, SREBPs are stabilized in the ER membrane by the INSIG proteins, thereby preventing their activation. Cholesterol and oxysterols like 25-OHC bind to and stabilize the INSIG proteins thereby preventing ER to Golgi transport and the subsequent transcriptional activation (145, 203). Summarising, one can say that oxysterol signalling via SREBPs leads to decreased cholesterol and fatty acid synthesis and decreased cholesterol uptake.

1.4.3 Smoothened and the hedgehog signalling pathway

The hedgehog signalling pathway is of extraordinary importance for the development of most vertebrate organs and tissues and has also been shown to be implicated in a number of birth defects and tumors (204-206). In contrast to LXR and SREBP signalling, the hedgehog signalling pathway is characterised by binding of oxysterols to a membrane associated receptor. The essential transmembrane proteins for the activation of the signalling pathway, patched (PTCH) and smoothened (SMO) (a seven transmembrane-spanning domain protein), are located within the primary cilium (207). Nearly all kinds of mammalian cells have a primary cilium consisting of nine microtubule doublets, without a central pair of microtubules, which is found only in motile cilia (208). After disruption of the primary cilium, the hedgehog-signalling and some other developmental pathways are also disrupted (209).

The most widespread activator, sonic hedgehog (SHH), is processed autocatalytically from a 45 kDa form to a 19 kDa lipidated protein, which is secreted to the extracellular matrix (210). SHH has two covalent lipid modifications. The first one contains a palmitic acid residue at the N-terminus (211) and the second one contains a cholesterol residue at the C-terminus (212).

In the absence of the signal, PTCH inhibits the function of SMO and keeps the pathway turned off. After binding of secreted SHH protein to PTCH, PTCH becomes inactive and SMO is activated (207). SMO then signals via a cytoplasmic transduction cascade that ultimately regulates the GLI family of zinc finger transcription factors with Gli1 and Gli2 as primary transcription factors in vertebrates (210).

It was stated for a long time that, besides the “natural” protein ligand, oxysterols are capable of activating the SHH signalling pathway (207, 213-215), until it was shown that oxysterols are allosteric activators of SMO (216).

This means that oxysterols break the “dogma” that bioactive cholesterol derivatives bind to and activate only intracellular binding sites, like the LXR receptor or the ER membrane-associated INSIG protein. Instead they, besides being involved in the regulation of lipid metabolism, can directly interfere with pathways affecting cell growth and differentiation.

1.4.4 G protein-coupled receptor 183 (EBI2)

Another seven transmembrane-spanning domain membrane receptor, which can be activated via oxysterol ligand binding, is the chemotactic receptor EBI2 (GPR183), which signals via $G\alpha_i$ (217, 218).

It was originally found that activated B cells move to inner and outer follicular regions by the action of an, at that time so-called “orphan”, G protein-coupled receptor, EBI2, and that $EBI2^{-/-}$ B cells favour the follicle and intermingle with the centre follicular dendritic cell (DC) network (219, 220). It was also reported that EBI2 is expressed by helper T cells, by various types of DCs, and it is also abundantly expressed in some CD8+ cytotoxic T cells (221).

In 2011, EBI2 was shown to be activated by 7α,25-dihydroxycholesterol and some other oxysterols (among them 25-OHC) and to be responsible for the observed B cell movement (222, 223). Moreover, EBI2 plays an important role in DCs, by regulating homeostasis and movement, and by influencing their immunological function (224).

The observation that EBI2, besides forming homodimers, also forms heterodimers with CXC-motive chemokine receptor (CXCR) 5, thereby modulating cellular calcium flux and MAPK activation, leads to the assumption that EBI2 is part of a complex receptor system, which integrates environmental signals on each stage of B cell activation (225).

1.5 Oxysterols in cancer

Summarizing evidence presented above, one may conclude that there are two distinct receptor families represented among the effectors that are known to bind oxysterols, namely the nuclear receptor transcription factors and G protein-coupled seven transmembrane-spanning domain receptors. Consequently oxysterols are able to interfere with tumor growth via multiple pathways:

a) by direct growth stimulation via activation of the hedgehog signalling pathway, as it was demonstrated for medulloblastoma (214) or

b) through regulation of the pro-inflammatory potential of immune cells by dampening the anti-tumor response of DCs in an LXR-dependent manner (226) or

c) by recruiting a population of (pro-tumorigenic) immune cells via LXR-independent pathways (227).

Only recently it was demonstrated that the mutated EGFR present in a high percentage of GBMs overcomes normal cell regulatory mechanisms to feed large amounts of cholesterol to brain cancer cells (181). It was shown that EGFRvIII upregulates SREBP1 cleavage and LDL receptor expression, thereby promoting cholesterol uptake, which favours growth and survival of GBM cells (228, 229). This pathway, which renders tumor cells exquisitely sensitive to LXR agonist-mediated apoptosis (181), could also feed excess cholesterol into the oxysterol synthetic pathways.

Oxysterols modulate the immune responses and as such could be effectors of the tumor environment: 25-OHC impairs IgA production in B-lymphocytes (230) and induces the secretion of the pro-inflammatory and angiogenic cytokine IL-8 (231, 232). Of note, oxysterols (in particular 7α,25-OHC) are potent chemoattractants for immune cells via EBI2 (222, 223). Besides regulating normal function of the immune system, this pathway might be of importance in the tumor environment, contributing

to chemotactic recruitment of monocytes across the tumor vasculature and subsequent deposition of tumor-associated macrophages.

LXR- and SREBP-mediated pathways interfere with cholesterol metabolism and, therefore, it is not surprising that oxysterols in the micromolar range are able to inhibit cancer cell proliferation including glioblastoma (228), breast (233), and prostate cancer cells (234) as well as prostate cancer xenografts (235). LXR agonists interfere with several cell cycle checkpoints inducing cell cycle arrest and phytosterols (plant LXR agonists) were suggested to reduce the incidence of colon cancer (236).

On the other hand, it has been demonstrated that oxysterols can dampen the function of DCs by inhibiting the functional expression of C-C chemokine receptor type 7 (CCR7) on maturing DCs via LXRα activation (226). As CCR7 is needed for the migration of DCs to secondary lymphoid organs, where they present antigens to T and B cells (237-239), a crucial step for the initiation of antigen-specific immune responses is blunted. Indeed, genetic or pharmacological inactivation of the LXR-oxysterol interaction restored DC migration to lymph nodes and antitumor responses in mouse tumor models (226).

In vitro studies demonstrated that 20(S)-hydroxycholesterol may interact with membrane receptors, activating the hedgehog signalling pathway via binding to the oncoprotein SMO (216). In a similar manner 25-OHC promotes medulloblastoma growth via activation of the SHH pathway (214). Conversion of 25-OHC to the more polar 25-OHC-3-sulfate by tumor cells decreases LXR affinity and exerts LXR antagonistic properties via peroxisome proliferator activated receptor (PPAR)γ activation (240) leading to increased tumor cell growth and tumor immune escape (241).

1.6 Hypotheses and aims

We first hypothesized that high expression of CH25H in primary glioblastoma samples and several cell lines (http://biogps.org) offers a growth advantage for tumor cells. This could be mediated via LXR-dependent and -independent mechanisms, such as stimulation of the hedgehog signalling pathway or recruitment of immunocompetent cells towards the tumor.

Second, we hypothesized that expression of CH25H and consequently production of 25-OHC is increased under the influence of pro-inflammatory cytokines in order to e.g. dampen DC function.

Therefore, the present thesis aimed at investigating CH25H expression on mRNA and protein level in three GBM cell lines. The effects of TNFα, IL1β, and IFNγ (cytokines secreted by GBM cells (242-244)) on CH25H transcription, translation, and product formation (25-OHC) were investigated in GBM cell lines. In addition 25-OHC concentrations were analysed in human GBM tissue by GC-MS. Growth curves were used to study the direct influence of 25-OHC on glioma cells and MTT tests aimed at investigating oxysterol toxicity. To examine the influence of oxysterols on the hedgehog signalling pathway, RT-qPCR was used and the relative amount of the Gli1 and PTCH gene products were quantified in oxysterol-treated and untreated cells.

Using THP-1 monocytes we studied the effects of exogenous 25-OHC and GBM-conditioned medium on cell migration, since monocyte-derived macrophages are known to contribute to increased aggressiveness and invasiveness of glioblastoma (245). Finally, the involvement of the G protein-coupled receptor EBI2 in 25-OHC-mediated migration of THP-1 cells and primary human monocytes was investigated.

The last part of the thesis aimed at elucidating the question if the observed *in vitro* effects (increased synthesis of oxysterols) are likely to occur *in vivo*, as well. C57/Bl6

mice were injected with LPS in order to achieve high plasma and tissue TNFα, IL1β, and IL6 concentrations. Subsequently, alterations in their lipid profile, especially tissue concentrations of side chain-oxidized sterols (24S-OHC, 25-OHC and 27-OHC), were analyzed.

2 Materials and methods

2.1 Materials

25-OHC and all standard solvents were from Sigma (Vienna, Austria). Deuterated (26,26,26,27,27,27-D_6-)25-OHC was from Dr. Ehrenstorfer GMBH (Augsburg, Germany). Cell culture supplies, TNFα and IL1β were from Gibco (Invitrogen, Vienna) or PAA Laboratories (Linz, Austria). LPS was from Sigma (Vienna, Austria) and silica gel (0.063-0.200 mm) for solid phase extraction was from Merck (Darmstadt, Germany). Kits for photometric free cholesterol, total cholesterol, and triglyceride quantitation were from DiaSys (Holzheim, Germany) and kits for phospholipid quantitation were from Roche (Mannheim, Germany).

The following antibodies were used: Monoclonal mouse-anti CH25H antibody (230), rabbit polyclonal antibody raised against calnexin was from Santa Cruz Biotechnology (CA, USA) and rabbit polyclonal antibody raised against EBI2 was from LSBiosciences (WA, USA). HRP-labelled goat anti-mouse IgG was from Santa Cruz Biotechnology and HRP-labelled goat anti-rabbit IgG was from Pierce (Thermo Scientific, MA, USA). Mouse anti-human vimentin, blocking solution, and antibody diluent were from DAKO (Jena, Germany). Cyanine-3 (Cy3) goat-anti mouse antibody was from Jackson laboratories (Bar Harbour, ME, USA), and DAPI solution was from Partec (Münster, Germany).

BCA protein assay kit and SuperSignal Western blot detection reagent kit were from Pierce (Thermo Scientific, MA, USA). ECL Plus Western Blotting Reagents were form Amersham Biosciences (Vienna). SuperScript II Reverse Transcriptase was from

Invitrogen (Vienna). Random hexamer primer were from Thermo Scientific. RNeasy Plus Kit, QuantiFast SYBR Green PCR kit, QuantiTect primer assays Cholesterol-25-hydroxylase (Hs_CH25H_1_SG), G protein-coupled-receptor 183 (Hs_EBI2_1_SG), Hydroxymethylbilanesynthase (Hs_HMBS_1_SG), Glyceraldehyde-3-phosphate-dehydrogenase (Hs_GAPDH_2_SG), and the siRNAs targeting EBI2 were from Qiagen (Hilden, Germany). Non-targeting siRNA (scrambled siRNA) was from Dharmacon (Thermo Scientific). GenMute transfection reagent was from SignaGen laboratories (MD, USA). Transwell plates with 8.0 µm polycarbonate membrane inserts (24-well plates) for cell migration experiments were from Costar (Vienna).

2.2 Cell culture

U87, A172 and GM133 cells were cultured in DMEM medium (Invitrogen) supplemented with 10% (v/v) FCS and 0.1% penicillin/streptomycin (Invitrogen). GM133 cells are derived from a glioblastoma patient biopsy; their culture has been previously described in detail (246). Before use for experiments cells were kept under serum-free conditions for at least 4 h. The only exception was oxysterol efflux experiments, where FCS was used as lipid acceptor. Cytokine stimulation was performed with TNFα (0.3 to 30 ng/ml) or IL1β (0.05 to 5 ng/ml).

2.3 Animals

Animal experiments were performed in accordance with the standards established by the Austrian Federal Ministry for Science and Research. C57/Bl6 mice (Himberg,

Austria) were maintained in a clean environment on a regular light-dark cycle (12 h light, 12 h dark) and were kept on standard chow diet.

10-12 week old male mice were injected intraperitoneally (i.p.) daily with LPS (0.83 mg/g body weight), dissolved in PBS. Every three days, five mice were sacrificed as described below and brain and plasma were taken.

2.4 Dissections

Mice were anesthetised deeply with Nembutal (150 µg/g body weight). After absence of reflexes, blood was taken retroorbitally (into Eppendorf tubes containing 20 µl 0.5 M EDTA) and mice were cut open with surgical instruments. A butterfly needle was injected into the left ventricle and the right atrium was opened for buffer perfusion. The blood was removed from the body by perfusion with PBS containing 1 mM EDTA for 11 minutes and brain was taken out.

2.4.1 Plasma

Blood samples were centrifuged at 5000 x g for 5 min and the supernatant was taken. Enzymatic analyses (total and free cholesterol, triglycerides, phospholipids) were performed immediately (2 µl each) using the kits for photometric analysis. The remaining volume was stored at -20 °C for further analysis.

2.4.2 Brain

Brain samples (one hemisphere) were stored at -70 °C and were frozen in liquid nitrogen for homogenisation using a bio-pulverizer (BioSpec Products, Bartlesville, USA). The whole homogenate was used for lipid extraction (three times, $CHCl_3/CH_3OH$ 2:1, for details see lipid extraction). Dried lipids were taken up into 5 ml of $CHCl_3/CH_3OH$ 2:1 (= brain lipid extract).

2.5 Cholesterol and triglyceride measurement

Brain lipid extracts were obtained as described above. 500 µl of lipid extract were mixed with 48 µl 10% (v/v) Triton X-100 in $CHCl_3$ dried under a stream of nitrogen. The oily residue was redissolved in 120 µl of distilled water and ultrasonicated in order to yield lipid-containing Triton vesicles. 2 µl were used for photometric cholesterol, triglyceride, and phospholipid measurement according to the manufacturer's instructions. Absorbance was measured on a Victor 1420 multilabel counter (Wallac).

2.6 Analysis of fatty acid composition

10 µg of C_{15} internal standard fatty acid were added to 150 µl plasma or to 2 ml of brain lipid extracts.

Lipid extraction of plasma samples was performed as described below and the dried lipid extracts were taken up into 1 ml toluene per each.

200 µl of plasma lipid extract was mixed with 800 µl toluene and 1 ml of BF_3-methanol (20%).

500 µl of brain lipid extract was dried under a gentle stream of nitrogen and resuspended into 1 ml toluene and mixed with 1 ml of BF_3-methanol (20%).

Derivatisation was performed at 110 °C for 1 h. After that, fatty acids were extracted using 400 µl of water/hexane (1:1). 100 µl of the hexane/toluene phase were removed, dried under a stream of nitrogen, and redissolved in 50 µl toluene. 1 µl of this solution was used for GC analysis.

A Thermo Scientific TRACE GC Ultra Gas Chromatograph equipped with a WCOT fused silica column (25 m x 0.32 mm), coupled to an FID-detector was used for analysis. The injection temperature was set to 230 °C and the detection temperature was 250 °C. The split ratio was set to 1:7. The time protocol used was as following:

Initial temperature was set to 150 °C increased with 2.5 °C/min to a plateau of 215 °C (held for 10 min); In a second ramping step temperature was increased again with 10 °C/min to reach a final temperature of 230 °C (held for 12.5 min).

2.7 Real time qPCR

RNA was extracted using an RNA Extraction Kit (Qiagen) according to the manufacturer's suggestions. Before reverse transcription, RNA concentration was determined using a Nanodrop ND-1000 spectrophotometer (Peqlab). One to three µg of RNA were used for reverse transcription, which was performed with the SuperScript II Reverse Transcription Kit and random hexamer primers (Invitrogen) according to the manufacturer's protocol. The temperature profile was: 25 °C for 10 min, 42 °C for 50 min, and 70 °C for 15 min. Real-time PCR analysis was performed using SyBr Green PCR kit and Quantitec primer assays (Qiagen) according to the manufacturer's protocol using a 7900 Fast Real-Time-PCR-System (Applied Biosciences).

GAPDH and HMBS were used as housekeeping genes. The following primers were used: CH25H (Hs_CH25H_1_SG), EBI2 (Hs_EBI2_1_SG), GAPDH (Hs_GAPDH_2_SG), and HMBS (Hs_HMBS_1_SG). Statistical analyses of qPCR analyses were performed using the REST software (http://www.gene-quantification.de; Ref. (247)).

2.8 Western blotting

Cells were lysed in 50 µl Ripa buffer (50 mM Tris-HCl, 1% (v/v) nonoxinol 40, 150 mM NaCl, 1 mM Na_3VO_4, 1 mM NaF, and 1 mM EDTA) containing protease inhibitors and PMSF. The lysate was kept on ice for 10 min, centrifuged at 10,000 x *g* for 10 min and the supernatant was collected. Protein content was measured using the BCA protein assay kit according to the manufacturer's protocol. Proteins were separated by SDS-PAGE (12%; 150 V) and transferred to PVDF membranes (150 mA, 1 h). CH25H was detected using a mouse monoclonal antibody. Calnexin and EBI2 were detected using polyclonal rabbit antibodies. Antibodies were diluted 1:1000 in antibody diluent. Immunoreactive bands were visualized using HRP-conjugated secondary antibodies and subsequent ECL Plus development. Luminescence was detected using a ChemiDocMP system (BioRad) followed by densitometric analysis with the ImageLab software (BioRad).

2.9 Lipid extraction

Cell lipid extraction: A172, U87, or GM133 cells were plated in 10 cm (diameter) Petri dishes and grown to 70-80% confluence. Cells were treated with cytokines at indi-

cated concentrations for 24 h. Thereafter, medium was collected and centrifuged to remove remaining cells. Cells were washed twice with PBS and scraped with 200 µl PBS. 20 ng D_6-25-OHC (MW = 408.69 Da) and/or 200 pmol epicoprostanol (MW = 388.67 Da) was added as internal standard. Tissue samples were collected as described above and directly subjected to lipid extraction. Lipid extraction was performed according to Folch (248). In brief, lipids were hydrolyzed in 2 ml ethanolic KOH (5 ml 5.88 M KOH in 100 ml EtOH); after neutralization with acetic acid (7 M, 120 µl) and addition of NaCl (200 µmol per extraction) lipids were extracted (twice for cell culture samples, three times for tissue samples) with chloroform/methanol (2:1; v/v). The chloroform phases were collected, unified and dried under a gentle stream of nitrogen with gentle heating. The dried lipids were derivatized with 100 µl MSTFA/pyridine (2:1; v/v) containing 1% (v/v) TMCS at 37 °C for 30 min.

2.10 Solid phase extraction

The solid phase extraction was performed using 1 mg silica gel columns. The columns were equilibrated with hexane (2 x 5 ml). Thereafter, samples were dissolved in 150 µl hexane:ether (2:1) and added onto the column. Columns were washed with 40 ml hexane:ether (4:1), 10 ml hexane:ether (2:1) and 6 ml hexane:ether (1:2). After that, the oxysterol-containing fraction was eluted with 12 ml ether and 10 ml ethylacetate. The unified fractions (ether + ethylacetate) were dried under a nitrogen stream. The dried lipids were derivatized with 70 µl MSTFA/pyridine (2:1; v/v) containing 1% (v/v) TMCS at 37 °C for 30 min.

2.11 Gas chromatography-mass spectroscopy (GC-MS) analysis

A Fisons model 8000 gas chromatograph, equipped with an HT5 fused silica capillary column (25 m × 0.22 mm i.d., 0.1 µm film thickness; SGE Analytical Science, Griesheim, Germany), coupled to a Fisons MD 800 quadrupole mass spectrometer, was used for detection. The splitless Grob-injector was kept at 220 °C. Helium was used as carrier gas with a constant flow of 1 ml/min. The initial column temperature of 200 °C was held for 1 min, followed by an increase of 15 °C/min to 280 °C, a hold at 280 °C for 10 min, followed by an increase of 15 °C/min to 300 °C, and a final isothermal hold of 7 min. The connection between GC and MS instrument was kept at 300 °C. The ion source temperature was 200 °C. Mass spectra were recorded with an electron ionization energy of 70 eV and an emission current of 100 µA. The diagnostic ions used for (two-fold) silylated 25-OHC were at m/z = 131.1, 456.4, and 546.4. Silylated D_6-25-OHC was detected at m/z = 137.1, 462.4 and 552.4.

2.12 Immunofluorescence

Cells were centrifuged onto glass slides using a Cytospin 2 centrifuge (Shandon), dried for 20 min, and stored at -20 °C until experimental use. Then cells were fixed with ice-cold acetone for 5 min, dried for 30 min, and blocked for 10 min using blocking solution (DAKO) for 10 min. The anti-vimentin antibody was diluted 1:50 in antibody diluent and was kept on the cells in a humidified chamber for 45 min. Slides were rinsed 5 times in PBS and then incubated with Cy3-labeled goat anti-mouse antibody (1:300, 30 min). Finally, the slides were counterstained with DAPI (Partec; 1:500, 5 min), rinsed 3 times in distilled water, and were mounted in Moviol. Microscopy was performed on a confocal laser-scanning microscope (Leica SP2, Leica La-

sertechnik GMBH, Heidelberg, Germany) using excitation wavelength at 543 nm (Cy3) and 405 nm (DAPI). Detected emission wavelengths were 555 nm to 620 nm for Cy3 and 430 nm to 450 nm for DAPI, respectively.

2.13 MTT test

Cells were plated in 24-well plates, grown to 80% confluence, and set serum-free 24 h before the start of the experiment. 25-OHC was added in concentrations between 0.1 nM and 10 µM for 6 h, 24 h and 72 h. After that MTT-medium (1.2 mM MTT in serum-free DMEM) was added and kept for 30 min at 37 °C. Cells were lysed in 2-propanol/1 M HCl (25:1) and the absorbance was read at 544 nm and at 650 nm (to measure background absorption) on a Victor 1420 multilabel counter.

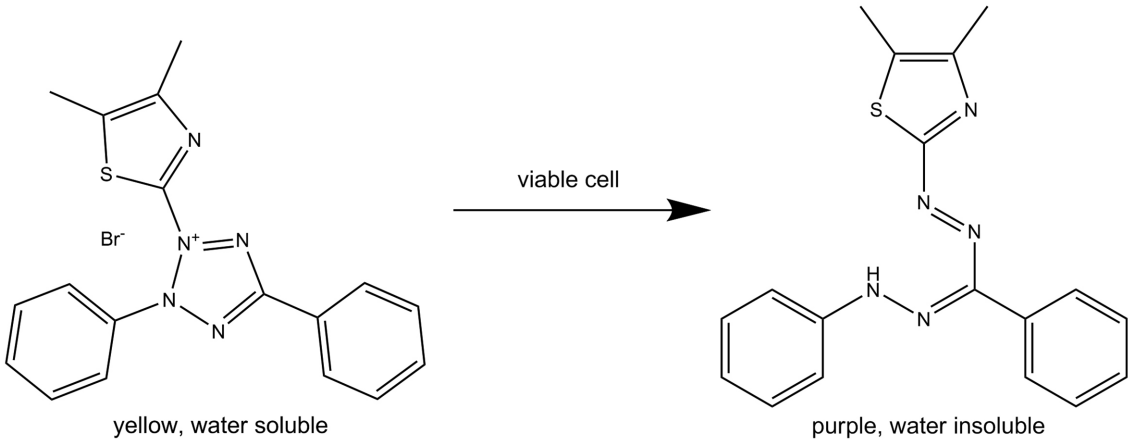

Figure 17: MTT reaction principle

MTT (left) is reduced by the succinyl-CoA reductase into the purple coloured, water insoluble form (right), which can be dissolved in an isopropanol/1 M HCl (25:1) mixture and used for photometric detection.

2.14 Growth curves

Cells were plated in 6 cm (diameter) petri dishes and were cultured in DMEM medium supplemented with 5% LPDS at the indicated concentrations of 25-OHC for the indicated times. To determine the cell number, cells were trypsinized and counted using a CASY cytometer.

2.15 Preparation of the GM133-conditioned medium extract

GM133 cells were plated in a 75 cm² flask and were grown to 80% confluence. Fresh medium (10 ml) was added and kept on the cells for 2 days. Medium lipid extraction was performed as described above. Dreid lipid extracts were reconstituted in 30 µl ethanol. For migration experiments and 0.5 µl per 500 µl medium were used.

2.16 Cell migration

Non-differentiated THP-1 cells were trypsinized, centrifuged, and resuspended in serum-free RPMI medium. Cell number was determined using a Bürker-Türk hemocytometer and 100,000 cells (in 100 µl) were plated in the upper chamber of a 6.5 mm² transwell chamber (Corning) with 8.0 µm pore size. The lower chamber was filled with 500 µl RPMI medium containing 0.1% (w/v) BSA (as an oxysterol acceptor), vehicle (0.1% ethanol; v/v), 25-OHC (2.5, 25, and 75 nM), GM133-conditioned medium extract (0.5 µl/500 µl medium), and/or pertussis toxin (PTX; 30 ng/ml). After 18 h, the number of migrated THP-1 cells into the lower chamber was determined by counting using a hemocytometer (at least nine large squares per sample) and cell number was normalized to the vehicle-containing (0.1% BSA, 0.1% ethanol) control.

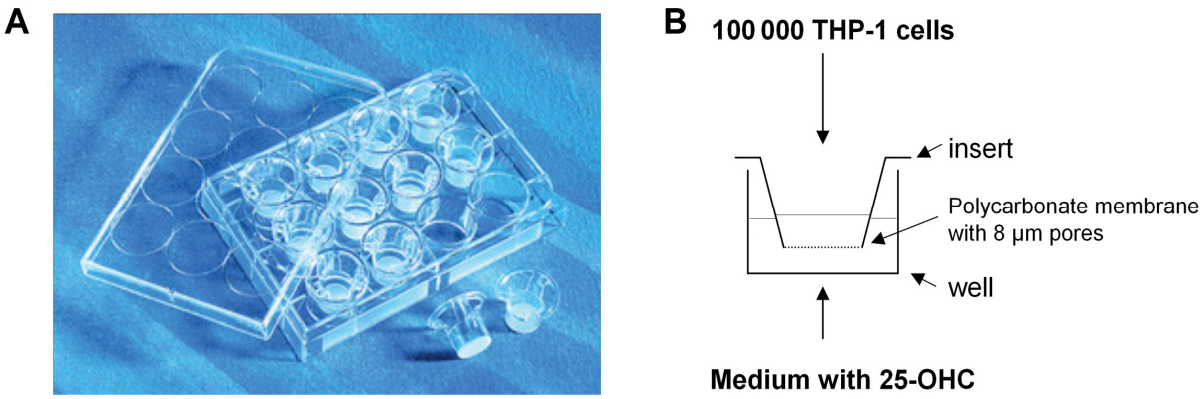

Figure 18: Transwells® and their principle of function

Corning Transwells® are shown in A (taken from www.sigmaaldrich.com), their principle of function is shown in B. 100,000 THP-1 cells were transferred into the insert, while the well contains medium supplemented with the chemoattractant. Well and insert are separated by a polycarbonate membrane with 8 µm pores. Cells can actively migrate across this barrier and can finally be counted inside the well.

2.17 siRNA transfection

400,000 THP-1 cells were plated in a 6-well plate and transfected with either 40 pmol EBI2 siRNAs (Hs_EBI2_1, Hs_EBI2_3, Hs_EBI2_4, and Hs_EBI2_5, respectively) or scrambled siRNA using the GenMute transfection reagent according to the manufacturer's suggestions. Forty-eight hours post transfection, migration experiments, RT-PCR, or Western blotting experiments were performed as described above.

2.18 Statistical analysis

Statistical analysis was performed using the GraphPad Prism 5 software. For determination of statistical significance the unpaired two-tailed t-test and one way ANOVA with or without Bonferroni post-hoc test were used. For *in vivo* results, two way ANOVA with Dunnett's post hoc test was used. p values < 0.05 were considered statistically significant.

3 Results

3.1 Analysis of tumor tissue samples

To get an indication, whether the *in silico* data for astrocytomas are compatible with our hypothesis, five astrocytoma samples were subjected to GC-MS analysis (for analytical details, see section 3.2.3, page 65). 25-OHC concentrations in GBM (astrocytoma grade IV) samples ranged between 0.55 and 2.2 ng/mg tissue wet weight compared to 0.12 ng/mg tissue wet weight in the pilocytic astrocytoma sample (grade I) (**Fig. 19**).

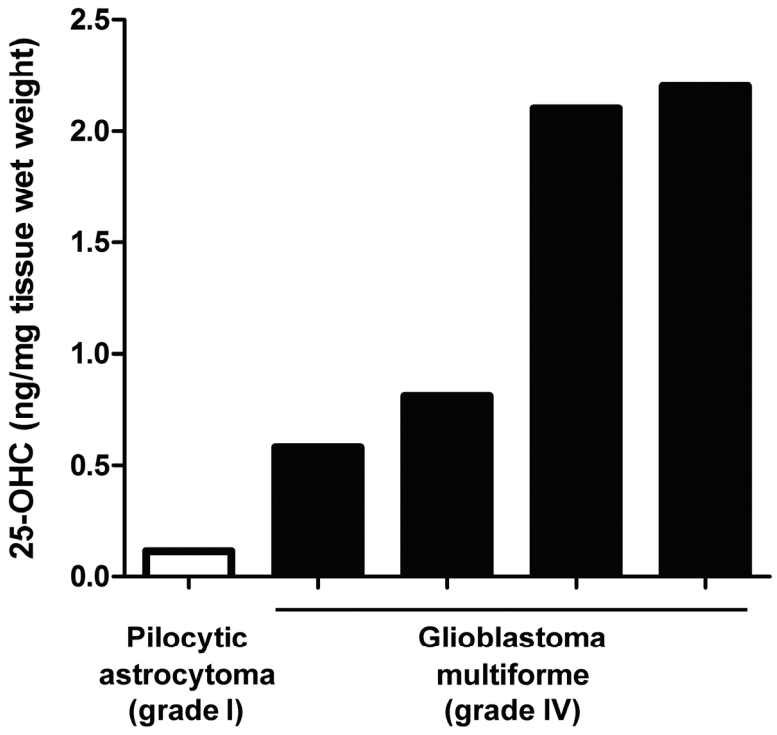

Figure 19: 25-OHC concentrations in astrocytoma tissue samples

Lipids of five tumor tissue samples were extracted and 25-OHC concentration were analyzed via GC-MS. All four glioblastoma tissue samples had a higher 25-OHC content than the pilocytic astrocytoma.

Although the experimental value of this observation is hampered by the lack of healthy control tissue, these data indicate that GBM 25-OHC amounts are indeed elevated *in vivo*.

3.2 Regulation of CH25H in glioblastoma cell lines A172, U87, and GM133

3.2.1 CH25H gene is upregulated in response to cytokine stimulation in GBM cell lines

The glioblastoma cell lines A172, U87, and GM133 were investigated by real time qPCR for their CH25H mRNA levels. *In silico* analysis using BioGPS (http://biogps.org) revealed that GM133 cells show highest CH25H expression among all cancer cell lines, included in the NCI-60 dataset. As cytokines act as important modulators of the tumor environment, the effects of TNFα, IL1β, and IFNγ on CH25H expression in A172, U87 and GM133 were examined.

In A172 cells, exogenously added TNFα and IFNγ did not result in significant upregulation of CH25H mRNA levels (**Fig. 20A** and **C**). In contrast, IL1β treatment resulted in 2.2-, 4.2-, and 9.0-fold upregulation at 0.05, 0.5 and 5 ng/ml, respectively (**Fig. 20B**).

In U87 cells, TNFα treatment resulted in significant upregulation of CH25H mRNA levels (2.1-, 7.2-, and 11-fold at 0.3, 3.0, and 30 ng/ml, respectively) (**Fig. 20D**). In contrast, IL1β had less pronounced effects on CH25H mRNA expression reaching a maximum induction of 4.5-fold (**Fig. 20E**). IFNγ treatment only reached a 2.1 fold CH25H gene expression induction at maximum (**Fig. 20F**).

Stimulation of GM133 cells with TNFα resulted in a maximum increase of CH25H mRNA expression by 4.6-fold (**Fig. 20G**). In contrast, IL1β treatment was more efficient with regards to transcriptional regulation of CH25H by increasing mRNA levels up to 5.3-, 7.8-, and 11-fold at IL1β concentrations of 0.05, 0.5, and 5 ng/ml, respectively (**Fig. 20H**).

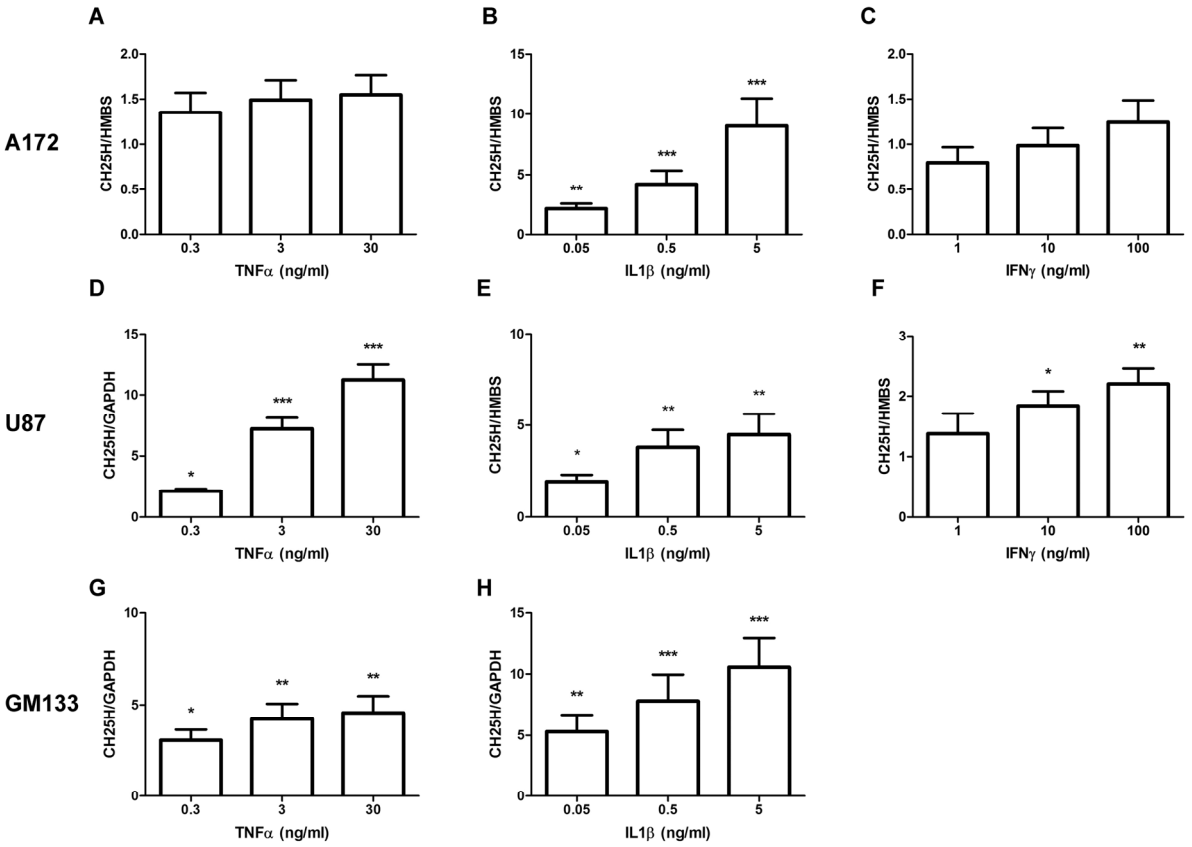

Figure 20: Cytokines are potent inducers of CH25H transcription in glioblastoma cell lines.

Three glioblastoma cell lines have been incubated with TNFα, IL1β, und IFNγ, respectively. After 6 h, cells were lysed, RNA was isolated and used for qPCR analysis. HMBS and GAPDH were used as housekeeping genes. Gene expression ratios were calculated by REST and analyzed by a pair-wise fixed random reallocation test. Data are shown as mean ± SD of 3 independent experiments. * $p < 0.05$, ** $p < 0.01$, *** $p < 0.001$

All observed responses were concentration dependent and represent the regulative status in glioma cell lines after 6 h of treatment. However, to get an indication about the time course of CH25H gene upregulation, we investigated CH25H response in TNFα treated U87 cells at different timepoints by qPCR (**Fig. 21**). The maximal upregulation of the CH25H gene (17-fold) was achieved after 12 h. After 24 h mRNA levels declined again and were only 10-fold increased at the endpoint of the experiment after 48 h.

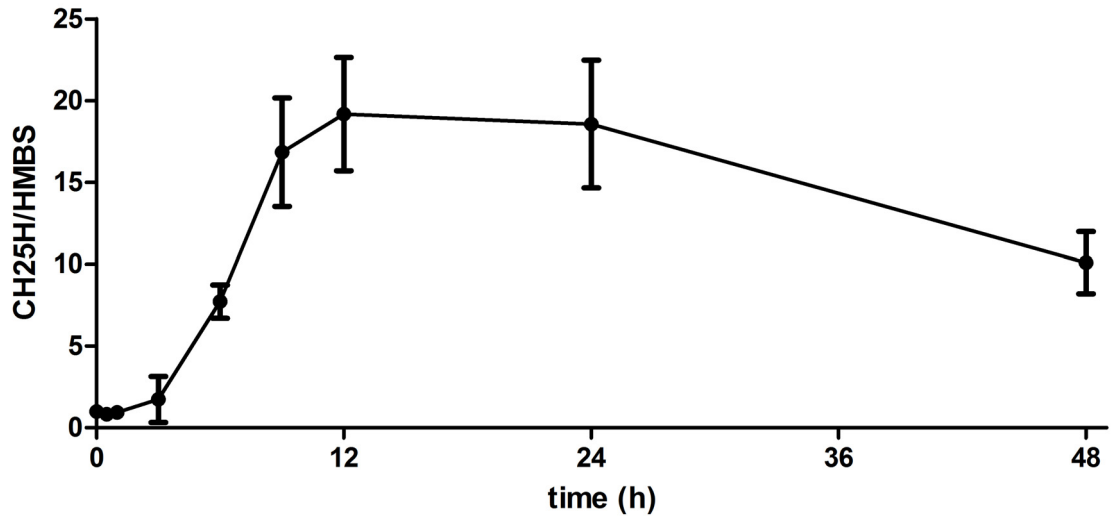

Figure 21: CH25H is upregulated for at least 48 h after cytokine stimulation with a maximum at 12 h.

U87 cells were treated with 30 ng/ml TNFα. At the indicated timepoints mRNA was extracted, reversely transcribed, and the amount of CH25H was quantitated by qPCR. Results are expressed as relative ratio of CH25H/HMBS compared to controls and represent mean values ± SD of triplicates.

3.2.2 Cytokine stimulation results in increased amounts of CH25H protein as revealed by Western blot analysis

To investigate whether increased mRNA amounts are accompanied by increased CH25H protein, Western blot analysis was performed. Data from these analyses revealed that the protein content of CH25H is increased in U87 and GM133 cells in response to 24 h stimulation with TNFα (30 ng/ml) and IL1β (5 ng/ml), respectively (**Fig. 22A** and **B**). In contrast, CH25H protein was below detection limit in protein lysates of cytokine-stimulated and unstimulated A172 cells.

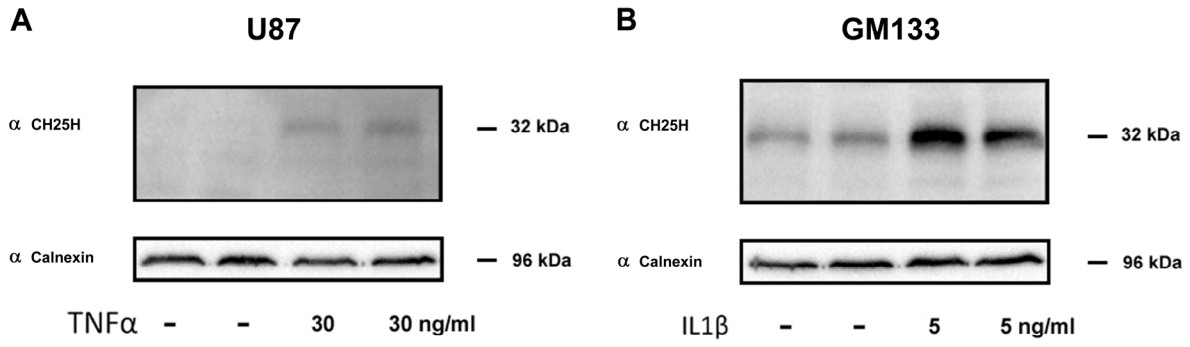

Figure 22: Upregulation of CH25H protein in response to TNFα and IL1β treatment.

U87 (**A**) and GM133 (**B**) were treated with the indicated cytokines at the indicated concentrations. After 24 h, cells were lysed, protein was extracted, and Western blot analysis was performed in duplicates using a monoclonal antibody against CH25H. Calnexin was used as loading control.

3.2.3 25-OHC concentrations are increased in cytokine-stimulated GBM cell lines

Taken together, the results described above indicate that cytokine stimulation of glioblastoma cells is strong enough and long enough to result in increased cellular protein levels. However, as enzymes can be modulated in activity by post-translational modifications (e.g. phosphorylations), the next set of experiments aimed

to clarify, whether increased levels of intracellular CH25H are accompanied by increased product generation. Cellular and medium lipid extracts of TNFα- and IL1β-treated glioblastoma cells were analyzed by GC-MS as the corresponding trimethylsilyl (TMS) derivatives. Selected ion-monitoring traces of TMS derivatives of 25-OHC (analyzed from cellular lipid extracts of untreated GM133 cells; diagnostic ions at m/z = 131.1) and D_6-25-OHC (m/z = 137.1; internal standard) are shown in **Fig. 23 A** and **B**. Full scan electron impact spectra for TMS derivatives of 25-OHC and D_6-25-OHC are shown in **Fig. 23 C** and **D**. The proposed fragmentation patterns for both analytes are shown as insets in Fig. 23 C and D.

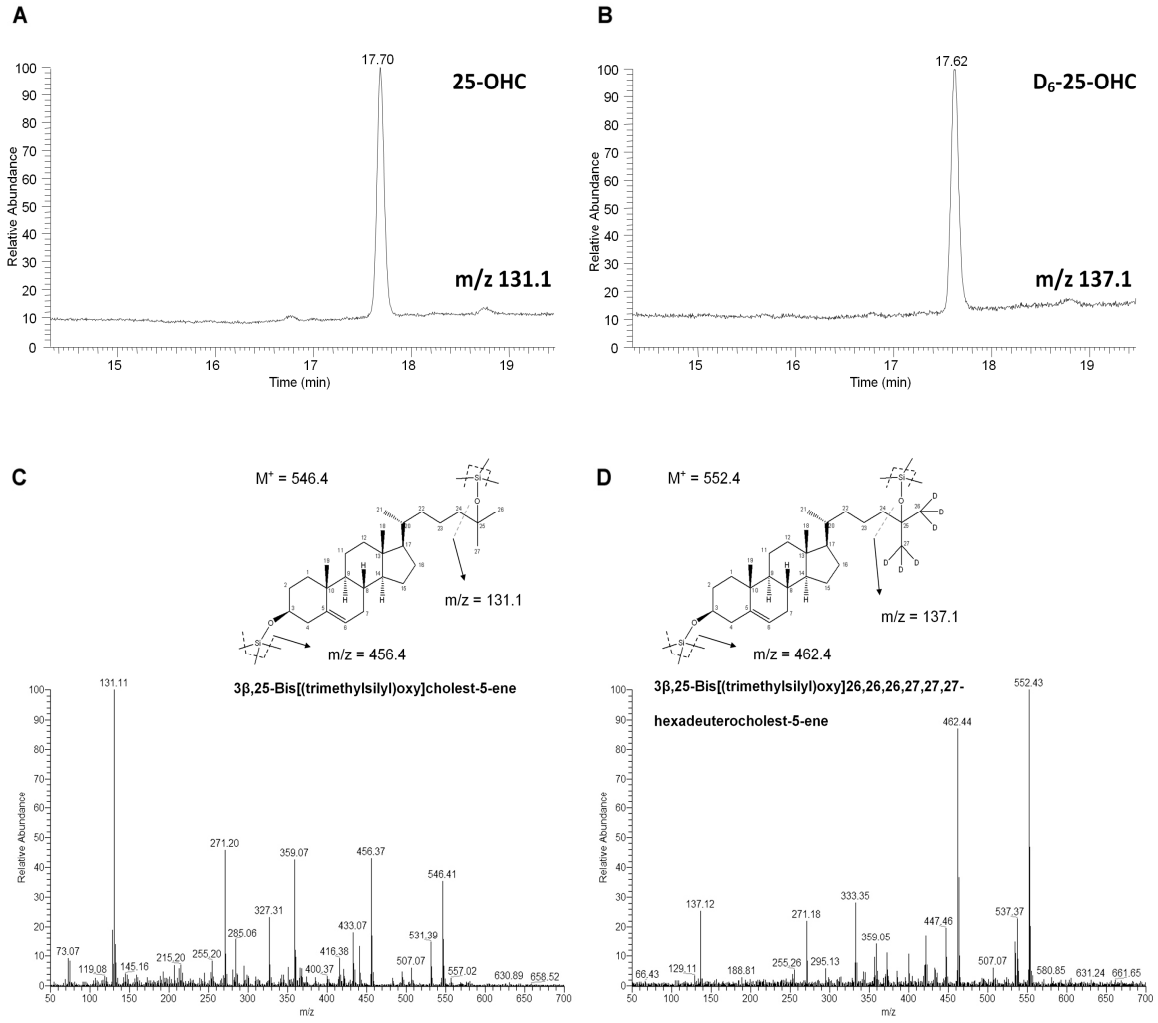

Figure 23: Selective ion chromatograms and full scan spectra of 25-OHC and D6-25-OHC.

Selective ion chromatograms of 25-OHC (**A**) and D_6-25-OHC (**B**). Proposed fragmentation patterns with mass assignment and representative full scan spectra of 25-OHC (**C**) and D_6-25-OHC (**D**).

After treatment with IL1β (5 ng/ml, 24 h), intracellular 25-OHC concentrations did not increase in A172 cells. However, extracellular 25-OHC concentrations significantly increased from 6.6 to 14.8 ng/mg cell protein.

Intracellular U87 25-OHC concentrations increased from 9.9 to 15 ng/mg cell protein in response to TNFα (30 ng/ml, 24 h) (**Fig. 24**). Concentrations of secreted 25-OHC increased significantly ($p<0.05$) from 5.8 to 18 ng/mg cell protein. In line with high

mRNA and protein levels of CH25H in GM133 cells (Fig. 20 and 22) cellular and medium 25-OHC concentrations under basal conditions were 10- to 30-fold higher as compared to U87 cells. Exogenously added IL1β provoked an intracellular increase of 25-OHC from 66 to 95 ng/mg cell protein ($p<0.05$) while extracellular 25-OHC concentrations increased from 160 to 300 ng/mg cell protein ($p<0.01$) (**Fig. 24**). In line with the qPCR findings (Fig. 20), exogenously added TNFα increased extracellular 25-OHC levels from 120 to 160 ng/mg cell protein ($p<0.05$) and resulted in a slight, but statistically not significant increase of intracellular 25-OHC amounts from 71 to 80 ng/mg cell protein (Fig. 24).

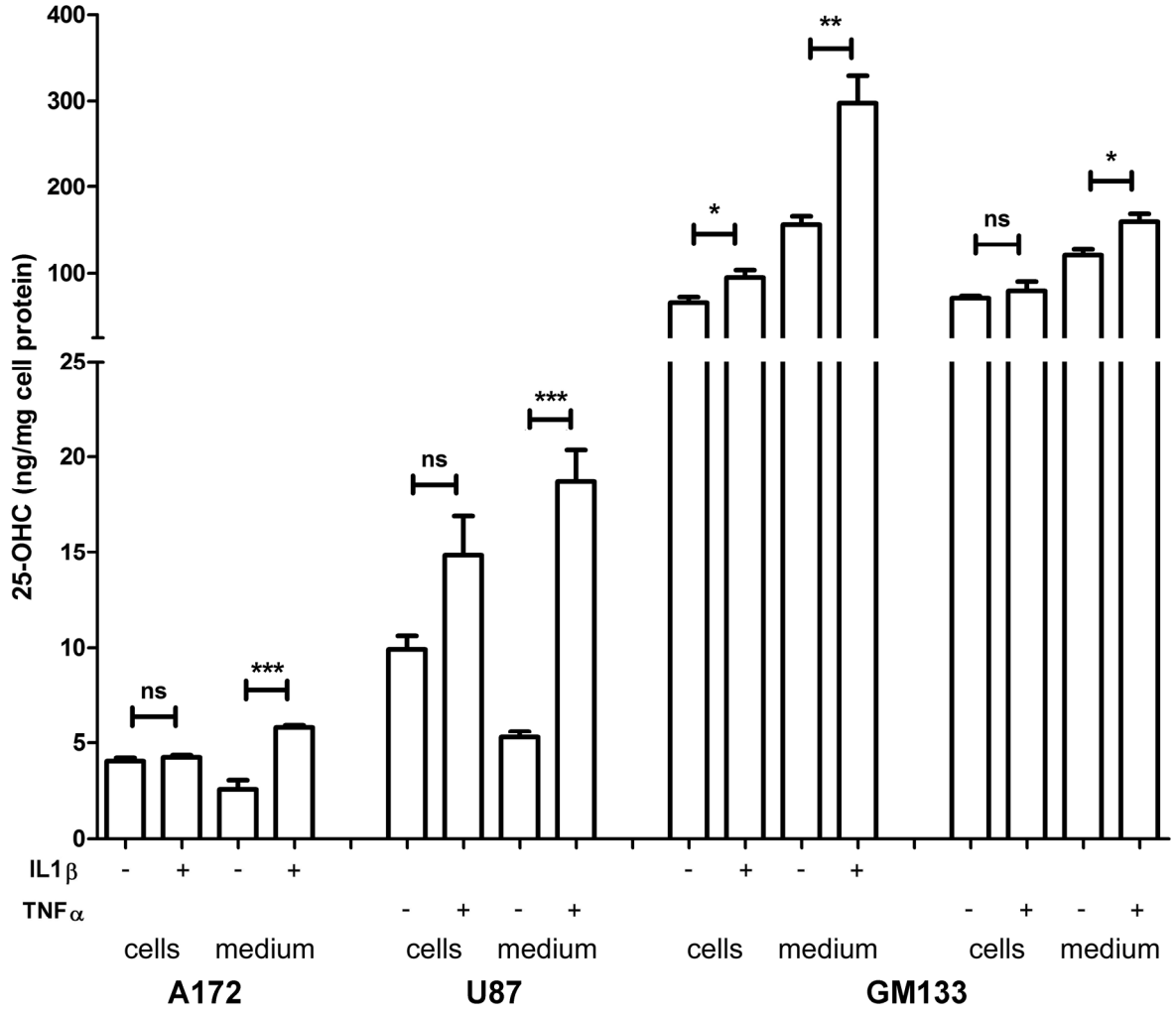

Figure 24: 25-OHC levels in cell and medium lipid extracts of cytokine-treated GBM cells.

A172, U87, and GM133 cells were incubated with either 5 ng/ml IL1β and/or 30 ng/ml TNFα as indicated. After 24 h medium and cells were collected separately, lipids were extracted, derivatised with MSTFA, and analyzed by means of GC-MS. D_6-25-OHC was used as internal standard and m/z = 131.1 and 137.1 were used as diagnostic ions for quantitation. Data are shown as mean ± SD of quadruplicates. * $p < 0.05$, ** $p < 0.01$, *** $p < 0.001$

3.3 Effects of lipopolysaccharide on U87 oxysterol production

As it has been shown in macrophages by Diczfalusy et al. (183) that LPS is able to upregulate CH25H gene transcription, we investigated the impact of LPS stimulation on CH25H transcription in U87 cells. We treated U87 cells with LPS (100 ng/ml) and analysed CH25H levels at timepoints of 1, 2, 3, 4, 6 and 24 h by qPCR. The maximal upregulation (2.5 fold) was observed after 2 h treatment (Fig. 25). We observed a rapid decline to 1.8-fold after 3 h, which remained almost unchanged up to 6 h and declined again to control level after 24 h (**Fig. 25**).

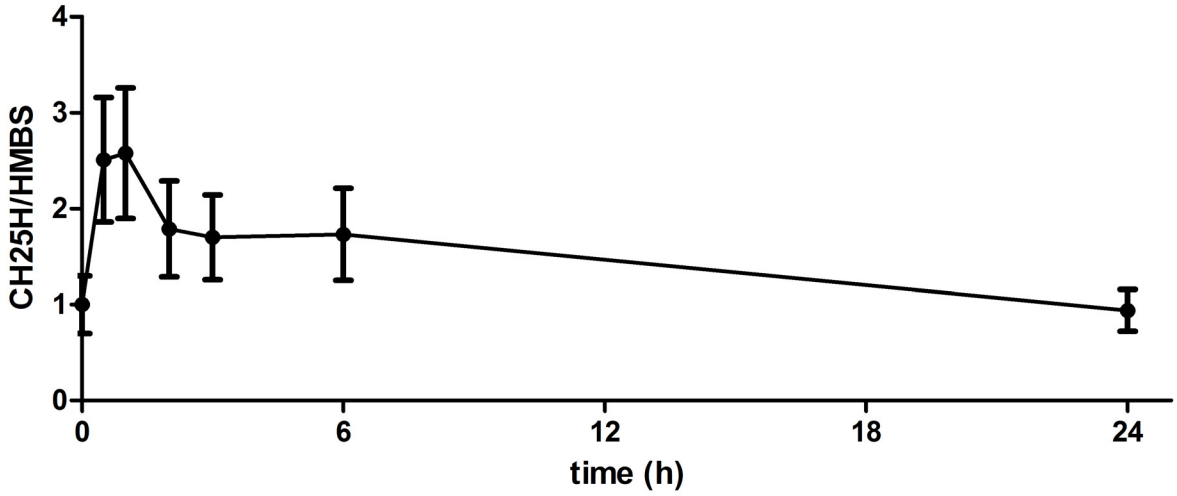

Figure 25: LPS exerts rather short term than long term effects on CH25H transcription.
U87 cells were stimulated with LPS (100 ng/ml). At the indicated timepoints mRNA was extracted, reversely transcribed, and analyzed by real time qPCR. CH25H mRNA amounts were normalized to HMBS. Results are expressed as relative ratio of CH25H/HMBS compared to controls and represent mean values ± SD.

As changes in CH25H expression were minimal, we wanted to figure out changes in LPS-treated U87 cells in absolute oxysterol amounts. Using GC-MS analysis, we were able to detect and quantify four different oxysterols in cellular and medium lipid

extracts: 7α-OHC, 24S-OHC, 25-OHC, and 27-OHC. Despite a slight intracellular increase of 24S-OHC from 200 to 230 ng/mg cell protein, we were not able to detect statistically significant changes (except for cell-associated 24S-OHC) in intracellular or extracellular oxysterol amounts (**Fig. 26A-D**). Nevertheless, 25- and 27-OHC levels showed a tendency to increase in response to LPS treatment.

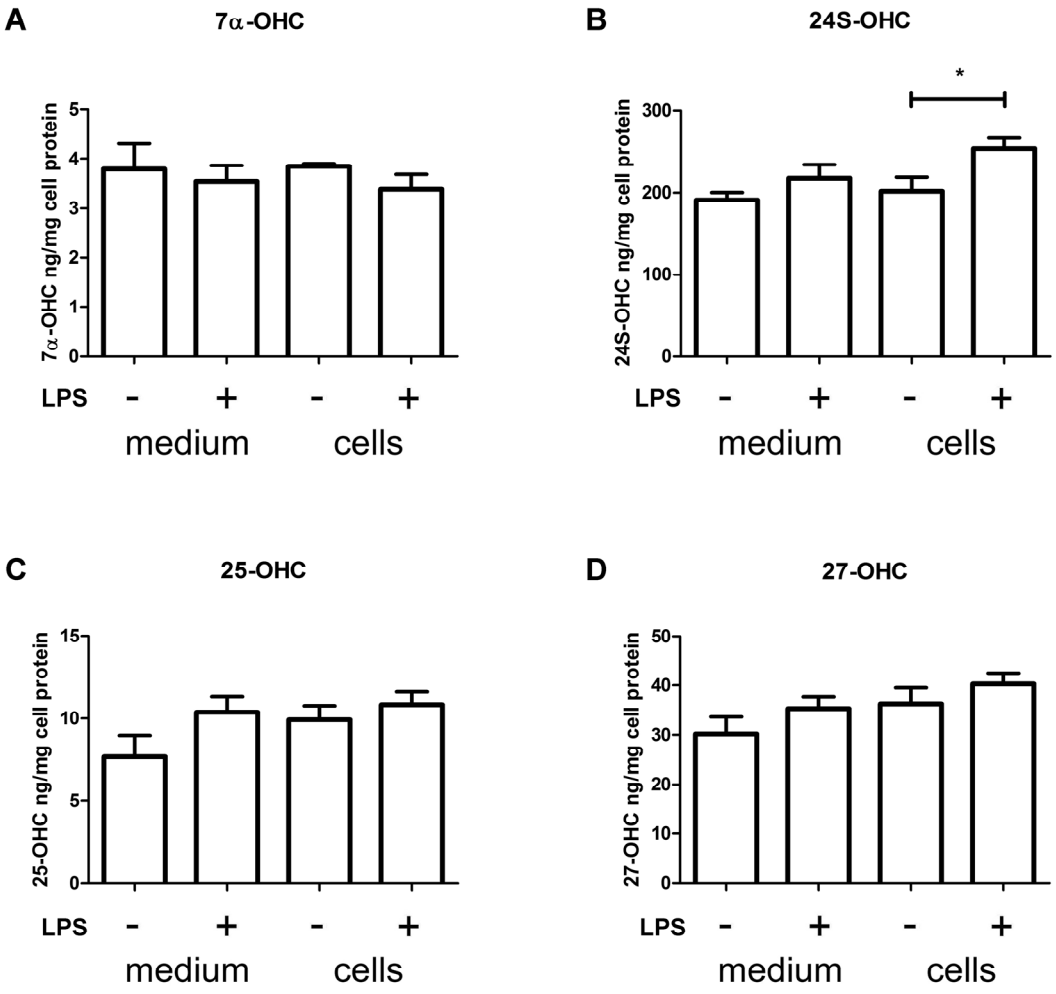

Figure 26: Oxysterol profile of U87 cells is marginally altered in response to LPS treatment. U87 cells were incubated for 24 h with 1 µg/ml LPS. Subsequently, medium and cells were collected and lipids were extracted, converted to the corresponding trimethylsilylether-derivatives with MSTFA, and analysed by means of GC-MS. D_6-25-OHC and epicoprostanol were used as internal standards. Data are shown as mean ± SD of quadruplicates. * $p < 0.05$

3.4 Toxicity of side chain-oxidized cholesterols

Oxysterols have been reported to be pro-apoptotic and cell toxic and Yamanaka et al. (249) demonstrated that neuronal death in response to 24-OHC is induced through necroptosis, which represents a programmed form of necrosis. Therefore, in this set of experiments four different cell lines (A172, U87, GM133 and THP-1) were treated with three different oxysterols (20S-OHC, 24S-OHC, and 25-OHC; THP-1 cells with 25-OHC only) at concentrations of 10 nM, 100 nM, 1 µM and 10 µM, respectively, and cell viability was measured after 24 and 72 h using the MTT test.

Results revealed that all tested cell lines were susceptible to oxysterol treatment > 10 µM for 72 h. However, cell death-inducing 25-OHC concentrations are one order of magnitude lower as compared to 20S-OHC and 24S-OHC (**Fig. 27A-F**). In detail, we found that after 24 h, 20S-OHC and 24S-OHC had almost no effects on cell viability up to 10 µM (Fig. 27A and C) whereas 25-OHC led to 30% decrease in cell viability in U87 cells at 1 µM and 10 µM (Fig. 27E) and a 20% and 30% reduction in viability of THP-1 cells at concentrations of 1 µM and 10 µM, respectively (Fig. 27E). 25-OHC had no effects on viability of A172 and GM133 cells up to 10 µM after treatment for 24 h (Fig. 27E).

After 72 h, 20S-OHC was without effect up to 1 µM, but at 10 µM it decreased cell viability by 20% in A172, 70% in U87, and by 90% in GM133 cells (Fig. 27B). 24S-OHC provoked a 20% reduction of cell viability after 72 h at 1 µM and 60% reduction of cell viability at 10 µM in U87 and GM133 cells, whereas cell viability of A172 remained unchanged up to 10 µM (Fig. 27D). 25-OHC, which turned out to be the most toxic among the tested oxysterols led at 1 µM to a 60%, 30%, and 40% reduction of cell viability in U87, GM133, and THP-1 cells, respectively. At 10 µM cell viability was

reduced in A172 by 80%, in U87 by 100%, and in GM133 and THP-1 cells by 90% (Fig. 27F).

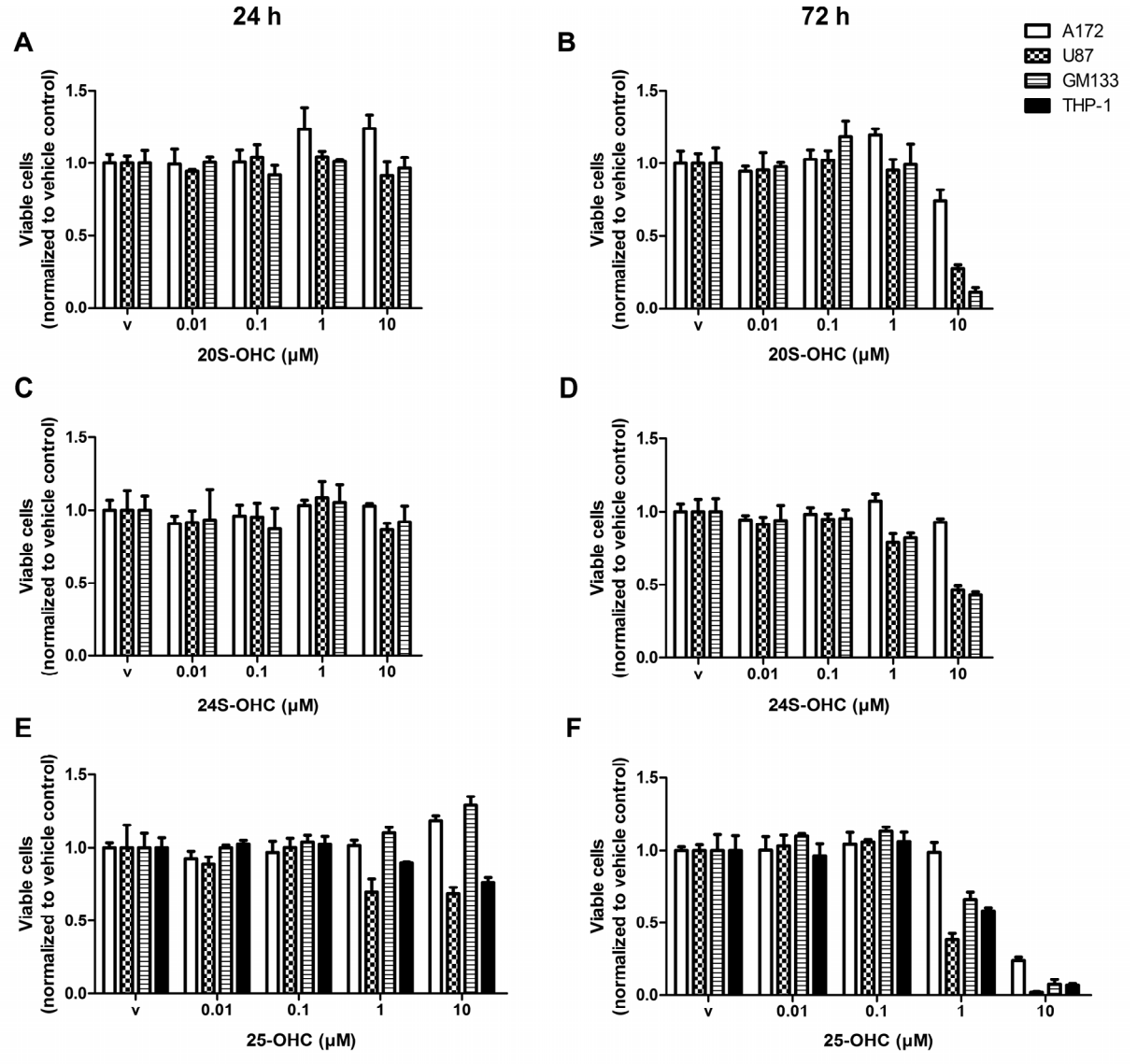

Figure 27: Estimation of cytotoxicity of different oxysterols in GBM cell lines.

Cells were plated in 24-well dishes and after 24 h they were treated with the indicated amounts of oxysterols (in medium containing 1% FCS). After 24 h (**A**, **C**, **E**) or 72 h (**B**, **D**, **F**) cell viability was assessed by the MTT-test as described in materials and methods. Absorbance (A_{544}/A_{650}) was normalized to the vehicle control (v). Bars represent means ± SD of triplicates.

3.5 Autocrine effects of 25-OHC on U87 cells

Our next aim was to clarify autocrine effects of 25-OHC on U87 cells. These experiments should support the hypothesis that 25-OHC exerts growth promoting effects, potentially mediated via SMO and the SHH pathway or via modulating metabolic pathways from a catabolic to a more anabolic state.

3.5.1 U87 cell proliferation is not increased by treatment with exogenously added 25-OHC

To test this hypothesis, we first performed cell proliferation experiments with U87 cells. We plated 50,000 cells into 12-well plates and counted cells after 2 and 4 days under 25-OHC-treated and untreated conditions. The experiment was performed either in medium containing 4.5 g/l glucose as in medium containing 1 g/l glucose to get an indication of a possible growth promoting role of 25-OHC under low glucose supply. When 4.5 g/l glucose was present in the culture medium, 25-OHC had no effect on cell growth compared to untreated cells (**Fig. 28A**). In contrast, when the culture medium contained 1 g/l glucose, we could even observe a concentration dependent, slight reduction of U87 cell growth (**Fig. 28B**).

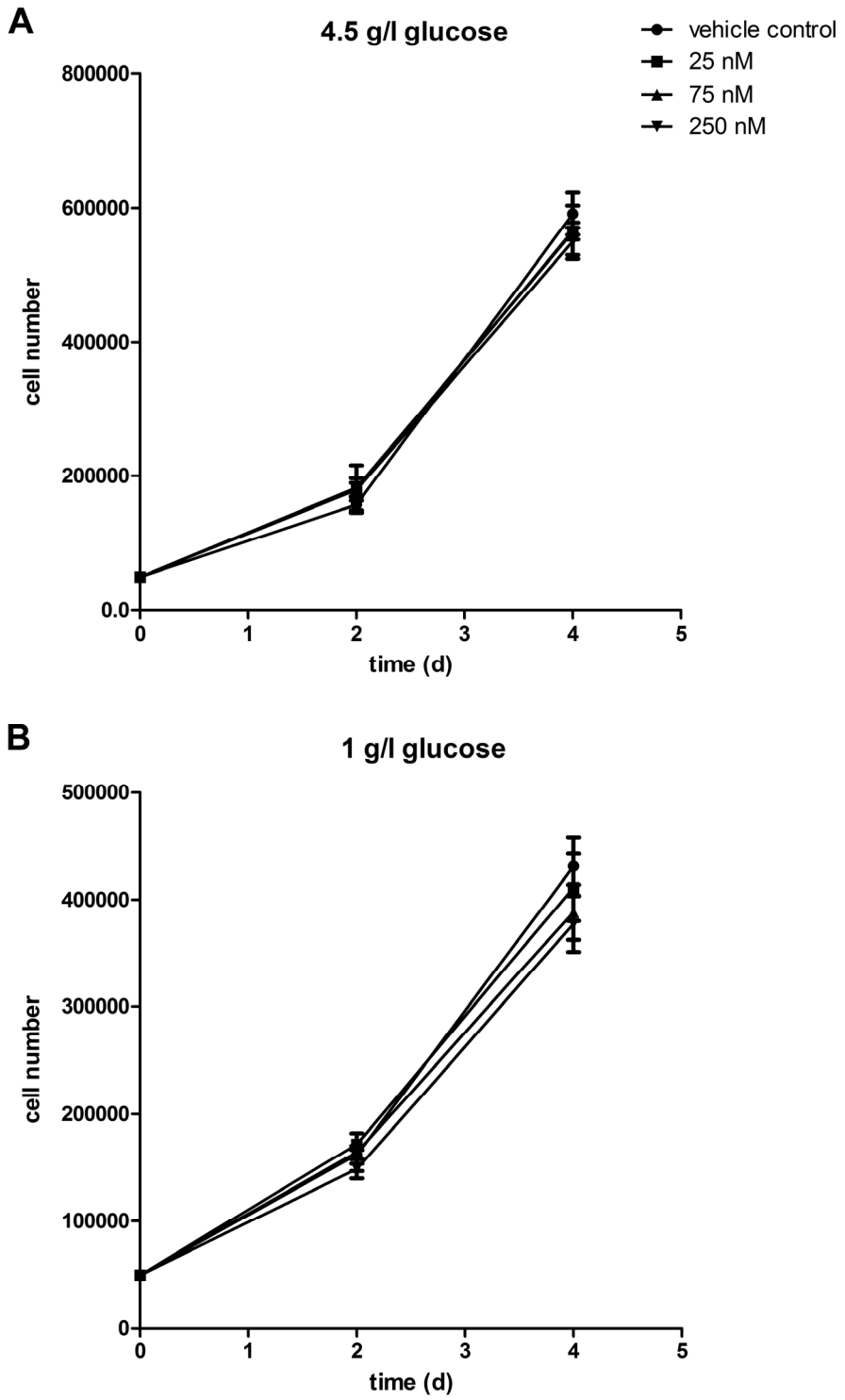

Figure 28: Exogenously-added 25-OHC does not accelerate U87 growth.

50,000 U87 cells were seeded into 12-well dishes and grown either in high glucose DMEM (**A**) or low glucose DMEM (**B**). On day 2 and 4 cells were trypsinised and counted by means of a CASY cytometer. Points represent means ± SD of triplicates.

3.5.2 The SHH pathway is marginally activated in response to 25-OHC treatment

Only recently it was demonstrated that 20S-OHC and also, to a lesser extent, 25-OHC are activators of the protein SMO, which is the key receptor of the SHH pathway (216). It was also shown that the SHH pathway is crucially important for medulloblastoma growth (214). Therefore, we were interested, if this molecular mechanism could be of importance in glioblastoma cells. *In silico* analysis of *geoprofiles* gene expression data (www.ncbi.nlm.nih.gov/geoprofiles) revealed that U87 and also A172 cells express the key protein SMO. When testing for transcriptional activation by 25-OHC, however, we could only observe a 1.4-fold induction of PTCH1 transcription (**Fig. 29**) which is an important reporter gene for the SHH pathway. The other important reporter gene, GLI1 was neither induced in U87, nor in A172 cells indicating (at least under the experimental conditions used here) a minor role for the SHH pathway in glioblastoma cell lines.

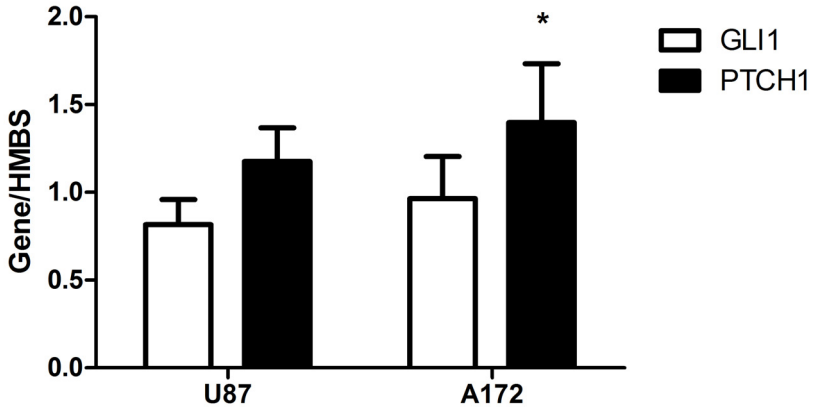

Figure 29: SHH reporter genes are only induced marginally by 25-OHC treatment.

U87 and A172 cells were treated with 25-OHC (1 µM). After 24 h cells were lysed, RNA was extracted, and reversely transcribed. Detection of the SHH activation-induced genes GLI1 and PTCH1 was performed by real time qPCR. Data are shown as mean ± SD of three independent experiments. * $p < 0.05$

3.5.3 25-OHC induces cholesterol turnover in U87 cells

After these negative results regarding growth promoting effects of 25-OHC, we were interested to assess the effects of 25-OHC on the metabolic genes ABCA1, acetyl coenzyme A carboxylase (ACC), fatty acid synthase (FASN), HMGCR, and glucose uptake transporter (GLUT) 1 and 3, because we expected a probable switch in cell lipid or glucose metabolism being the reason for the described effects. These analyses revealed that ABCA1, a cholesterol efflux transporter, is upregulated 3-fold in 4.5 g/l glucose medium and 2-fold in 1 g/l glucose medium, indicating increased cholesterol excretion in response to 25-OHC. In line with this finding, the key gene for cholesterol biosynthesis, HMGCR, was downregulated 5-fold in 4.5 g/l glucose medium (**Fig. 30A**) and 4 fold in 1 g/l glucose medium (**Fig. 30B**), indicating decreased cholesterol biosynthesis, whereas ACC was only slightly, but not significantly downregulated. Interestingly, also FASN, the gene encoding fatty acid synthase, was decreased to the same extent as HMGCR, i.e. 5-fold in 4.5 g/l glucose medium and 4-fold in 1 g/l glucose medium, indicating not only decreased cholesterol, but also decreased fatty acid synthesis in response to 25-OHC. The genes for the glucose transporters GLUT1 and GLUT3, which we expected to be upregulated under low glucose conditions, remained unchanged in both experimental settings (Fig. 30A and B).

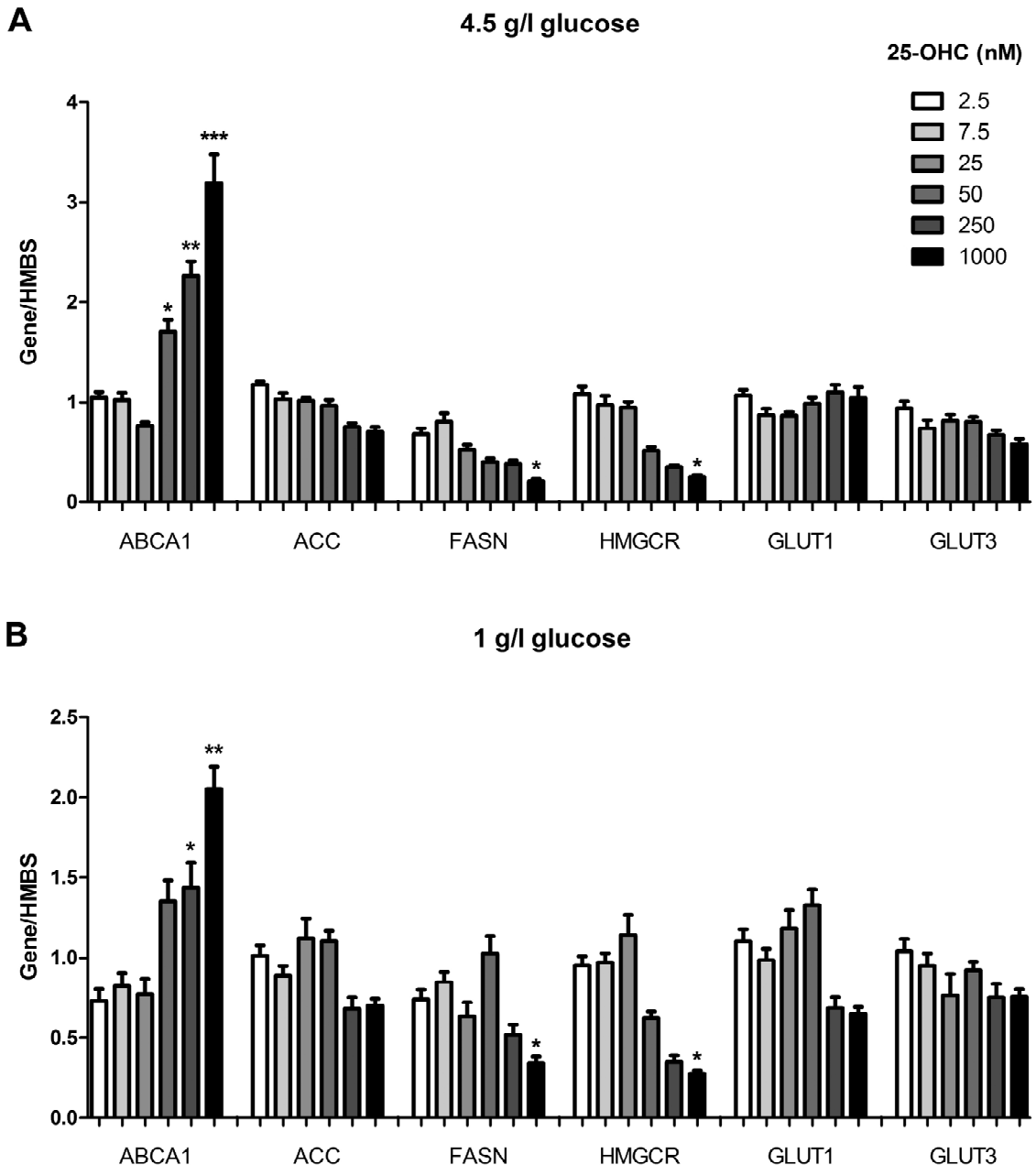

Figure 30: 25-OHC treatment increases cholesterol catabolism on the transcriptional level.

U87 cells were plated in 6-wells and were treated overnight with increasing concentrations of 25-OHC. After 24 h cells were lysed, RNA was extracted, and reversely transcribed. Detection of the LXR target genes ABCA1, ACC, FASN, HMGCR, GLUT1, and GLUT3 was performed by real time qPCR as described in materials and methods. Data are shown as mean ± SD of three independent experiments. * $p < 0.05$, ** $p < 0.01$, *** $p < 0.001$

3.6 25-OHC induces migration of human THP-1 monocytes

3.6.1 25-OHC increases THP-1 monocytes migration at low nanomolar concentrations

Next, we were interested, if 25-OHC has a pro-migratory effect towards THP-1 cells. To test this hypothesis, we used a Transwell® approach, which has been shown to be a suitable model for detection of primary blood monocyte and THP-1 migration (250, 251). As described in the materials and methods section, the lower chamber was filled with 25-OHC- or vehicle-containing medium, whereas the upper chamber was supplied with 100,000 THP-1 cells. After 18 h, cell number was assessed by counting the cells present in the lower chamber with a hemocytometer. As shown in **Fig. 31**, the maximal increase of migrated cells could be observed by treatment with 25 nM 25-OHC (1.5-fold, $p < 0.001$). Up to this concentration, the increase was concentration-dependent (1.3-fold at 2.5 nM, $p < 0.01$), however, at higher concentrations the number of migrated cells declined again (1.2-fold at 75 nM, $p < 0.01$ and 0.8-fold at 1 µM, $p < 0.01$), probably due to the cytotoxic effects of 25-OHC, which were shown above (Fig. 30). FCS (10%) was used as positive control and resulted in a 1.7-fold maximal induction of migrated THP-1 cells.

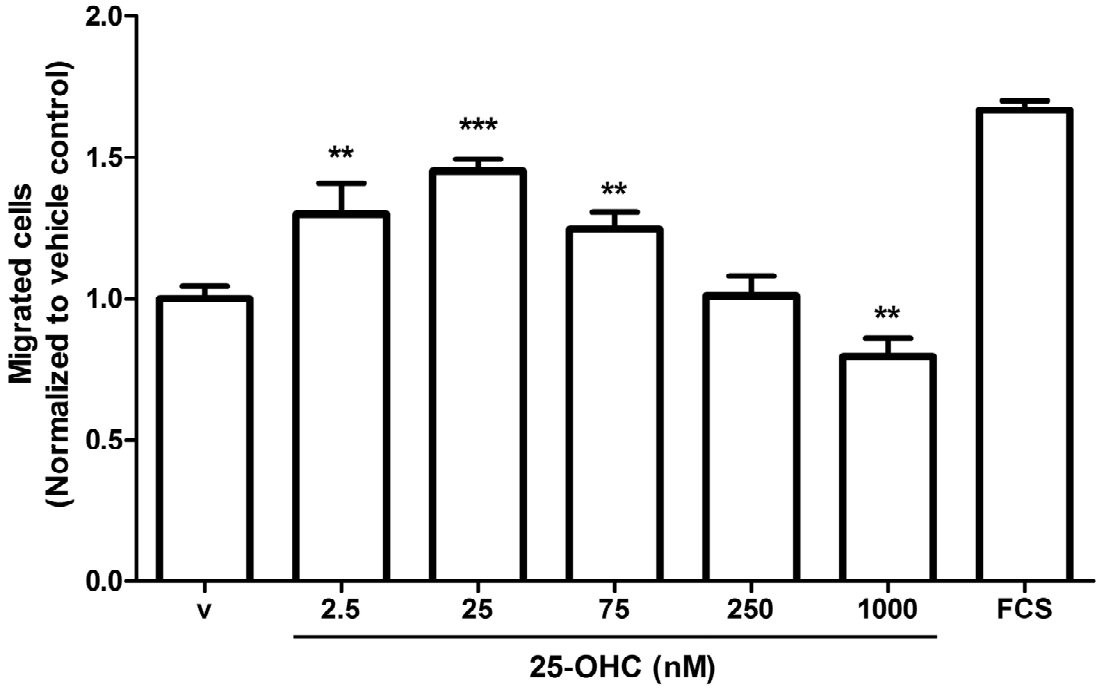

Figure 31: 25-OHC exerts a concentration dependent pro-migratory effect on THP-1 cells.

100,000 THP-1 cells were plated in the upper chamber of a Transwell aparatus. The lower chamber contained medium supplemented with ethanol (0.1%, vehicle, 'v'), 25-OHC (at the indicated concentrations), or 5% FCS (positive control). After 18 h, transmigrated cells were counted and cell numbers were normalized to the vehicle control. Data shown represent mean ± SD of at least 3 independent experiments. ** $p < 0.01$, *** $p < 0.001$

3.6.2 GM133-conditioned medium lipid extract is able to increase THP-1 migration

As the observed effects from the previous experiment occur at rather low 25-OHC concentrations, and as the known LXR-dependent oxysterol effects occur at micromolar concentrations (151), we hypothesized that the observed effects could be due to activation of a membrane receptor, possibly a G protein-coupled receptor.

Given the rather efficient secretion of 25-OHC in the cellular supernatant of GM133 cells we reasoned that lipid extracts prepared from conditioned GM133 medium would be able to affect THP-1 migration. Therefore, we extracted lipids from GM133-conditioned medium and extracts were reconstituted in ethanol and added to the medium in the lower chamber of the Transwell to result in a 25-OHC concentration of approx. 25 nM. These experiments revealed that the medium lipid extracts from GM133 cells promote migration to a similar extent (1.7-fold) as observed for the same concentration of exogenously added 25-OHC (**Fig. 32**). To narrow the mechanism, we also added pertussis toxine (PTX), an inhibitor of the αi subunits of G protein-coupled receptors, which abrogated completely the observed increases in cell migration in both experimental settings (Fig. 32).

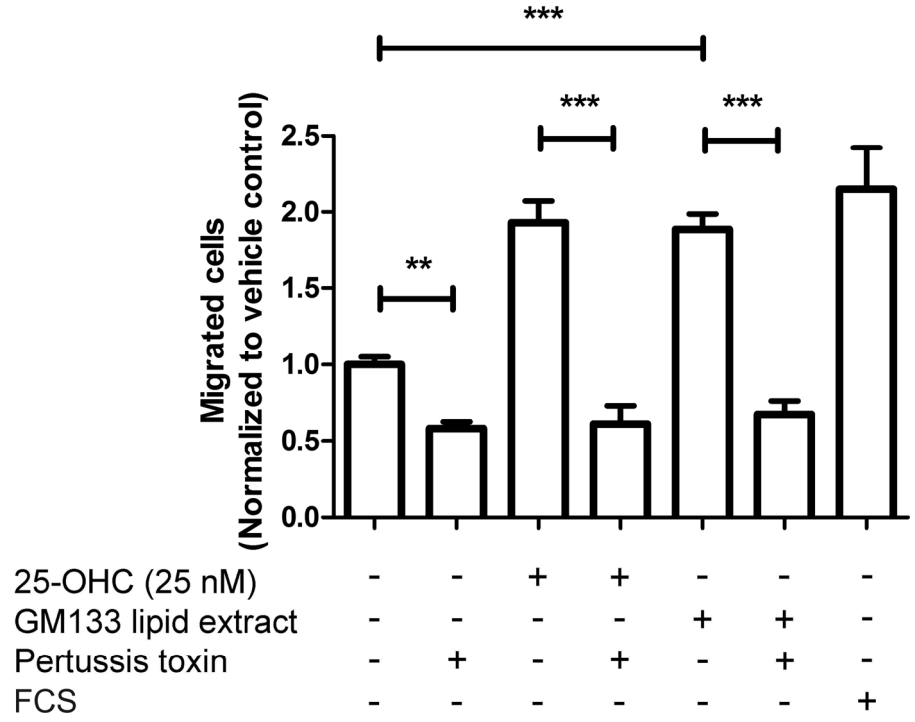

Figure 32: GM133-conditioned medium lipid extract is able to increase THP-1 migration in a similar manner as 25-OHC.

100,000 THP-1 cells were plated in the upper chamber of a Transwell apparatus. The lower chamber contained medium with ethanol (0.1%, vehicle, 'v'), 25-OHC (25 nM), GM133-conditioned medium lipid extracts (0.5 µl of reconstituted lipid extracts in ethanol was added to the medium to result in a 25-OHC concentration of approx. 25 nM) in the absence or presence of PTX (30 ng/ml), or 5% FCS (positive control. After 18 h, transmigrated cells were counted and cell numbers were normalized to the vehicle control. Data shown represent mean ± SD of 3 independent experiments. ** $p < 0.01$, *** $p < 0.001$

3.6.3 25-OHC treatment induces cytoskeletal changes in THP-1 cells

To get an indication whether the observed migratory effects are accompanied with morphologic changes in cell shape, we performed hematoxyline eosine (HE) staining of vehicle (ethanol)-, 25-OHC (25 nM)-, 25-OHC (25 nM) + PTX (30 ng/ml)-, or FCS (10%)-treated THP-1 cells. As changes in cell shape could be observed in microscopy, we took photographs and assigned the cells into the two groups “round cells” and “cells with protuberances”. After treatment with 25-OHC, we could observe a significant increase in cells with protuberances from 30% (control group) to 40% (25-OHC-treated group) and a significant decrease to 20% in the 25-OHC + PTX-treated group (**Fig. 33E**). Untreated controls and FCS-treated positive controls displayed no obvious morphological difference.

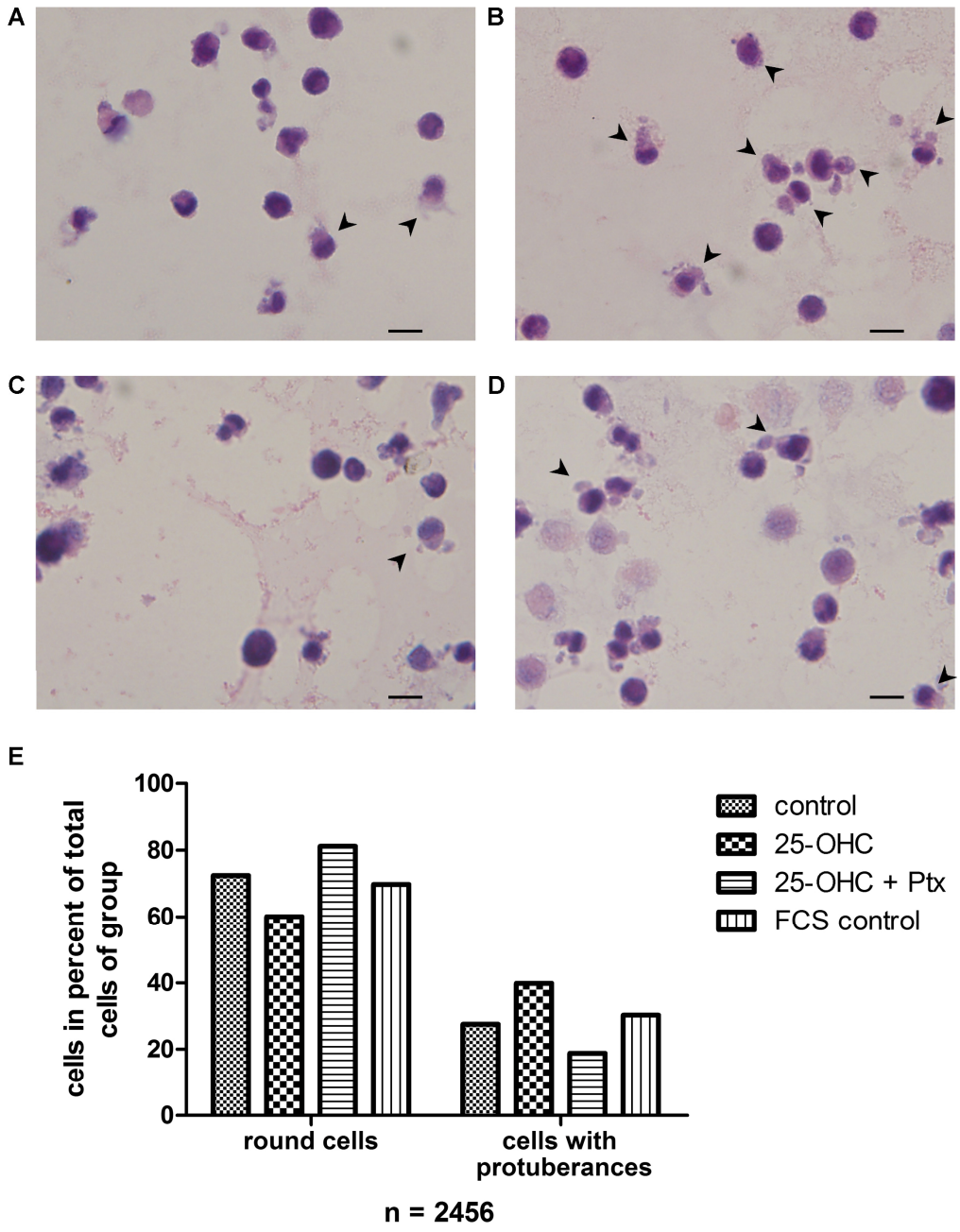

Figure 33: 25-OHC induces morphological alterations at THP1 cells.

HE staining of either vehicle- (**A**), 25-OHC- (25 nM) (**B**), 25-OHC with PTX- (30 ng/ml) (**C**), or FCS- (10%, positive control) (**D**) treated THP-1 cells. Arrows indicate example cells with changes in the (normally round) cell shape. The scale bars indicate 20 µm. (**E**) At least 500 cells of each treated group (2456 total) were counted optically and assigned to the two groups “round cells” and “cells with protuberances”. All changes were highly significant ($p < 0.001$) as assessed by chi-square test, except at the FCS positive control which was non-significant (compared to the vehicle control).

To investigate, whether the observed changes in cell shape are accompanied by changes in the intermediate filaments of the THP-1 cytoskeleton, vimentin, an important regulatory protein of cell motility, was visualized by immunofluorescence microscopy. As shown in **Fig. 34A** and **B**, exogenously added 25-OHC changed the vimentin intermediate filament architecture in THP-1 cells from a cytoplasmic distribution to a more cortical location with multiple extensions, indicative of monocyte polarization in response to 25-OHC (Fig. 34B; arrows).

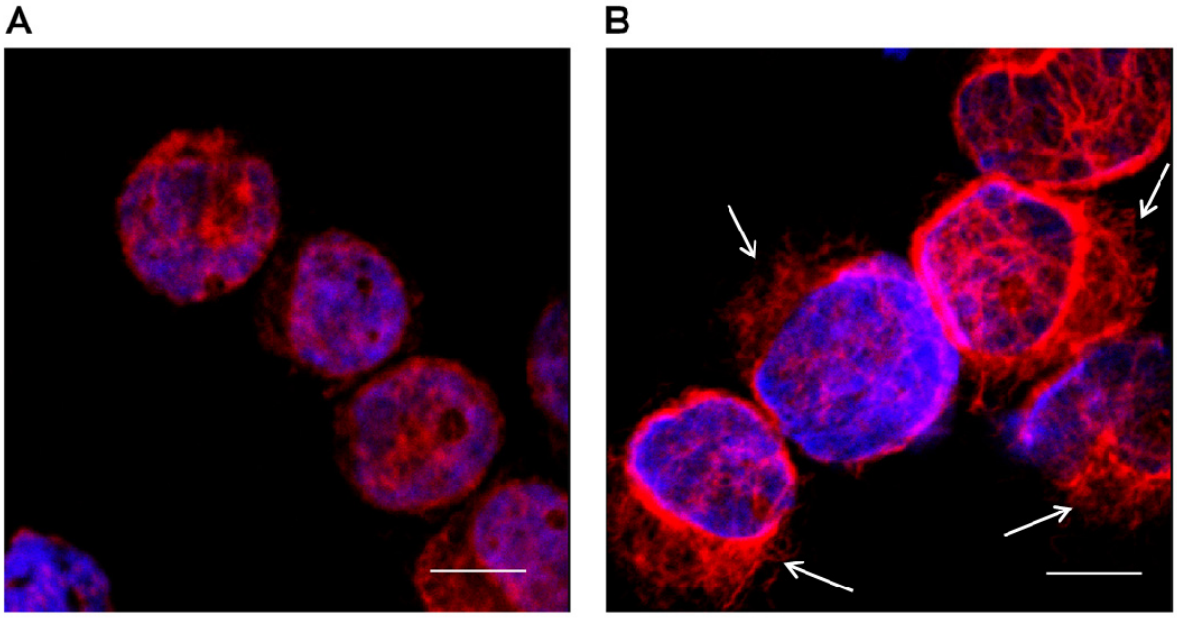

Figure 34: 25-OHC induces cellular polarisation in THP-1 cells.

Vehicle- (**A**) or 25-OHC (25 nM, 18 h)-treated THP-1 cells (**B**) were fixed with acetone and vimentin was immunostained with mouse anti-human vimentin and a Cy3-labeled anti-mouse IgG. Nuclei were counterstained with DAPI. The scale bar indicates 10 µm. Arrows indicate areas of vimentin intermediate filament polarisation.

3.6.4 Chemotactic properties of 25-OHC depend on EBI2.

It has been recently shown that 25-OHC has pro-migratory effects on B-lymphocytes via activation of EBI2 (GPR183) (222, 223). *In silico* research revealed that mRNA for this receptor can be found in primary monocytes as well as in THP-1 cells (http://biogps.org). It was also recently shown that this receptor is expressed in macrophages (252), but to a lesser extent than in B-lymphocytes. We used Western blot analysis to show that EBI2 is also detectable on protein level in THP-1 cells (**Fig. 35**), thereby confirming *in silico* findings.

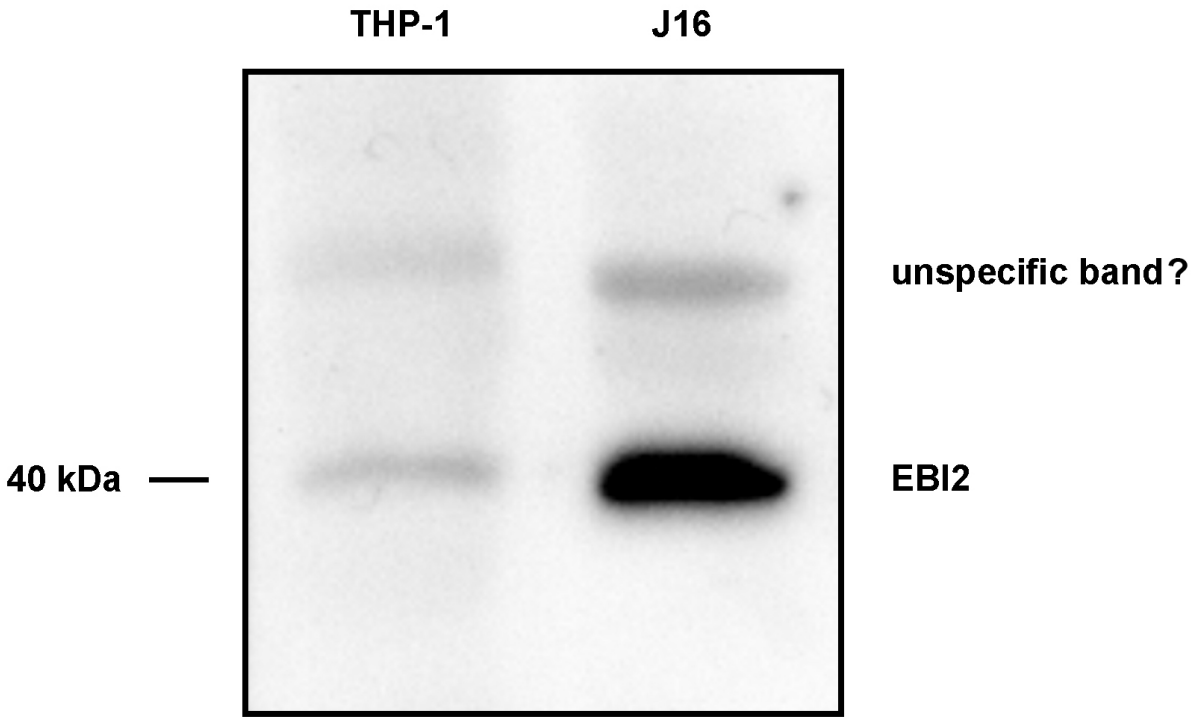

Figure 35: The G protein-coupled receptor EBI2 is expressed by THP-1 cells.

Fifty µg of each, THP-1 and J16 Jurkat cell (positive control) lysate were separated by SDS PAGE on a 12% polyacrylamide gel, blotted onto a PVDF membrane, and incubated with primary antibody against EBI2. Immunoreactive bands were visualised with peroxidase-conjugated secondary antibody.

Thus, it is likely that EBI2 could, at least partially, mediate the observed pro-migratory effects on THP-1 monocytes in response to 25-OHC. We decided to use an siRNA approach for further investigation. First, silencing efficiency of EBI2 was analyzed on mRNA and protein level. On mRNA level EBI2 was decreased by 83 and 68% (24 and 48 h post silencing, respectively; **Fig. 36A** and **B**) in response to siRNA transfection. On protein level mock transfection slightly increased EBI2 protein expression, whereas scrambled siRNA was without pronounced effects. Silencing of EBI2 resulted in an approximately 60% reduction (in comparison to scrambled siRNA) of EBI2 on protein level as calculated by densitometric analysis of immunoreactive bands (**Fig. 36C**). Next, migration experiments were performed in the presence of 25-OHC. Mock transfection reduced the number of transmigrated cells by 38%, scrambled siRNA by 55%, and siEBI2 by 76% (**Fig. 36D**). Thus, in comparison to scrambled siRNA, silencing of EBI2 resulted in a 46% reduction of migrated cells.

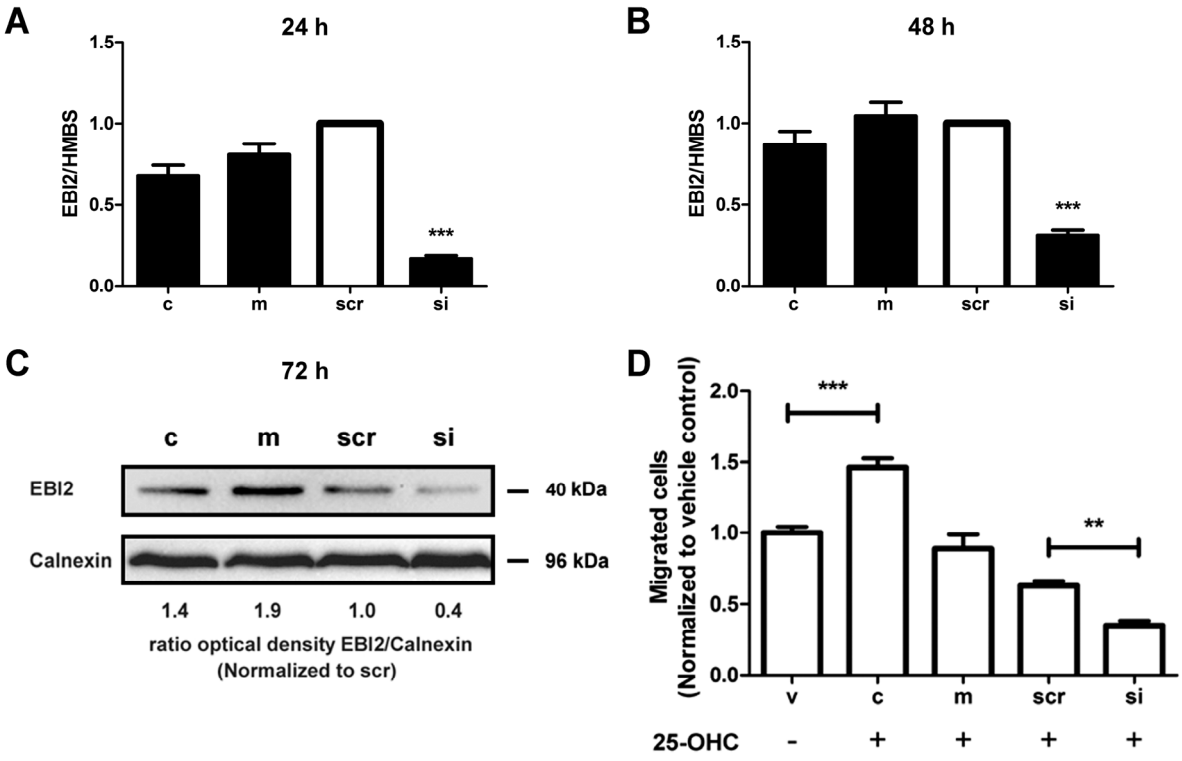

Figure 36: Silencing of EBI2 leads to decreased THP-1 migration in response to 25-OHC.

THP-1 cells were cultured under standard conditions and transfected with siRNA against EBI2 as described in materials and methods. After 24 h (**A**) and 48 h (**B**), cells were lysed, and mRNA was extracted and reversely transcribed for qPCR analysis. (**C**) After 72 h, cells were lysed and protein extracts (150 µg) were separated by SDS-PAGE (12%) and electrophoretically transferred to a PVDF membrane and EBI2 (40 kDa) was detected using a polyclonal antibody. Immunoreactive bands were visualized using peroxidase-coupled secondary antibody. (**D**) 100,000 THP-1 cells of each group (v = vehicle-treated; control = untransfected; m = mock, scr = scrambled; si = EBI2 siRNA transfected cells) were plated in the upper chamber of a Transwell apparatus. The lower chamber contained medium supplemented with ethanol (0.1%, vehicle, '-'), or 25-OHC (25 nM, '+'). After 18 h transmigrated cells were counted. The migration experiment was started 60 h after siRNA transfection. Data shown represent mean ± SD of three independent experiments. One-way ANOVA with Bonferroni multiple comparison test was used. ** $p < 0.01$, *** $p < 0.001$

3.7 Lipopolysaccharide influences lipid metabolism *in vivo*

LPS is a strong pro-inflammatory stimulus that has been widely used in experimental sepsis models (253) and is a well-characterized inducer of the acute phase reaction and stimulates the expression of the pro-inflammatory cytokines TNFα, IL1β and IL6 in e.g. tissue macrophages and circulating monocytes (253-255). Furthermore, LPS is a strong inducer of CH25H in macrophages (183), acting via TLR 4 (256). Therefore, we aimed to investigate whether or not peripherally administered LPS would impact on cerebral lipid homeostasis (with focus on oxysterol patterns) in C57/Bl6 mice. Moreover, it has been demonstrated that LPS treatment of GBM-bearing mice is beneficial in terms of survival (257). Consequently, the last part of these experiments deals with *in vivo* effects of LPS on plasma and brain fatty acid, cholesterol and oxysterol composition.

3.7.1 Side chain-oxidized sterol profile in LPS-treated brains of C57/Bl6 mice

In the experimental setup used here mice received 0.83 mg LPS/kg body weight/day. Every three days, five mice were sacrificed and plasma and brains were collected. As our in vitro data indicate a short term transcriptional upregulation of sterol side chain oxidizing enzymes via TLR4 and a long term upregulation via TNFα and/or IL1β, we expected increased concentrations of side chain oxidized sterols in brains of LPS-treated C57/Bl6 mice. Therefore, brain lipids were extracted, oxysterols were separated by solid phase extraction, and 24S-OHC, 25-OHC and 27-OHC were quantitated by GC-MS.

LPS treatment resulted in a significant increase of 24S-OHC (41.8 to 55.5 ng/mg wet tissue) and 27-OHC concentrations (4.61 to 6.52 ng/mg wet tissue) (**Fig. 37**). 25-OHC concentrations exhibited a 1.35-fold, but statistically not significant increase from 74 (day 0) to 100 (day 3) pg/mg wet tissue. Thus, these experiments demonstrate that a fully-blown peripheral inflammation favours neuroinflammatory conditions that lead to altered oxysterol homeostasis in the brain.

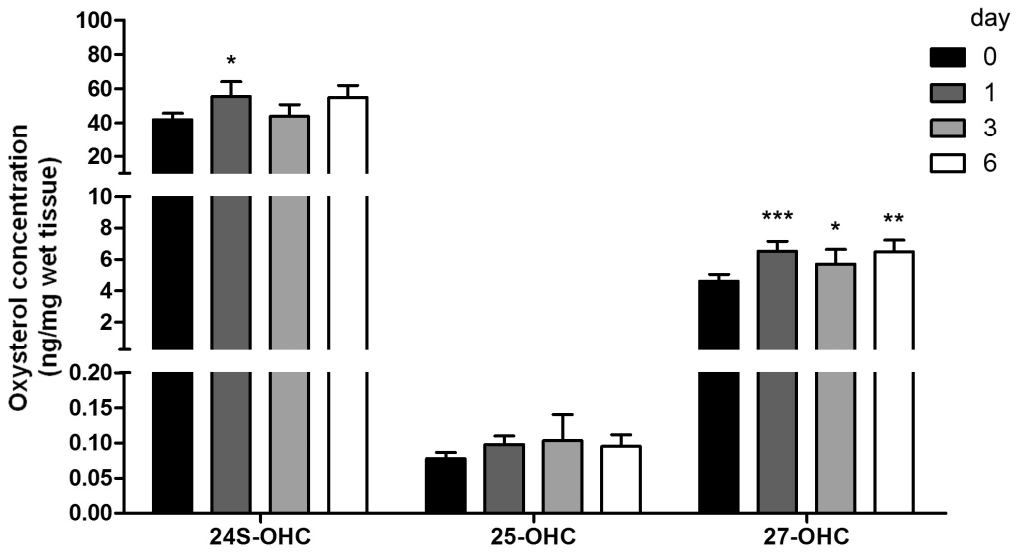

Figure 37: LPS administration alters brain oxysterol profile.

C57/Bl6 mice were daily treated with LPS (0.83 mg/kg body weight). On day 0, 1, 3, and 6, five mice were sacrificed, brain lipids were extracted, and oxysterols were measured as described in materials and methods. Data shown represent mean ± SEM of five animals. One-way ANOVA with Dunnett's post hoc test was used. * $p < 0.05$, ** $p < 0.01$, *** $p < 0.001$

3.7.2 Side chain-oxidized sterol profile in plasma of LPS-treated C57/Bl6 mice

To get an indication whether the observed effects are confined to the brain or are also evident in the peripheral circulation, we analysed plasma side chain-oxidized

sterol composition. Therefore, oxysterols were extracted from mouse plasma samples and quantitated by GC-MS. Results revealed a significant increase of 24S-OHC (from 123 to 588 nM), 25-OHC (from 18.2 to 67.2 nM) and 27-OHC (from 80.6 to 552 nM) concentrations on day 3 in case of LPS treatment (**Fig. 38**). After day 3 mean oxysterol levels decreased to control levels. No significant changes in 22-OHC concentrations were detected after LPS treatment.

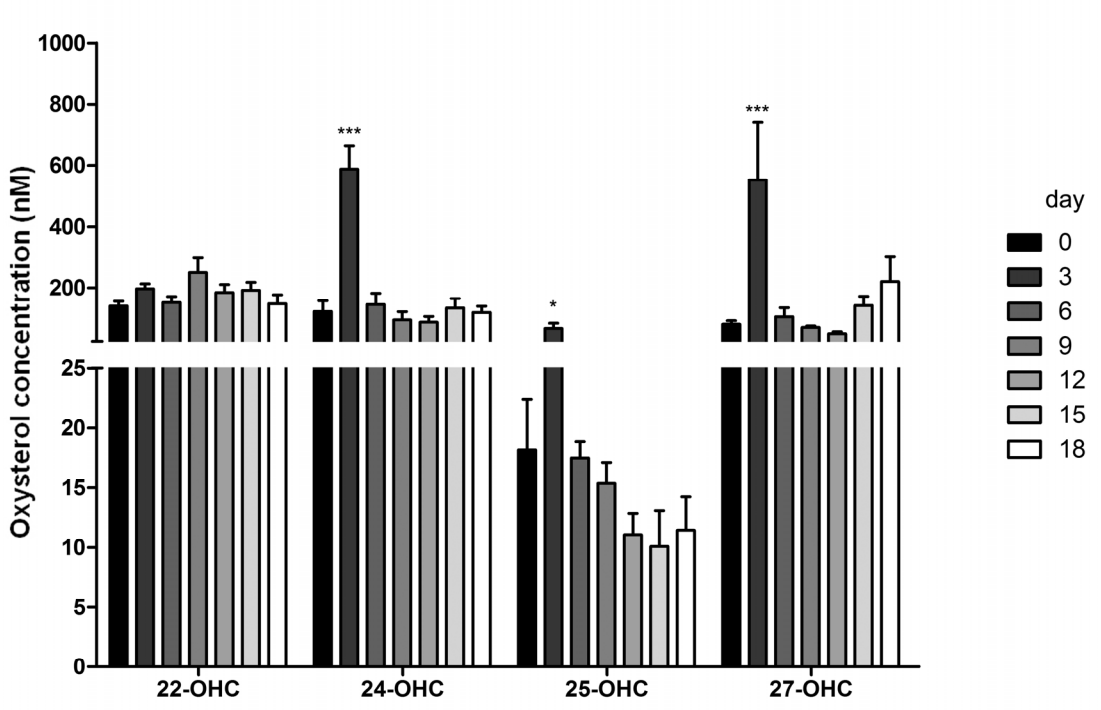

Figure 38: LPS administration alters plasma oxysterol profile of C57/Bl6 mice.

C57/Bl6 mice were daily treated with LPS (0.83 mg/kg body weight). Every three days, five mice were sacrificed, plasma lipids were extracted and oxysterols were measured as described in materials and methods. Data shown represent mean ± SEM of five individuals. One-way ANOVA with Dunnett's post hoc test was used. * $p < 0.05$, *** $p < 0.001$

3.7.3 Cholesterol, triglyceride and phospholipids profile of LPS-treated C57/Bl6 mice

It is known that LPS administration induces systemic inflammation which provokes dysfunction of the endothelial monolayer at the BBB (258-260). To elucidate effects

of LPS on brain lipid metabolism, brain cholesterol (represents 99% of total brain cholesterol), triglycerides and phospholipids were quantitated. These analyses revealed a moderate, time dependent decrease of brain cholesterol concentrations during the first nine days after treatment from 13.4 (day 0) to 10.9 (day 9) µg/mg brain wet weight. After day 9 cholesterol concentrations remained more or less unchanged. Interestingly, brain triglyceride concentrations increased during the first six days from 0.96 (day 0) to 1.39 (day 6) µg/mg brain wet tissue and then remained unchanged until day 18. Phospholipid concentrations decreased in a time dependent manner (similar to what was observed for brain cholesterol) from 14.8 (day 0) to 12.3 (day 18) µg/mg brain wet tissue (**Fig. 39**).

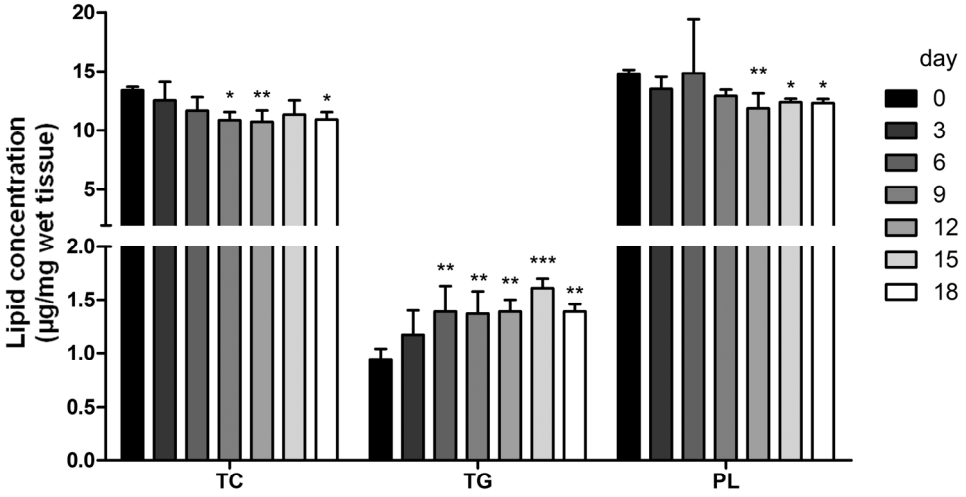

Figure 39: LPS administration increases triglyceride concentrations and slightly decreases the amounts of total cholesterol and phospholipids in brains of C57/Bl6 mice.

C57/Bl6 mice were daily treated with LPS (0.83 mg/kg body weight). Every three days, five mice were sacrificed, brain lipids were extracted, and total cholesterol (TC), triglycerides (TG), and phospholipids (PL) were measured as described in materials and methods. Data shown represent mean ± SEM of five animals. One-way ANOVA with Dunnett's post hoc test was used. * $p < 0.05$, ** $p < 0.01$, *** $p < 0.001$

3.7.4 Cholesterol and triglyceride profiles in plasma of LPS-treated C57/Bl6 mice

Shifts in plasma cholesterol and triglyceride concentrations in response to LPS treatment have already been described in previous publications (261-266). Therefore, plasma lipids were analysed to get an indication whether LPS-induced inflammation leads to comparable results under the experimental conditions applied. These analyses revealed that the levels of free cholesterol did not change significantly in

course of LPS treatment, whereas the amount of total cholesterol (unesterified and esterified cholesterol) was increased on day 3 (from 75 (experimental start) to 90 mg/dl, **Fig. 40**). We also observed significantly increased plasma triglyceride concentrations on day 9 (120 mg/dl), indicating increased secretion of triglyceride-rich lipoproteins from the liver (Fig. 40).

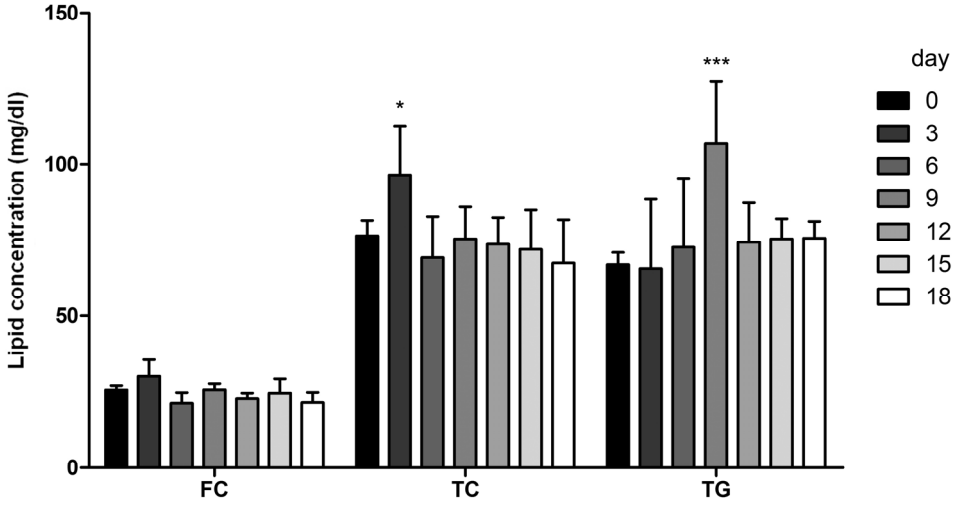

Figure 40: LPS administration moderately increases amounts of total cholesterol and triglycerides in plasma of C57/Bl6 mice.

C57/Bl6 mice were daily treated with LPS (0.83 mg/kg body weight). Every three days, five mice were sacrificed, plasma lipids were extracted and free cholesterol (FC), total cholesterol (TC), and triglycerides (TG) were measured as described in materials and methods. Data shown represent mean ± SEM of five animals. One-way ANOVA with Dunnett's post hoc test was used. * $p < 0.05$, *** $p < 0.001$

3.7.5 Fatty acid composition in brains of LPS-treated C57/Bl6 mice

As we could observe changes in the triglyceride, total cholesterol, and phospholipids pattern in brains of LPS-treated C57/Bl6 mice, we additionally wanted to investigate changes in fatty acid composition of total brain lipids (cholesterol esters, triglycerides, phospholipids). GC analysis revealed that changes in the fatty acid profile were mar-

ginally altered in course of LPS treatment. Stearic acid (C18:0) containing lipid species increased from 6.8 (day 0) to 7.5 (day 18) µg/mg tissue wet weight, oleic acid (C18:1) containing species increased from 6.5 (day 0) to 7.5 (day 18) µg/mg tissue wet weight, and linolic acid (C18:2) containing species increased from 0.18 (day 0) to 0.26 (day 3) µg/mg tissue wet weight (**Fig. 41**). Concentrations of palmitic acid (C16:0), palmitoleic acid (C16:1), arachidonic acid (C20:4) and cervonic acid (C22:6) containing lipids were not significantly changed.

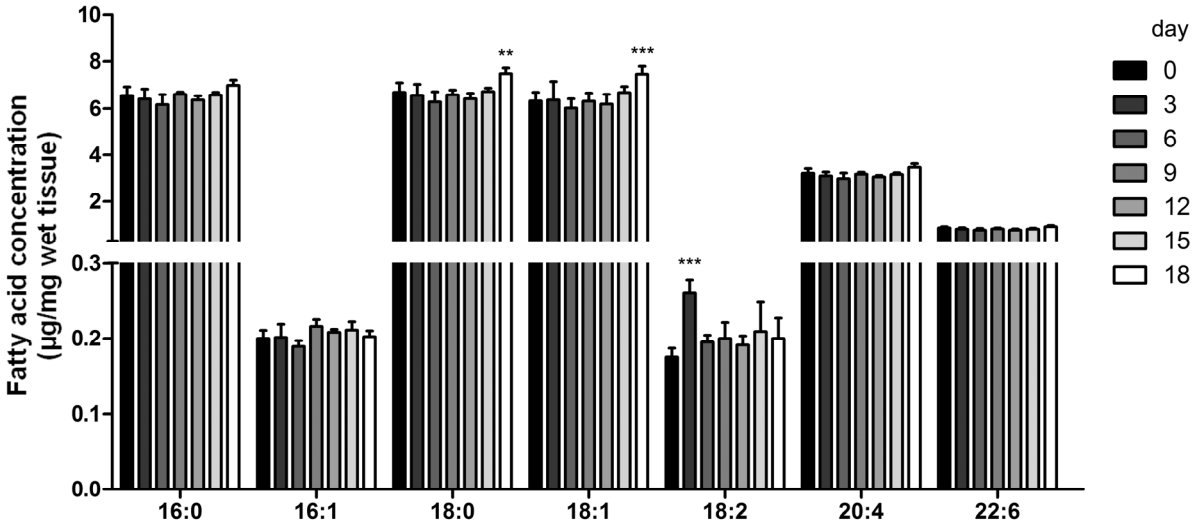

Figure 41: LPS administration increases the amounts of C18:0, C18:1, and C18:2 fatty acids in brain lipids of C57/Bl6 mice.

C57/Bl6 mice were daily treated with LPS (0.83 mg/kg body weight). Every three days, five mice were sacrificed, brain lipids were extracted, and fatty acids were measured as described in materials and methods. Data shown represent mean ± SEM of five individuals. One-way ANOVA with Dunnett's post hoc test was used. ** $p < 0.01$, *** $p < 0.001$

3.7.6 Fatty acid composition in plasma of LPS-treated C57/Bl6 mice

As expected, alterations in fatty acid composition due to LPS administration were more pronounced in plasma than in brain. Palmitic acid (C16:0) was found increased

from 380 µg/ml plasma (experimental start) to 560 µg/ml plasma (day 9) and to 550 µg/ml plasma (day 18). Oleic acid (C18:1) levels increased from 272 µg/ml plasma (day 0) to 638 µg/ml plasma (day 9) and 523 µg/ml plasma (day 18). Linoleic acid (C18:2) concentrations were found elevated from 442 µg/ml plasma (day 0) to 653 µg/ml plasma (day 3), and 649 µg/ml plasma (day 9) and remained at that level (606 µg/ml) until day 18 (**Fig. 42**). No significant changes were found in C16:1, C18:0, C20:4, C20:5, and C22:6 fatty acids levels.

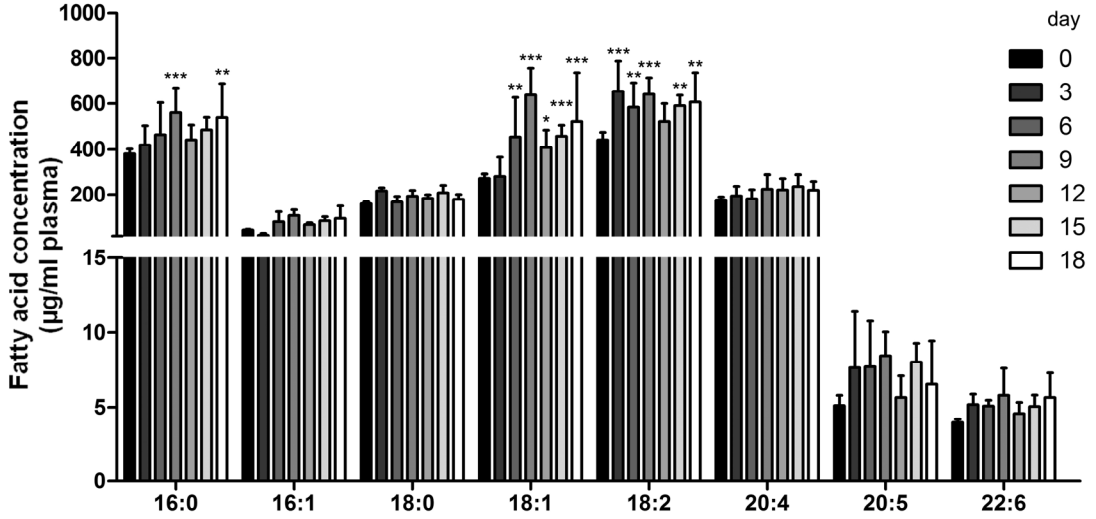

Figure 42: LPS administration alters the fatty acid profile of plasma lipids in C57/Bl6 mice.

C57/Bl6 mice were daily treated with LPS (0.83 mg/kg body weight). Every three days, five mice were sacrificed, plasma lipids were extracted, and fatty acids were measured as described in materials and methods. Data shown represent mean ± SEM of five animals. One-way ANOVA with Dunnett's post hoc test was used. * $p < 0.05$, ** $p < 0.01$, *** $p < 0.001$

4 Discussion

4.1 Oxysterols and glioblastoma cells

Oxysterols display their bioactive effects at a variety of different points of action. Among these, LXR activation, SREBP inhibition, SHH activation, EBI2 activation, or modulation of plasma membrane properties by compromising lipid rafts are the most important ones (177, 267, 268). Although oxysterols have been studied intensively during the past two decades, there is still potential for new and surprising discoveries, like immunomodulatory or antiviral effects, which were reported recently (222, 223, 269, 270).

Data obtained during the present study demonstrate that A172, GM133 and U87MG GBM cell lines express CH25H on mRNA and protein level in a cytokine-inducible manner and that these cell lines are able to synthesize and secrete 25-OHC. In GBM tissue samples, elevated concentrations of 25-OHC were detected. However, exogenously added 25-OHC did not affect U87MG proliferation and was without effect on SHH signalling in A172 and U87MG cells. Although exogenously added 25-OHC exerted toxic effects towards the tumor cells at high concentrations, it promoted chemotactic migration of THP-1 cells and primary human peripheral monocytes at low nanomolar concentrations. Furthermore, lipid extracts obtained from GM133-conditioned medium induced chemotactic migration of THP-1 cells in an EBI2-dependent manner. Thus GBM-derived 25-OHC has the potential to act as a chemotactic signal that induces recruitment of monocytes towards tumor cells and could facilitate the deposition of tumor-associated macrophages. In future studies it would

be important to investigate whether 25-OHC affects macrophage polarization towards an M1 (tumor inhibiting) or M2 (tumor promoting)-like phenotype.

Results of this study revealed upregulated CH25H transcription and translation in GBM cells. Interestingly, among the NCI-60 data set contained within the BioGPS gene portal GBM cells take a unique role in terms of highest CH25H expression (http://biogps.org). This was further supported by the results obtained from tumor tissue samples (Fig. 19).

25-OHC concentrations in glioma samples ranged between 0.5 and 2 ng/mg tissue wet weight, whereas 25-OHC levels in normal brain are between 60 and 100 pg/mg in mice (271) (Fig. 42). Lütjohann et al. reported 25-OHC concentrations in human samples to be below 3% of 24S-OHC concentrations (3.8-4.8 ng/mg tissue wet weight for cerebellum and 8.6-15.1 ng/mg tissue wet weight for cerebrum) (160), which corresponds to a maximum 25-OHC concentration of 140 pg/mg for cerebellum and 450 pg/mg for cerebrum. These values closely resemble the concentration of 25-OHC that was detected in the single pilocytic astrocytoma sample (120 pg/mg tissue wet weight, Fig. 19). However, further data is needed in order to clarify the correlation between tumor grade and 25-OHC concentrations, which has not been published yet.

The response of the tested GBM cell lines to TNFα, IL1β, and IFNγ was different with respect to cytokine selectivity in the two cell lines studied here (Fig. 20). *In silico* (www.bioGPS.org) analysis of the NCI-60 data set revealed that U87MG express higher amounts of the TNFα receptor TNFR1 in comparison to A172 and GM133 cells. GM133 are expressing higher amounts of the IL1β receptor IL1R1, whereas U87MG and A172 cells have similar expression levels. The IFNγ receptor (IFNGR) is expressed in all three cell lines in comparable amounts. Despite this, even 100 ng/ml

IFNγ increased CH25H expression only marginally thus indicating a minor role of IFNγ compared to TNFα and IL1β for induction of CH25H expression. Whether this is due to lower IFNγ receptor expression is currently not clear. However, all cytokines used here may activate JAK/STAT pathways. TNFα activates JAK/STAT1 (272) and IL1β activates STAT1 (273) and a STAT-like factor, leading to activation of gene transcription (274). Therefore our observations are compatible with a pathway inducing transcriptional activation of CH25H identified in DCs and macrophages (182).

In line with findings reported for LPS-activated macrophages (183), we have observed efficient secretion of 25-OHC into the cellular supernatant. In experiments analyzing free transfer of cholesterol or 25-OHC from erythrocytes and plasma to liposomes, exchange of 25-OHC was found to occur about 2,000 times faster than that of cholesterol (156). The rate of transfer of oxysterols from a monolayer to acceptor particles followed a clear rank order with the highest rate of transfer observed for 25-OHC (275). As reported for the quantitatively dominating oxysterols 24S- and 27-OHC, also 25-OHC is transported in association with circulating lipoproteins including HDL (276). This might be of functional importance for gliomagenesis since HDL containing sphingosine-1-phosphate (S1P; a potent lipid GBM mitogen; (277)) induced increased DNA synthesis, ERK phosphorylation, and Ca^{2+} mobilization in glioma cells (278).

As LXR ligand 25-OHC induces ABCA1 transcription (Fig. 30, (279)), which is an active exporter of S1P in astrocytes (280, 281). It is widely accepted that elevated amounts of S1P lead to increased growth signalling and cell survival in several tumor cells (282). This rationale led us to hypothesize that 25-OHC itself could have growth stimulatory potential. To support this hypothesis we performed proliferation studies with U87MG cells stimulated by exogenously added 25-OHC. However, data obtained from these experiments did not support our hypothesis that 25-OHC directly

increases growth of tumor cells. This result was additionally supported by the results obtained from MTT viability assays. These data consequently indicate that either the high 25-OHC amounts required for activation of the described LXR/ABCA1/S1P axis are too high and already exert cytotoxic effects towards tumor cells, or that the secreted S1P concentrations are too low to exert any substantial effect on cell growth and survival.

MTT tests further revealed that higher amounts of 25-OHC reduced U87MG cell growth and viability in a concentration dependent manner, indicating that 25-OHC has pro-apoptotic effects at concentrations > 1 µM, which is consistent with previous findings (283). Mechanistically, this effect is most probably mediated via EGFR/SREBP-mediated mechanisms, as suggested by Guo et al. (228).

The general, widely accepted mechanism for the action of oxysterols in tumors is via LXR activation. It has been shown that LXR activation has the potential to inhibit proliferation of multiple cancer (breast, liver, lung, melanoma or prostate) cell lines (233, 284). This anti-proliferative and pro-apoptotic effect is not confined to tumor cells, as demonstrated recently (285). However, it is known that LXR stimulation inhibits DC recruitment through the expression of CCR7, which paradoxically enhances tumor growth by decreasing antigen processing and presentation to the immune system (226). These two opposite effects of LXR activation in cancer need to be evaluated carefully before being addressed to therapeutic usage.

25-OHC mediated LXR activation occurs at concentrations > 1 µM (151). 24S-OHC is a stronger LXR agonist than 25-OHC, but exerts lower cytotoxic activity towards all GBM cell lines and in THP-1 cells (Fig. 27). Thus, toxicity is most likely not mediated solely via LXR. Whether these effects are mediated via SREBP-dependent mechanisms or via cell membrane toxicity (e.g. compromising lipid rafts etc.) remains to be elucidated.

On the contrary, statin-induced depletion of cholesterol (leading to decreased oxysterol amounts), and its effects on tumors have been investigated: For example, a retrospective study on cancer development showed a correlation between depletion of cholesterol by statins and a decreased risk in developing colorectal cancer (286).

Recent investigations revealed that signalling via the SHH pathway, that is oxysterol-dependent, is often implicated in abnormal and neoplastic cell growth (214). Oxysterols bind to the extracellular domain of SMO and are necessary for maximal activation of the pathway (287). As this effect already occurs at nanomolar oxysterol concentrations, we examined SHH activation in glioma cell lines, because we were expecting an increase in SHH signalling. However, our results revealed no increased SHH target gene transcription, neither in U87MG, nor in A172 cell lines (Fig. 29).

Significant progress has been made in elucidating the functional significance of oxysterol-induced B and T cell migration in lymphoid organs (217, 222, 223, 288, 289). It is now widely accepted that EBI2-mediated chemotaxis represents an important molecular mechanism directing follicular B cell migration and localization. Of note, oxysterols represent natural ligands for EBI2 (222, 223, 288) activation. In line with findings from the present study (Fig. 32), PTX suppressed 7α,25-OHC-stimulated and EBI2-mediated binding of GTP (223). However, PTX-insensitive ERK activation in response to EBI2 engagement was also reported (217). The functional potency of different oxysterols towards EBI2 is 7α,25-OHC>7α,27-OHC>7α-OHC>25-OHC>27-OHC (289). Of relevance for the present study 25-OHC also confers agonist activity towards EBI2 albeit with lower affinity (243, 244). In line, silencing of EBI2 using 21-mer siRNA reduced 25-OHC-induced THP-1 migration by 46% (Fig. 36). The reason why mock transfection and transfection with scrambled siRNA reduced migration of GM133 in response to 25-OHC is currently not clear. However, lipid-based transfection reagents impact on cellular phospholipid composition (enrichment in C16:0- or

C22:6-containing phosphatidylcholine species; personal communication from Dr. Sasa Frank; Institute of Biochemistry and Molecular Biology, MUG), which could account for different receptor responsiveness.

To get an indication whether GBM-derived 25-OHC could act as a chemotactic signal for monocytes, lipid extracts of GM133 media were used in THP-1 migration assays. Although an indirect approach, these experiments revealed that medium lipid extracts induced monocyte migration in a quantitatively similar manner as identical concentrations of exogenously added 25-OHC (Fig. 32). A question remaining is how 25-OHC would contribute to monocyte attraction in the tumor environment.

Association of secreted 25-OHC with lipoproteins would be a plausible explanation. In light of the facts that HDL particles transport 25-OHC in the circulation (276), shuttle oxysterols between the circulation and the brain (109), and are potent effectors of the monocytic migratory response (290) this hypothesis could be reasonable. Silva and colleagues showed that an oxysterol-containing lipid fraction isolated from osteoblast-conditioned medium potently induces migration of human breast cancer cells, raising the possibility that oxysterols even contribute to tumor invasion and metastasis (291).

Results of the present study not only demonstrate differences in cell shape (Fig. 33), but also that 25-OHC treatment of THP-1 monocytes induced vimentin intermediate filament reorganization to more cortical structures and a polarized phenotype (Fig. 34). Vimentin is the major intermediate filament protein present in leukocytes and plays an important role in leukocyte motility and endothelial diapedesis (292). In line, vimentin intermediate filaments play a crucial role during adhesion molecule assembly that is needed during adhesion and transendothelial migration (293), an event accompanying the recruitment of circulating monocytes across the tumor vasculature (294). A characterization of human glioblastoma-associated immune cells revealed

that besides lymphocytes and microglia, monocytes/macrophages represent the dominating inflammatory cell population infiltrating these tumors (295).

In summary, data obtained during the present study make it attractive to hypothesize that GBM-derived 25-OHC is able to attract EBI2-expressing immune cells to the tumor environment. Thereby, 25-OHC may contribute to the recruitment of tumor-associated microglia/macrophages that are potent modulators of gliomagenesis (65).

4.2 *In vivo* effects of LPS on lipid metabolism in C57/Bl6 mice

LPS is a strong pro-inflammatory stimulus that has been widely used in experimental animal (and human) sepsis models (253). Nevertheless, there is some concern that these models are unphysiological, as LPS concentrations during bacterial sepsis are much lower as compared to experimental endotoxinemia, resulting in different temporal profiles of cytokine release (296). Despite these concerns, LPS is a well-characterized inducer of the acute phase reaction and the release of pro-inflammatory cytokines like TNFα, IL1β, and IL6 in tissue macrophages and circulating monocytes (253-255). Furthermore, LPS is a strong inducer of CH25H expression in macrophages (183), acting via binding to TLR 4 (256). In this part of the study we tried to reproduce the findings from glioma cells, i.e. that pro-inflammatory conditions impact on oxysterol synthesis in brain. In addition, the effect of endotoxemia on the lipid profile in the peripheral circulation was addressed.

Impaired brain cholesterol homeostasis might be a contributing factor during the pathogenesis of neurodegenerative diseases. Oxysterols could play an important role during these processes, as they are able to traverse the BBB. Under physiological

conditions this mechanism is used to clear 24-OHC (formed from excess brain cholesterol) from brain to blood. However, it could conversely allow toxic concentrations of peripheral oxysterols to reach the brain and this pathway definitively operates for 27-OHC (297).

LPS is known to disturb BBB integrity (258-260) and 25-OHC levels were found to be elevated in response to LPS treatment in brain of C57/Bl6 mice (Fig. 37). Additionally, levels of 24S- and 27-OHC were increased at approximately 20%. 27-OHC is known to be able to diffuse from blood into the brain (297). However, brain 24S-, 25- and 27-OHC levels on day 3 were rather low in comparison to the their increase of concentrations found in plasma (Fig. 38). This is indicative that oxysterols are primarily enriched in plasma and that diffusion into the brain parenchyma is of minor importance. Whether the observed oxysterol increase in brain tissue is due to *de novo* synthesis or diffusion across the BBB remains to be elucidated. It is also not clear so far, whether these minor alterations in brain oxysterol content would be able to impact on the pathogenesis of neurological diseases. Although it is accepted that secretion of 24-OHC protects the brain from the accumulation of excess cholesterol, it can also potentiate the pro-amyloidogenic effects of 1–42 amyloid-β ($A\beta_{1–42}$) on neuronal cell lines (298). This study demonstrated that the interaction between Aβ and 24-OHC leads to increased intracellular ROS production. Of note, histochemical studies provided evidence for co-localization of CYP46A1 with Aβ deposits in brains of Alzheimer diseased patients (299).

Plasma oxysterols (24S-, 25- and 27-OHC) were highly increased (approximately three- to five-fold) after LPS treatment (Fig. 38). The only exception from this was 22-OHC, which remained rather unchanged. Inflammatory processes are known to

cause lipid peroxidation *in vivo* (300) and considering the fact that 24S-OHC, 25-OHC and 27-OHC are classical cholesterol peroxidation products (167) increased ROS production could (besides increased enzyme activities of the corresponding hydroxylases) contribute to these findings. Similar to oxidized phospholipids, oxysterols are able to promote endothelial cell dysfunction that characterizes the onset of the atheromasic plaque (301). In particular, 7α-OHC, 7β-OHC, and 7- ketocholesterol are able to elicit an inflammatory phenotype in human endothelial cells (302). In addition 7-ketocholesterol is able to induce the formation of foam cells (303).

It is well-accepted that bacterial infection causes alterations in peripheral lipid homeostasis. Patients with bacterial infections have increased serum triglyceride levels (304-306). LPS administration in mice leads to similar results producing hypertriglyceridemia, mainly via increased hepatic fatty acid synthesis and secretion of triglyceride-rich lipoprotein particles (261-264). Of note, these studies also reported increased lipolysis under inflammatory conditions and higher lipoprotein concentrations, which are beneficial due to their ability to scavenge LPS. In line with these findings, we were able to observe increased triglyceride levels in this study (Fig. 39 and 40).

In addition, our results revealed increased total serum cholesterol levels on day 3 (Fig. 40), which can be explained by the fact that LPS stimulates hepatic cholesterol synthesis by increasing transcription rate, mRNA expression, and activity of HMG-CoA reductase in rodents (265, 266). However, the situation in humans may be different, as some studies reported decreased cholesterol plasma levels in humans after LPS administration (305, 307, 308).

Regarding fatty acid metabolism, we observed increased incorporation of C16:0, C18:1 and 18:2 fatty acids into complex lipid species in plasma. The levels of C18 fatty acids remained elevated until the end of the experiment (day 18; Fig. 38). In the brain LPS treatment augmented the levels of linoleate (C18:2; Fig. 41). Linoleate is one of the most important fatty acids due to the fact that it can be converted to arachidonate (C20:4) via desaturation and elongation (309). Arachidonate is the precursor for prostaglandine, leukotriene, and thromboxane synthesis, which play important roles in many pathophysiologic processes, including inflammation (310). Interestingly, C20:4 levels were slightly, but statistically not significantly upregulated in plasma (Fig. 42).

4.3 Conclusion

When we performed the LPS treatment of C57/Bl6 mice, we expected elevated 25-OHC levels in plasma and brain. However, whereas significantly increased concentration of 25-OHC could be detected in plasma, increased brain 25-OHC levels did not reach statistical significance in LPS-treated mice. Anyhow, these results are concordant with other studies, which showed that treatment of mice with the selective TLR4 agonist KDO induced upregulation of CH25H expression in the brain (230). Macrophages and DCs respond to TLR4 ligands by upregulating CH25H expression (182, 183), which is a possible explanation for the increased plasma 25-OHC concentrations on day 3 (Fig. 38). In the latter cell type TLR-dependent upregulation is mediated via a signalling pathway that involves NFκB and IFNγ secretion and converges on activation of the JAK/STAT1 pathway (182).

Our *in vitro* experiments using LPS treatment as a stimulus for 25-OHC production in GBM cell lines only resulted in a moderate short term induction of CH25H (Fig. 25) with slightly, but not significantly increased 25-OHC amounts after 24 h (Fig. 26). The fact that LPS is a more potent stimulus in macrophages than in GBM cell lines is possibly due to different TLR4 receptor expression levels, which are high for monoblasts and low for A172, GM133, and U87MG cells (www.biogps.org; NCI-60 dataset).

Interestingly, LPS administration to glioma bearing mice is able to improve survival rates (257). As the authors were not able not provide a precise mechanistic explanation, they have raised speculations that GBM growth is possibly less aggressive under pro-inflammatory conditions. According to our data, the observed effect could also be due to highly increased tumoral CH25H transcription and the resulting excessively increased 25-OHC amounts leading to some kind of “self-intoxication” of the malignant glioma cells.

However, the situation *in vivo* is virtually much more complex, as for example the discovery of the perivascular niche has given evidence (86). Therefore it is difficult to anticipate, which cell types are affected by increased oxysterol concentrations. There are two possible explanations in which way elevated levels of 25-OHC could promote tumor malignancy:

Increased 25-OHC concentrations could provoke astrocyte cell death, thereby increasing tumor aggressiveness and invasion, which requires that glia cells and neurons are more susceptible towards oxysterol-mediated toxicity than GBM cells themselves *in vivo*.

Alternatively, 25-OHC could act in the tumor microenvironment at low concentration (< 1 µM). Concomitantly, peripheral monoblasts are recruited and could polarize into the pro-tumorigenic M2 phenotype under the influence of the IL-containing tumor en-

vironment. Additionally, oxysterols lead to an induction in expression of MMPs via PKC and NFκB (311).

Another most recently discovered 25-OHC-mediated action is cellular defense against enveloped viruses (269, 270). These publications give evidence that 25-OHC may act as an intrinsic anti-viral substance by compromising membrane fusion via interaction with a (so-far unknown) protein and not only via simple membrane intercalation. This means that 25-OHC possibly exerts similar properties in immunologic mechanisms, for example when a tumor cell membrane is being attacked by the complement membrane attack complex or perforins of NK cells.

Taken together, the question remains, whether overexpression of CH25H or intratumoral 25-OHC administration would increase GBM malignancy *in vivo*, or if oxysterol treatment exhibits increased cytotoxicity versus GBM cells and has therefore beneficial properties. These open questions should be addressed by using an intracranial GBM mouse model (wild-type and $CH25H^{-/-}$), which could give a first experimental *in vivo* evidence whether or not CH25H could represent a potential therapeutic target in GBM therapy.

5 Table of abbreviations

Abbr.	Description
24S-OHC	24S-hydroxycholesterol
7α-OHC	7α-hydroxycholesterol
ABCA1	ATP-binding cassette transporter A1
ABCG1	ATP-binding cassette transporter G1
ABCG8	ATP-binding cassette transporter G8
ACC	acetyl coenzyme A carboxylase
AKT	protein kinase B
ANOVA	analysis of variances
ANS	autonomous nervous system
APOC	apolipoprotein C
apoE	apolipoprotein E
ATP	adenosine triphosphate
BAD	Bcl-2-associated death promoter
BAX	Bcl-2-associated X protein
BCL-2	B cell lymphoma protein 2
bFGF	basic fibroblast growth factor
bHLH-LZ	basic Helix-Loop-Helix Leucine Zipper
BSA	bovine serum albumin
BTSCs	brain tumor stem-like cells
CCR7	C-C chemokine receptor type 7
CD45	cluster of differentiation 45
CDK4	cyclin-dependent kinase 4
CH25H	cholesterol 25-hydroxylase
CNS	central nervous system
COPII	coat protein complex II

CSF	cerebro-spinal fluid
CTX	cerebrotedinous xanthomasis
CYP27A1	cytochrome P450, family 27, subfamily A, polypeptide 1 (gene encoding for cholesterol-27-hydroxylase)
CYP3A4	cytochrome P450, family 3, subfamily A, polypeptide 4
CYP46A1	cytochrome P450, family 46, subfamily A, polypeptide 1 (gene encoding for cholesterol-24-hydroxylase)
CYP7A1	cytochrome P450, family 7, subfamily A, polypeptide 1 (gene encoding for cholesterol-7a-hydroxylase)
DAPI	4',6-diamidino-2-phenylindole
DC	dendritic cell
DNA	desoxyribonucleic acid
EBI2 = GPR183	Epstein-Barr virus induced protein 2 = G protein-coupled receptor 183
EGF	epidermal growth factor
EGFR	epidermal growth factor receptor
EGFRvIII	mutant EGFR lacking exons
ER	endoplasmic reticulum
ERBB2	erythroblastic Leukemia Viral Oncogene Homolog 2
ERK	extracellular-signal Regulated Kinase
FASN	fatty acid synthase
FCS	fetal calf serum
FDS	farnesyl diphosphate synthase
FOXO1	Forkhead box protein O1
GBM	glioblastoma mutiforme
GC-MS	gas chromatography - mass spectrometry
GFAP	glial fibrillary acidic protein
GLI	gene encoding for the GLI family zinc finger 1 protein
Gli1	GLI family zinc finger 1 protein

GLUT1	glucose uptake transporter 1
GLUT3	glucose uptake transporter 3
GLUT4	glucose uptake transporter 4
GTP	guanosine triphosphate
GW3965	synthetic LXRα and β agonist
HDAC	histone-deacetylase
HDL	high density lipoprotein
HE	hematoxyline eosine staining
HER2	human epidermal growth factor receptor 2 = ERBB2
HIF-1	hypoxia induced factor 1
HMBS	hydroxymethylbilane synthase
HMG	hydroxymethylglutaric acid
HMGCR	hydroxymethylglutaryl coenzyme A reductase
HMGCS	hydroxymethylglutarylcoenzyme A synthase
HRP	horse raddish peroxidase
IDH	isocitrate dehydrogenase
IFN	interferon
INSIG	insulin-induced gene anchor protein
LDL	low density lipoprotein
LOH	loss of heterozygosity
LPS	lipopolysaccharide
LXR	liver-X-receptor
MAP	mitogen-activated protein
MAPK	mitogen-activated protein kinases
MCP3	monocyte chemotactic protein-3
MDM2	mouse double minute 2 homolog = E3 ubiquitin-protein ligase
MEK	mitogen-activated protein kinase kinase
MIP	macrophage inflammatory protein
MMP	matrix metalloproteinase

MSTFA	N-Methyl-N-(trimethylsilyl) trifluoroacetamide
MTIC	5-(3-methyltriazen-1-yl)imidazole-4-carboxamide
mTOR	mammalian target of rapamycin protein
MTT	3-(4,5-Dimethylthiazol-2-yl)-2,5-diphenyltetrazoliumbromid
NF1	neurofibromin-1
NFκB	nuclear factor kappa B
NO	nitric oxide
NPCs	neuronal precursor cells
p16INK4a	cyclin-dependent kinase inhibitor 2A
p53	protein 53
PBS	phosphate-buffered saline
PCR	polymerase chain reaction
PDGF-BB	platelet-derived growth factor (with two B chains)
PDGFR	platelet-derived growth factor receptor
PDGFs	platelet-derived growth factors
PI3K	phosphatidylinositol-3-kinase
PIP2	phospholipid phosphatidylinositol(4,5)diphophsphate
PIP3	phosphatidylinositol(3,4,5)triphosphate
PKC	protein kinase C
PMSF	phenylmethylsulfonylfluorid
PNS	peripheral nervous system
pRB	retinoblastoma protein
PTCH	patched
PTEN	phosphatase and tensin homolog
PTX	pertussis toxine
RAF	rapidly accelerated fibrosarcoma protein
RAS	rat sarcoma protein
REST	relative expression software tool
RTKs	receptor tyrosine kinases

RXR	retinoid-X-receptor
S1P	sphingosine-1-phosphate
SCAP	SREBP cleavage activating protein
SHH	sonic hedgehog
siRNA	small interfering RNA
SMO	smoothened
SREBP	sterol responsive element binding protein
T0901317	synthetic LXRa and b agonist
TGF	transforming growth factor
THP-1	a human monocytic cell line derived from an acute monocytic leukemia patient
TLR4	toll-like receptor 4
TLR9	toll like receptor 9
TMCS	trimethylchlorosilane
TMS	trimethylsilyl-
TNF	tumor necrosis factor
TP53	tumor suppressor protein 52
VEGF	vascular endothelial growth factor
VEGFR	vascular endothelial growth factor receptor
Wnt	proto-oncogene protein for the WNT-signalling pathway

6 References

1. Trepel M. Neuroanatomie : Struktur und Funktion ; mit 27 Tabellen. 3., neu bearb. Aufl., 2. Nachdr ed. München [u.a.]: Urban & Fischer; 2004.

2. Zigmond MJ. Fundamental neuroscience. San Diego: Academic Press; 1999.

3. Nieuwenhuys R, Donkelaar HJt, Nicholson C. The central nervous system of vertebrates. Berlin ; New York: Springer; 1998.

4. Swanson LW. Mapping the human brain: past, present, and future. Trends Neurosci. 1995 Nov;18(11):471-4.

5. Zhang S-x, editor. An atlas of histology. New York: Springer; 1999.

6. Barker RA, Barasi S, Neal MJ. Neuroscience at a glance. Oxford ; Malden, MA: Blackwell Science; 1999.

7. Johanson CE, Duncan JA, 3rd, Klinge PM, Brinker T, Stopa EG, Silverberg GD. Multiplicity of cerebrospinal fluid functions: New challenges in health and disease. Cerebrospinal Fluid Res. 2008;5:10.

8. Abbott NJ. Evidence for bulk flow of brain interstitial fluid: significance for physiology and pathology. Neurochem Int. 2004 Sep;45(4):545-52.

9. Gadani SP, Cronk JC, Norris GT, Kipnis J. IL-4 in the brain: a cytokine to remember. J Immunol. 2012 Nov 1;189(9):4213-9.

10. Somjen GG. Nervenkitt: notes on the history of the concept of neuroglia. Glia. 1988;1(1):2-9.

11. Wang DD, Bordey A. The astrocyte odyssey. Prog Neurobiol. 2008 Dec 11;86(4):342-67.

12. Oberheim NA, Wang X, Goldman S, Nedergaard M. Astrocytic complexity distinguishes the human brain. Trends Neurosci. 2006 Oct;29(10):547-53.

13. Kimelberg HK. The problem of astrocyte identity. Neurochem Int. 2004 Jul-Aug;45(2-3):191-202.

14. Bushong EA, Martone ME, Jones YZ, Ellisman MH. Protoplasmic astrocytes in CA1 stratum radiatum occupy separate anatomical domains. J Neurosci. 2002 Jan 1;22(1):183-92.

15. Ogata K, Kosaka T. Structural and quantitative analysis of astrocytes in the mouse hippocampus. Neuroscience. 2002;113(1):221-33.

16. Kettenmann H, Ransom BR. Neuroglia. New York: Oxford University Press; 1995.

17. Cheng C, Sourial M, Doering LC. Astrocytes and developmental plasticity in fragile X. Neural Plast. 2012;2012:197491.

18. Volterra A, Meldolesi J. Astrocytes, from brain glue to communication elements: the revolution continues. Nat Rev Neurosci. 2005 Aug;6(8):626-40.

19. Abbott NJ, Ronnback L, Hansson E. Astrocyte-endothelial interactions at the blood-brain barrier. Nat Rev Neurosci. 2006 Jan;7(1):41-53.

20. Verkhratsky A, Rodriguez JJ, Parpura V. Neurotransmitters and integration in neuronal-astroglial networks. Neurochem Res. 2012 Nov;37(11):2326-38.

21. Kimelberg HK. Supportive or information-processing functions of the mature protoplasmic astrocyte in the mammalian CNS? A critical appraisal. Neuron Glia Biol. 2007 Aug;3(3):181-9.

22. Santello M, Volterra A. TNFalpha in synaptic function: switching gears. Trends Neurosci. 2012 Oct;35(10):638-47.

23. Stupp R, Gander M, Leyvraz S, Newlands E. Current and future developments in the use of temozolomide for the treatment of brain tumours. Lancet Oncol. 2001 Sep;2(9):552-60.

24. DeAngelis LM. Brain tumors. N Engl J Med. 2001 Jan 11;344(2):114-23.

25. Böcker W, Denk H, Heitz PU, Aguzzi A, Böcker Denk H. Pathologie : mit 164 Tabellen ; 3., völlig überarb. Aufl., [Nachdr.] ed. München [u.a.]: Elsevier; 2006.

26. Grzmil M, Hemmings BA. Deregulated signalling networks in human brain tumours. Biochim Biophys Acta. 2010 Mar;1804(3):476-83.

27. Ohgaki H. Genetic pathways to glioblastomas. Neuropathology. 2005 Mar;25(1):1-7.

28. Comprehensive genomic characterization defines human glioblastoma genes and core pathways. Nature. 2008 Oct 23;455(7216):1061-8.

29. Maher EA, Furnari FB, Bachoo RM, Rowitch DH, Louis DN, Cavenee WK, et al. Malignant glioma: genetics and biology of a grave matter. Genes Dev. 2001 Jun 1;15(11):1311-33.

30. Chakravarti A, Dicker A, Mehta M. The contribution of epidermal growth factor receptor (EGFR) signaling pathway to radioresistance in human gliomas: a review of preclinical and correlative clinical data. Int J Radiat Oncol Biol Phys. 2004 Mar 1;58(3):927-31.

31. Sonabend AM, Dana K, Lesniak MS. Targeting epidermal growth factor receptor variant III: a novel strategy for the therapy of malignant glioma. Expert Rev Anticancer Ther. 2007 Dec;7(12 Suppl):S45-50.

32. Ramnarain DB, Park S, Lee DY, Hatanpaa KJ, Scoggin SO, Otu H, et al. Differential gene expression analysis reveals generation of an autocrine loop by a mutant epidermal growth factor receptor in glioma cells. Cancer Res. 2006 Jan 15;66(2):867-74.

33. Hermanson M, Funa K, Hartman M, Claesson-Welsh L, Heldin CH, Westermark B, et al. Platelet-derived growth factor and its receptors in human glioma tissue: expression of messenger RNA and protein suggests the presence of autocrine and paracrine loops. Cancer Res. 1992 Jun 1;52(11):3213-9.

34. Plate KH, Breier G, Farrell CL, Risau W. Platelet-derived growth factor receptor-beta is induced during tumor development and upregulated during tumor progression in endothelial cells in human gliomas. Lab Invest. 1992 Oct;67(4):529-34.

35. Di Rocco F, Carroll RS, Zhang J, Black PM. Platelet-derived growth factor and its receptor expression in human oligodendrogliomas. Neurosurgery. 1998 Feb;42(2):341-6.

36. Weller M, Malipiero U, Aguzzi A, Reed JC, Fontana A. Protooncogene bcl-2 gene transfer abrogates Fas/APO-1 antibody-mediated apoptosis of human malignant glioma cells and confers resistance to chemotherapeutic drugs and therapeutic irradiation. J Clin Invest. 1995 Jun;95(6):2633-43.

37. Rieger L, Weller M, Bornemann A, Schabet M, Dichgans J, Meyermann R. BCL-2 family protein expression in human malignant glioma: a clinical-pathological correlative study. J Neurol Sci. 1998 Feb 18;155(1):68-75.

38. Jensen RL, Ragel BT, Whang K, Gillespie D. Inhibition of hypoxia inducible factor-1alpha (HIF-1alpha) decreases vascular endothelial growth factor (VEGF) secretion and tumor growth in malignant gliomas. J Neurooncol. 2006 Jul;78(3):233-47.

39. Sonoda Y, Kanamori M, Deen DF, Cheng SY, Berger MS, Pieper RO. Overexpression of vascular endothelial growth factor isoforms drives oxygenation and growth but not progression to glioblastoma multiforme in a human model of gliomagenesis. Cancer Res. 2003 Apr 15;63(8):1962-8.

40. Gomez-Manzano C, Fueyo J, Jiang H, Glass TL, Lee HY, Hu M, et al. Mechanisms underlying PTEN regulation of vascular endothelial growth factor and angiogenesis. Ann Neurol. 2003 Jan;53(1):109-17.

41. Yoshino Y, Aoyagi M, Tamaki M, Duan L, Morimoto T, Ohno K. Activation of p38 MAPK and/or JNK contributes to increased levels of VEGF secretion in human malignant glioma cells. Int J Oncol. 2006 Oct;29(4):981-7.

42. Tsai JC, Goldman CK, Gillespie GY. Vascular endothelial growth factor in human glioma cell lines: induced secretion by EGF, PDGF-BB, and bFGF. J Neurosurg. 1995 May;82(5):864-73.

43. Parsons DW, Jones S, Zhang X, Lin JC, Leary RJ, Angenendt P, et al. An integrated genomic analysis of human glioblastoma multiforme. Science. 2008 Sep 26;321(5897):1807-12.

44. Yan H, Parsons DW, Jin G, McLendon R, Rasheed BA, Yuan W, et al. IDH1 and IDH2 mutations in gliomas. N Engl J Med. 2009 Feb 19;360(8):765-73.

45. Zhao S, Lin Y, Xu W, Jiang W, Zha Z, Wang P, et al. Glioma-derived mutations in IDH1 dominantly inhibit IDH1 catalytic activity and induce HIF-1alpha. Science. 2009 Apr 10;324(5924):261-5.

46. McKay MM, Morrison DK. Integrating signals from RTKs to ERK/MAPK. Oncogene. 2007 May 14;26(22):3113-21.

47. Guha A. Ras activation in astrocytomas and neurofibromas. Can J Neurol Sci. 1998 Nov;25(4):267-81.

48. McGillicuddy LT, Fromm JA, Hollstein PE, Kubek S, Beroukhim R, De Raedt T, et al. Proteasomal and genetic inactivation of the NF1 tumor suppressor in gliomagenesis. Cancer Cell. 2009 Jul 7;16(1):44-54.

49. Hawkins PT, Anderson KE, Davidson K, Stephens LR. Signalling through Class I PI3Ks in mammalian cells. Biochem Soc Trans. 2006 Nov;34(Pt 5):647-62.

50. Maehama T, Dixon JE. The tumor suppressor, PTEN/MMAC1, dephosphorylates the lipid second messenger, phosphatidylinositol 3,4,5-trisphosphate. J Biol Chem. 1998 May 29;273(22):13375-8.

51. Fayard E, Tintignac LA, Baudry A, Hemmings BA. Protein kinase B/Akt at a glance. J Cell Sci. 2005 Dec 15;118(Pt 24):5675-8.

52. Angileri FF, Aguennouz M, Conti A, La Torre D, Cardali S, Crupi R, et al. Nuclear factor-kappaB activation and differential expression of survivin and Bcl-2 in human grade 2-4 astrocytomas. Cancer. 2008 May 15;112(10):2258-66.

53. Wang H, Zhang W, Huang HJ, Liao WS, Fuller GN. Analysis of the activation status of Akt, NFkappaB, and Stat3 in human diffuse gliomas. Lab Invest. 2004 Aug;84(8):941-51.

54. da Rocha AB, Mans DR, Regner A, Schwartsmann G. Targeting protein kinase C: new therapeutic opportunities against high-grade malignant gliomas? Oncologist. 2002;7(1):17-33.

55. Aeder SE, Martin PM, Soh JW, Hussaini IM. PKC-eta mediates glioblastoma cell proliferation through the Akt and mTOR signaling pathways. Oncogene. 2004 Dec 2;23(56):9062-9.

56. Levine AJ, Hu W, Feng Z. The P53 pathway: what questions remain to be explored? Cell Death Differ. 2006 Jun;13(6):1027-36.

57. Shvarts A, Steegenga WT, Riteco N, van Laar T, Dekker P, Bazuine M, et al. MDMX: a novel p53-binding protein with some functional properties of MDM2. EMBO J. 1996 Oct 1;15(19):5349-57.

58. Riemenschneider MJ, Buschges R, Wolter M, Reifenberger J, Bostrom J, Kraus JA, et al. Amplification and overexpression of the MDM4 (MDMX) gene from 1q32 in a subset of malignant gliomas without TP53 mutation or MDM2 amplification. Cancer Res. 1999 Dec 15;59(24):6091-6.

59. Gu J, Kawai H, Nie L, Kitao H, Wiederschain D, Jochemsen AG, et al. Mutual dependence of MDM2 and MDMX in their functional inactivation of p53. J Biol Chem. 2002 May 31;277(22):19251-4.

60. Adamson C, Kanu OO, Mehta AI, Di C, Lin N, Mattox AK, et al. Glioblastoma multiforme: a review of where we have been and where we are going. Expert Opin Investig Drugs. 2009 Aug;18(8):1061-83.

61. Henson JW, Schnitker BL, Correa KM, von Deimling A, Fassbender F, Xu HJ, et al. The retinoblastoma gene is involved in malignant progression of astrocytomas. Ann Neurol. 1994 Nov;36(5):714-21.

62. Nakamura M, Yonekawa Y, Kleihues P, Ohgaki H. Promoter hypermethylation of the RB1 gene in glioblastomas. Lab Invest. 2001 Jan;81(1):77-82.

63. Lam PY, Di Tomaso E, Ng HK, Pang JC, Roussel MF, Hjelm NM. Expression of p19INK4d, CDK4, CDK6 in glioblastoma multiforme. Br J Neurosurg. 2000 Feb;14(1):28-32.

64. Hanahan D, Weinberg RA. The hallmarks of cancer. Cell. 2000 Jan 7;100(1):57-70.

65. Charles NA, Holland EC, Gilbertson R, Glass R, Kettenmann H. The brain tumor microenvironment. Glia. 2011 Aug;59(8):1169-80.

66. Penfield W. Microglia and the Process of Phagocytosis in Gliomas. Am J Pathol. 1925 Jan;1(1):77-90 15.

67. Graeber MB, Scheithauer BW, Kreutzberg GW. Microglia in brain tumors. Glia. 2002 Nov;40(2):252-9.

68. Watters JJ, Schartner JM, Badie B. Microglia function in brain tumors. J Neurosci Res. 2005 Aug 1;81(3):447-55.

69. Badie B, Schartner JM. Flow cytometric characterization of tumor-associated macrophages in experimental gliomas. Neurosurgery. 2000 Apr;46(4):957-61; discussion 61-2.

70. Alterman RL, Stanley ER. Colony stimulating factor-1 expression in human glioma. Mol Chem Neuropathol. 1994 Feb-Apr;21(2-3):177-88.

71. Okada M, Saio M, Kito Y, Ohe N, Yano H, Yoshimura S, et al. Tumor-associated macrophage/microglia infiltration in human gliomas is correlated with MCP-3, but not MCP-1. Int J Oncol. 2009 Jun;34(6):1621-7.

72. Yamasaki R, Tanaka M, Fukunaga M, Tateishi T, Kikuchi H, Motomura K, et al. Restoration of microglial function by granulocyte-colony stimulating factor in ALS model mice. J Neuroimmunol. 2010 Dec 15;229(1-2):51-62.

73. Platten M, Kretz A, Naumann U, Aulwurm S, Egashira K, Isenmann S, et al. Monocyte chemoattractant protein-1 increases microglial infiltration and aggressiveness of gliomas. Ann Neurol. 2003 Sep;54(3):388-92.

74. Suzumura A, Sawada M, Yamamoto H, Marunouchi T. Transforming growth factor-beta suppresses activation and proliferation of microglia in vitro. J Immunol. 1993 Aug 15;151(4):2150-8.

75. Bettinger I, Thanos S, Paulus W. Microglia promote glioma migration. Acta Neuropathol. 2002 Apr;103(4):351-5.

76. Markovic DS, Glass R, Synowitz M, Rooijen N, Kettenmann H. Microglia stimulate the invasiveness of glioma cells by increasing the activity of metalloprotease-2. J Neuropathol Exp Neurol. 2005 Sep;64(9):754-62.

77. Markovic DS, Vinnakota K, Chirasani S, Synowitz M, Raguet H, Stock K, et al. Gliomas induce and exploit microglial MT1-MMP expression for tumor expansion. Proc Natl Acad Sci U S A. 2009 Jul 28;106(30):12530-5.

78. Farmer JP, Antel JP, Freedman M, Cashman NR, Rode H, Villemure JG. Characterization of lymphoid cells isolated from human gliomas. J Neurosurg. 1989 Oct;71(4):528-33.

79. Dunn GP, Dunn IF, Curry WT. Focus on TILs: Prognostic significance of tumor infiltrating lymphocytes in human glioma. Cancer Immun. 2007;7:12.

80. El Andaloussi A, Han Y, Lesniak MS. Prolongation of survival following depletion of CD4+CD25+ regulatory T cells in mice with experimental brain tumors. J Neurosurg. 2006 Sep;105(3):430-7.

81. Grauer OM, Nierkens S, Bennink E, Toonen LW, Boon L, Wesseling P, et al. CD4+FoxP3+ regulatory T cells gradually accumulate in gliomas during tumor growth and efficiently suppress antiglioma immune responses in vivo. Int J Cancer. 2007 Jul 1;121(1):95-105.

82. El Andaloussi A, Sonabend AM, Han Y, Lesniak MS. Stimulation of TLR9 with CpG ODN enhances apoptosis of glioma and prolongs the survival of mice with experimental brain tumors. Glia. 2006 Nov 1;54(6):526-35.

83. Aboody KS, Najbauer J, Danks MK. Stem and progenitor cell-mediated tumor selective gene therapy. Gene Ther. 2008 May;15(10):739-52.

84. Glass R, Synowitz M, Kronenberg G, Walzlein JH, Markovic DS, Wang LP, et al. Glioblastoma-induced attraction of endogenous neural precursor cells is associated with improved survival. J Neurosci. 2005 Mar 9;25(10):2637-46.

85. Staflin K, Honeth G, Kalliomaki S, Kjellman C, Edvardsen K, Lindvall M. Neural progenitor cell lines inhibit rat tumor growth in vivo. Cancer Res. 2004 Aug 1;64(15):5347-54.

86. Calabrese C, Poppleton H, Kocak M, Hogg TL, Fuller C, Hamner B, et al. A perivascular niche for brain tumor stem cells. Cancer Cell. 2007 Jan;11(1):69-82.

87. De Palma M, Naldini L. Role of haematopoietic cells and endothelial progenitors in tumour angiogenesis. Biochim Biophys Acta. 2006 Aug;1766(1):159-66.

88. Rafii S, Heissig B, Hattori K. Efficient mobilization and recruitment of marrow-derived endothelial and hematopoietic stem cells by adenoviral vectors expressing angiogenic factors. Gene Ther. 2002 May;9(10):631-41.

89. Du R, Lu KV, Petritsch C, Liu P, Ganss R, Passegue E, et al. HIF1alpha induces the recruitment of bone marrow-derived vascular modulatory cells to regulate tumor angiogenesis and invasion. Cancer Cell. 2008 Mar;13(3):206-20.

90. Le DM, Besson A, Fogg DK, Choi KS, Waisman DM, Goodyer CG, et al. Exploitation of astrocytes by glioma cells to facilitate invasiveness: a mechanism involving matrix metalloproteinase-2 and the urokinase-type plasminogen activator-plasmin cascade. J Neurosci. 2003 May 15;23(10):4034-43.

91. Sameshima T, Nabeshima K, Toole BP, Yokogami K, Okada Y, Goya T, et al. Glioma cell extracellular matrix metalloproteinase inducer (EMMPRIN) (CD147) stimulates production of membrane-type matrix metalloproteinases and activated gelatinase A in co-cultures with brain-derived fibroblasts. Cancer Lett. 2000 Sep 1;157(2):177-84.

92. Belien AT, Paganetti PA, Schwab ME. Membrane-type 1 matrix metalloprotease (MT1-MMP) enables invasive migration of glioma cells in central nervous system white matter. J Cell Biol. 1999 Jan 25;144(2):373-84.

93. Sawaya RE, Yamamoto M, Gokaslan ZL, Wang SW, Mohanam S, Fuller GN, et al. Expression and localization of 72 kDa type IV collagenase (MMP-2) in human malignant gliomas in vivo. Clin Exp Metastasis. 1996 Jan;14(1):35-42.

94. Uhm JH, Dooley NP, Villemure JG, Yong VW. Glioma invasion in vitro: regulation by matrix metalloprotease-2 and protein kinase C. Clin Exp Metastasis. 1996 Oct;14(5):421-33.

95. Folkins C, Man S, Xu P, Shaked Y, Hicklin DJ, Kerbel RS. Anticancer therapies combining antiangiogenic and tumor cell cytotoxic effects reduce the tumor stem-like cell fraction in glioma xenograft tumors. Cancer Res. 2007 Apr 15;67(8):3560-4.

96. Charles N, Ozawa T, Squatrito M, Bleau AM, Brennan CW, Hambardzumyan D, et al. Perivascular nitric oxide activates notch signaling and promotes stem-like character in PDGF-induced glioma cells. Cell Stem Cell. 2010 Feb 5;6(2):141-52.

97. Hess KR. Extent of resection as a prognostic variable in the treatment of gliomas. J Neurooncol. 1999 May;42(3):227-31.

98. Simpson JR, Horton J, Scott C, Curran WJ, Rubin P, Fischbach J, et al. Influence of location and extent of surgical resection on survival of patients with glioblastoma multiforme: results of three consecutive Radiation Therapy Oncology Group (RTOG) clinical trials. Int J Radiat Oncol Biol Phys. 1993 May 20;26(2):239-44.

99. Fadul C, Wood J, Thaler H, Galicich J, Patterson RH, Jr., Posner JB. Morbidity and mortality of craniotomy for excision of supratentorial gliomas. Neurology. 1988 Sep;38(9):1374-9.

100. Walker MD, Alexander E, Jr., Hunt WE, MacCarty CS, Mahaley MS, Jr., Mealey J, Jr., et al. Evaluation of BCNU and/or radiotherapy in the treatment of anaplastic gliomas. A cooperative clinical trial. J Neurosurg. 1978 Sep;49(3):333-43.

101. Karim AB, Maat B, Hatlevoll R, Menten J, Rutten EH, Thomas DG, et al. A randomized trial on dose-response in radiation therapy of low-grade cerebral glioma: European Organization for Research and Treatment of Cancer (EORTC) Study 22844. Int J Radiat Oncol Biol Phys. 1996 Oct 1;36(3):549-56.

102. Shaw E, Arusell R, Scheithauer B, O'Fallon J, O'Neill B, Dinapoli R, et al. Prospective randomized trial of low- versus high-dose radiation therapy in adults with supratentorial low-grade glioma: initial report of a North Central Cancer Treatment Group/Radiation Therapy Oncology Group/Eastern Cooperative Oncology Group study. J Clin Oncol. 2002 May 1;20(9):2267-76.

103. Karim AB, Afra D, Cornu P, Bleehan N, Schraub S, De Witte O, et al. Randomized trial on the efficacy of radiotherapy for cerebral low-grade glioma in the adult: European Organization for Research and Treatment of Cancer Study 22845 with the Medical Research Council study BRO4: an interim analysis. Int J Radiat Oncol Biol Phys. 2002 Feb 1;52(2):316-24.

104. Stupp R, Mason WP, van den Bent MJ, Weller M, Fisher B, Taphoorn MJ, et al. Radiotherapy plus concomitant and adjuvant temozolomide for glioblastoma. N Engl J Med. 2005 Mar 10;352(10):987-96.

105. Stupp R, Hegi ME, van den Bent MJ, Mason WP, Weller M, Mirimanoff RO, et al. Changing paradigms--an update on the multidisciplinary management of malignant glioma. Oncologist. 2006 Feb;11(2):165-80.

106. Burger PC, Green SB. Patient age, histologic features, and length of survival in patients with glioblastoma multiforme. Cancer. 1987 May 1;59(9):1617-25.

107. Simmons ML, Lamborn KR, Takahashi M, Chen P, Israel MA, Berger MS, et al. Analysis of complex relationships between age, p53, epidermal growth factor receptor, and survival in glioblastoma patients. Cancer Res. 2001 Feb 1;61(3):1122-8.

108. Dietschy JM, Turley SD. Thematic review series: brain Lipids. Cholesterol metabolism in the central nervous system during early development and in the mature animal. J Lipid Res. 2004 Aug;45(8):1375-97.

109. Bjorkhem I, Meaney S. Brain cholesterol: long secret life behind a barrier. Arterioscler Thromb Vasc Biol. 2004 May;24(5):806-15.

110. Rapp M, Segev I, Yarom Y. Physiology, morphology and detailed passive models of guinea-pig cerebellar Purkinje cells. J Physiol. 1994 Jan 1;474(1):101-18.

111. Gabella G, Blundell D. Nexuses between the smooth muscle cells of the guinea-pig ileum. J Cell Biol. 1979 Jul;82(1):239-47.

112. Jurevics H, Morell P. Cholesterol for synthesis of myelin is made locally, not imported into brain. J Neurochem. 1995 Feb;64(2):895-901.

113. Turley SD, Burns DK, Dietschy JM. Preferential utilization of newly synthesized cholesterol for brain growth in neonatal lambs. Am J Physiol. 1998 Jun;274(6 Pt 1):E1099-105.

114. Pfrieger FW. Outsourcing in the brain: do neurons depend on cholesterol delivery by astrocytes? Bioessays. 2003 Jan;25(1):72-8.

115. Dietschy JM. Central nervous system: cholesterol turnover, brain development and neurodegeneration. Biol Chem. 2009 Apr;390(4):287-93.

116. Vance JE, Pan D, Campenot RB, Bussiere M, Vance DE. Evidence that the major membrane lipids, except cholesterol, are made in axons of cultured rat sympathetic neurons. J Neurochem. 1994 Jan;62(1):329-37.

117. Campenot RB. Independent control of the local environment of somas and neurites. Methods Enzymol. 1979;58:302-7.

118. Harris FM, Tesseur I, Brecht WJ, Xu Q, Mullendorff K, Chang S, et al. Astroglial regulation of apolipoprotein E expression in neuronal cells. Implications for Alzheimer's disease. J Biol Chem. 2004 Jan 30;279(5):3862-8.

119. LaDu MJ, Gilligan SM, Lukens JR, Cabana VG, Reardon CA, Van Eldik LJ, et al. Nascent astrocyte particles differ from lipoproteins in CSF. J Neurochem. 1998 May;70(5):2070-81.

120. Minagawa H, Gong JS, Jung CG, Watanabe A, Lund-Katz S, Phillips MC, et al. Mechanism underlying apolipoprotein E (ApoE) isoform-dependent lipid efflux from neural cells in culture. J Neurosci Res. 2009 Aug 15;87(11):2498-508.

121. Xu Q, Bernardo A, Walker D, Kanegawa T, Mahley RW, Huang Y. Profile and regulation of apolipoprotein E (ApoE) expression in the CNS in mice with targeting of green fluorescent protein gene to the ApoE locus. J Neurosci. 2006 May 10;26(19):4985-94.

122. Xu Q, Li Y, Cyras C, Sanan DA, Cordell B. Isolation and characterization of apolipoproteins from murine microglia. Identification of a low density lipoprotein-like apolipoprotein J-rich but E-poor spherical particle. J Biol Chem. 2000 Oct 13;275(41):31770-7.

123. Yu C, Youmans KL, LaDu MJ. Proposed mechanism for lipoprotein remodelling in the brain. Biochim Biophys Acta. 2010 Aug;1801(8):819-23.

124. Snipes GJ, Suter U. Cholesterol and myelin. SuB cell Biochem. 1997;28:173-204.

125. Herman GE. Disorders of cholesterol biosynthesis: prototypic metabolic malformation syndromes. Hum Mol Genet. 2003 Apr 1;12 Spec No 1:R75-88.

126. Wojcicka G, Jamroz-Wisniewska A, Horoszewicz K, Beltowski J. Liver X receptors (LXRs). Part I: structure, function, regulation of activity, and role in lipid metabolism. Postepy Hig Med Dosw (Online). 2007;61:736-59.

127. Gaylor JL. Membrane-bound enzymes of cholesterol synthesis from lanosterol. Biochem Biophys Res Commun. 2002 Apr 19;292(5):1139-46.

128. Nieweg K, Schaller H, Pfrieger FW. Marked differences in cholesterol synthesis between neurons and glial cells from postnatal rats. J Neurochem. 2009 Apr;109(1):125-34.

129. de Chaves EI, Rusinol AE, Vance DE, Campenot RB, Vance JE. Role of lipoproteins in the delivery of lipids to axons during axonal regeneration. J Biol Chem. 1997 Dec 5;272(49):30766-73.

130. Mauch DH, Nagler K, Schumacher S, Goritz C, Muller EC, Otto A, et al. CNS synaptogenesis promoted by glia-derived cholesterol. Science. 2001 Nov 9;294(5545):1354-7.

131. Amaratunga A, Abraham CR, Edwards RB, Sandell JH, Schreiber BM, Fine RE. Apolipoprotein E is synthesized in the retina by Muller glial cells, secreted into the vitreous, and rapidly transported into the optic nerve by retinal ganglion cells. J Biol Chem. 1996 Mar 8;271(10):5628-32.

132. Beffert U, Stolt PC, Herz J. Functions of lipoprotein receptors in neurons. J Lipid Res. 2004 Mar;45(3):403-9.

133. Bu G. Apolipoprotein E and its receptors in Alzheimer's disease: pathways, pathogenesis and therapy. Nat Rev Neurosci. 2009 May;10(5):333-44.

134. Fryer JD, Demattos RB, McCormick LM, O'Dell MA, Spinner ML, Bales KR, et al. The low density lipoprotein receptor regulates the level of central nervous system human and murine apolipoprotein E but does not modify amyloid plaque pathology in PDAPP mice. J Biol Chem. 2005 Jul 8;280(27):25754-9.

135. Herz J. Apolipoprotein E receptors in the nervous system. Curr Opin Lipidol. 2009 Jun;20(3):190-6.

136. Hayashi H, Campenot RB, Vance DE, Vance JE. Glial lipoproteins stimulate axon growth of central nervous system neurons in compartmented cultures. J Biol Chem. 2004 Apr 2;279(14):14009-15.

137. Gordon I, Genis I, Grauer E, Sehayek E, Michaelson DM. Biochemical and cognitive studies of apolipoprotein-E-deficient mice. Mol Chem Neuropathol. 1996 May-Aug;28(1-3):97-103.

138. Masliah E, Samuel W, Veinbergs I, Mallory M, Mante M, Saitoh T. Neurodegeneration and cognitive impairment in apoE-deficient mice is ameliorated by infusion of recombinant apoE. Brain Res. 1997 Mar 21;751(2):307-14.

139. Oitzl MS, Mulder M, Lucassen PJ, Havekes LM, Grootendorst J, de Kloet ER. Severe learning deficits in apolipoprotein E-knockout mice in a water maze task. Brain Res. 1997 Mar 28;752(1-2):189-96.

140. Masliah E, Mallory M, Ge N, Alford M, Veinbergs I, Roses AD. Neurodegeneration in the central nervous system of apoE-deficient mice. Exp Neurol. 1995 Dec;136(2):107-22.

141. Martin M, Dotti CG, Ledesma MD. Brain cholesterol in normal and pathological aging. Biochim Biophys Acta. 2010 Aug;1801(8):934-44.

142. Pfrieger FW, Ungerer N. Cholesterol metabolism in neurons and astrocytes. Prog Lipid Res. 2011 Oct;50(4):357-71.

143. Espenshade PJ. SREBPs: sterol-regulated transcription factors. J Cell Sci. 2006 Mar 15;119(Pt 6):973-6.

144. Brown MS, Goldstein JL. The SREBP pathway: regulation of cholesterol metabolism by proteolysis of a membrane-bound transcription factor. Cell. 1997 May 2;89(3):331-40.

145. Goldstein JL, DeBose-Boyd RA, Brown MS. Protein sensors for membrane sterols. Cell. 2006 Jan 13;124(1):35-46.

146. Espenshade PJ, Hughes AL. Regulation of sterol synthesis in eukaryotes. Annu Rev Genet. 2007;41:401-27.

147. Peng Y, Schwarz EJ, Lazar MA, Genin A, Spinner NB, Taub R. Cloning, human chromosomal assignment, and adipose and hepatic expression of the CL-6/INSIG1 gene. Genomics. 1997 Aug 1;43(3):278-84.

148. Radhakrishnan A, Ikeda Y, Kwon HJ, Brown MS, Goldstein JL. Sterol-regulated transport of SREBPs from endoplasmic reticulum to Golgi: oxysterols block transport by binding to Insig. Proc Natl Acad Sci U S A. 2007 Apr 17;104(16):6511-8.

149. Rawson RB. The SREBP pathway--insights from Insigs and insects. Nat Rev Mol Cell Biol. 2003 Aug;4(8):631-40.

150. Lee SJ, Sekimoto T, Yamashita E, Nagoshi E, Nakagawa A, Imamoto N, et al. The structure of importin-beta bound to SREBP-2: nuclear import of a transcription factor. Science. 2003 Nov 28;302(5650):1571-5.

151. Janowski BA, Grogan MJ, Jones SA, Wisely GB, Kliewer SA, Corey EJ, et al. Structural requirements of ligands for the oxysterol liver X receptors LXRalpha and LXRbeta. Proc Natl Acad Sci U S A. 1999 Jan 5;96(1):266-71.

152. Janowski BA, Willy PJ, Devi TR, Falck JR, Mangelsdorf DJ. An oxysterol signalling pathway mediated by the nuclear receptor LXR alpha. Nature. 1996 Oct 24;383(6602):728-31.

153. Loane DJ, Washington PM, Vardanian L, Pocivavsek A, Hoe HS, Duff KE, et al. Modulation of ABCA1 by an LXR agonist reduces beta-amyloid levels and improves outcome after traumatic brain injury. J Neurotrauma. 2011 Feb;28(2):225-36.

154. Schweinzer C, Kober A, Lang I, Etschmaier K, Scholler M, Kresse A, et al. Processing of Endogenous AbetaPP in Blood-Brain Barrier Endothelial Cells is Modulated by Liver-X Receptor Agonists and Altered Cellular Cholesterol Homeostasis. J Alzheimers Dis. 2011 Aug 2.

155. Terwel D, Steffensen KR, Verghese PB, Kummer MP, Gustafsson JA, Holtzman DM, et al. Critical role of astroglial apolipoprotein E and liver X receptor-alpha expression for microglial Abeta phagocytosis. J Neurosci. 2011 May 11;31(19):7049-59.

156. Lange Y, Ye J, Strebel F. Movement of 25-hydroxycholesterol from the plasma membrane to the rough endoplasmic reticulum in cultured hepatoma cells. J Lipid Res. 1995 May;36(5):1092-7.

157. Meaney S, Bodin K, Diczfalusy U, Bjorkhem I. On the rate of translocation in vitro and kinetics in vivo of the major oxysterols in human circulation: critical importance of the position of the oxygen function. J Lipid Res. 2002 Dec;43(12):2130-5.

158. Lund EG, Guileyardo JM, Russell DW. cDNA cloning of cholesterol 24-hydroxylase, a mediator of cholesterol homeostasis in the brain. Proc Natl Acad Sci U S A. 1999 Jun 22;96(13):7238-43.

159. Lund EG, Xie C, Kotti T, Turley SD, Dietschy JM, Russell DW. Knockout of the cholesterol 24-hydroxylase gene in mice reveals a brain-specific mechanism of cholesterol turnover. J Biol Chem. 2003 Jun 20;278(25):22980-8.

160. Lutjohann D, Breuer O, Ahlborg G, Nennesmo I, Siden A, Diczfalusy U, et al. Cholesterol homeostasis in human brain: evidence for an age-dependent flux of 24S-hydroxycholesterol from the brain into the circulation. Proc Natl Acad Sci U S A. 1996 Sep 3;93(18):9799-804.

161. Xie C, Lund EG, Turley SD, Russell DW, Dietschy JM. Quantitation of two pathways for cholesterol excretion from the brain in normal mice and mice with neurodegeneration. J Lipid Res. 2003 Sep;44(9):1780-9.

162. Jusakul A, Yongvanit P, Loilome W, Namwat N, Kuver R. Mechanisms of oxysterol-induced carcinogenesis. Lipids Health Dis. 2011;10:44.

163. Myant NB, Mitropoulos KA. Cholesterol 7 alpha-hydroxylase. J Lipid Res. 1977 Mar;18(2):135-53.

164. Pikuleva IA. Cholesterol-metabolizing cytochromes P450. Drug Metab Dispos. 2006 Apr;34(4):513-20.

165. Chiang JY, Miller WF, Lin GM. Regulation of cholesterol 7 alpha-hydroxylase in the liver. Purification of cholesterol 7 alpha-hydroxylase and the immunochemical evidence for the induction of cholesterol 7 alpha-hydroxylase by cholestyramine and circadian rhythm. J Biol Chem. 1990 Mar 5;265(7):3889-97.

166. Pullinger CR, Eng C, Salen G, Shefer S, Batta AK, Erickson SK, et al. Human cholesterol 7alpha-hydroxylase (CYP7A1) deficiency has a hypercholesterolemic phenotype. J Clin Invest. 2002 Jul;110(1):109-17.

167. Teng JI, Smith LL. Sterol metabolism. XXIV. On the unlikely participation of singlet molecular oxygen in several enzyme oxygenations. J Am Chem Soc. 1973 Jun 13;95(12):4060-1.

168. Repa JJ, Mangelsdorf DJ. The role of orphan nuclear receptors in the regulation of cholesterol homeostasis. Annu Rev Cell Dev Biol. 2000;16:459-81.

169. Chiang JY. Bile acid regulation of hepatic physiology: III. Bile acids and nuclear receptors. Am J Physiol Gastrointest Liver Physiol. 2003 Mar;284(3):G349-56.

170. Russell DW. The enzymes, regulation, and genetics of bile acid synthesis. Annu Rev Biochem. 2003;72:137-74.

171. Feingold KR, Spady DK, Pollock AS, Moser AH, Grunfeld C. Endotoxin, TNF, and IL-1 decrease cholesterol 7 alpha-hydroxylase mRNA levels and activity. J Lipid Res. 1996 Feb;37(2):223-8.

172. Kren BT, Rodrigues CM, Setchell KD, Steer CJ. Posttranscriptional regulation of mRNA levels in rat liver associated with deoxycholic acid feeding. Am J Physiol. 1995 Dec;269(6 Pt 1):G961-73.

173. Heverin M, Bogdanovic N, Lutjohann D, Bayer T, Pikuleva I, Bretillon L, et al. Changes in the levels of cerebral and extracerebral sterols in the brain of patients with Alzheimer's disease. J Lipid Res. 2004 Jan;45(1):186-93.

174. Wang Y, Muneton S, Sjovall J, Jovanovic JN, Griffiths WJ. The effect of 24S-hydroxycholesterol on cholesterol homeostasis in neurons: quantitative changes to the cortical neuron proteome. J Proteome Res. 2008 Apr;7(4):1606-14.

175. Milagre I, Nunes MJ, Gama MJ, Silva RF, Pascussi JM, Lechner MC, et al. Transcriptional regulation of the human CYP46A1 brain-specific expression by Sp transcription factors. J Neurochem. 2008 Jul;106(2):835-49.

176. Shafaati M, O'Driscoll R, Bjorkhem I, Meaney S. Transcriptional regulation of cholesterol 24-hydroxylase by histone deacetylase inhibitors. Biochem Biophys Res Commun. 2009 Jan 23;378(4):689-94.

177. Diczfalusy U. On the formation and possible biological role of 25-hydroxycholesterol. Biochimie. 2013 Mar;95(3):455-60.

178. Lund EG, Kerr TA, Sakai J, Li WP, Russell DW. cDNA cloning of mouse and human cholesterol 25-hydroxylases, polytopic membrane proteins that synthesize a potent oxysterol regulator of lipid metabolism. J Biol Chem. 1998 Dec 18;273(51):34316-27.

179. Repa JJ, Li H, Frank-Cannon TC, Valasek MA, Turley SD, Tansey MG, et al. Liver X receptor activation enhances cholesterol loss from the brain, decreases neuroinflammation, and increases survival of the NPC1 mouse. J Neurosci. 2007 Dec 26;27(52):14470-80.

180. Laffitte BA, Repa JJ, Joseph SB, Wilpitz DC, Kast HR, Mangelsdorf DJ, et al. LXRs control lipid-inducible expression of the apolipoprotein E gene in macrophages and adipocytes. Proc Natl Acad Sci U S A. 2001 Jan 16;98(2):507-12.

181. Makoukji J, Shackleford G, Meffre D, Grenier J, Liere P, Lobaccaro JM, et al. Interplay between LXR and Wnt/beta-catenin signaling in the negative regulation of peripheral myelin genes by oxysterols. J Neurosci. 2011 Jun 29;31(26):9620-9.

182. Park K, Scott AL. Cholesterol 25-hydroxylase production by dendritic cells and macrophages is regulated by type I interferons. J Leukoc Biol. 2010 Dec;88(6):1081-7.

183. Diczfalusy U, Olofsson KE, Carlsson AM, Gong M, Golenbock DT, Rooyackers O, et al. Marked upregulation of cholesterol 25-hydroxylase expression by lipopolysaccharide. J Lipid Res. 2009 Nov;50(11):2258-64.

184. Wang JH, Tuohimaa P. Regulation of cholesterol 25-hydroxylase expression by vitamin D3 metabolites in human prostate stromal cells. Biochem Biophys Res Commun. 2006 Jun 30;345(2):720-5.

185. Anderson KE, Kok E, Javitt NB. Bile acid synthesis in man: metabolism of 7 -hydroxycholesterol- 14 C and 26-hydroxycholesterol- 3 H. J Clin Invest. 1972 Jan;51(1):112-7.

186. Lund E, Andersson O, Zhang J, Babiker A, Ahlborg G, Diczfalusy U, et al. Importance of a novel oxidative mechanism for elimination of intracellular cholesterol in humans. Arterioscler Thromb Vasc Biol. 1996 Feb;16(2):208-12.

187. Duane WC, Javitt NB. 27-hydroxycholesterol: production rates in normal human subjects. J Lipid Res. 1999 Jul;40(7):1194-9.

188. Bjorkhem I, Andersson O, Diczfalusy U, Sevastik B, Xiu RJ, Duan C, et al. Atherosclerosis and sterol 27-hydroxylase: evidence for a role of this enzyme in elimination of cholesterol from human macrophages. Proc Natl Acad Sci U S A. 1994 Aug 30;91(18):8592-6.

189. Fu X, Menke JG, Chen Y, Zhou G, MacNaul KL, Wright SD, et al. 27-hydroxycholesterol is an endogenous ligand for liver X receptor in cholesterol-loaded cells. J Biol Chem. 2001 Oct 19;276(42):38378-87.

190. Song C, Liao S. Cholestenoic acid is a naturally occurring ligand for liver X receptor alpha. Endocrinology. 2000 Nov;141(11):4180-4.

191. Apfel R, Benbrook D, Lernhardt E, Ortiz MA, Salbert G, Pfahl M. A novel orphan receptor specific for a subset of thyroid hormone-responsive elements and its interaction with the retinoid/thyroid hormone receptor subfamily. Mol Cell Biol. 1994 Oct;14(10):7025-35.

192. Willy PJ, Umesono K, Ong ES, Evans RM, Heyman RA, Mangelsdorf DJ. LXR, a nuclear receptor that defines a distinct retinoid response pathway. Genes Dev. 1995 May 1;9(9):1033-45.

193. Calkin AC, Tontonoz P. Transcriptional integration of metabolism by the nuclear sterol-activated receptors LXR and FXR. Nat Rev Mol Cell Biol. 2012 Apr;13(4):213-24.

194. Venkateswaran A, Laffitte BA, Joseph SB, Mak PA, Wilpitz DC, Edwards PA, et al. Control of cellular cholesterol efflux by the nuclear oxysterol receptor LXR alpha. Proc Natl Acad Sci U S A. 2000 Oct 24;97(22):12097-102.

195. Repa JJ, Turley SD, Lobaccaro JA, Medina J, Li L, Lustig K, et al. Regulation of absorption and ABC1-mediated efflux of cholesterol by RXR heterodimers. Science. 2000 Sep 1;289(5484):1524-9.

196. Kennedy MA, Venkateswaran A, Tarr PT, Xenarios I, Kudoh J, Shimizu N, et al. Characterization of the human ABCG1 gene: liver X receptor activates an internal promoter that produces a novel transcript encoding an alternative form of the protein. J Biol Chem. 2001 Oct 19;276(42):39438-47.

197. Repa JJ, Berge KE, Pomajzl C, Richardson JA, Hobbs H, Mangelsdorf DJ. Regulation of ATP-binding cassette sterol transporters ABCG5 and ABCG8 by the liver X receptors alpha and beta. J Biol Chem. 2002 May 24;277(21):18793-800.

198. Mak PA, Laffitte BA, Desrumaux C, Joseph SB, Curtiss LK, Mangelsdorf DJ, et al. Regulated expression of the apolipoprotein E/C-I/C-IV/C-II gene cluster in murine and human macrophages. A critical role for nuclear liver X receptors alpha and beta. J Biol Chem. 2002 Aug 30;277(35):31900-8.

199. Dalen KT, Ulven SM, Bamberg K, Gustafsson JA, Nebb HI. Expression of the insulin-responsive glucose transporter GLUT4 in adipocytes is dependent on liver X receptor alpha. J Biol Chem. 2003 Nov 28;278(48):48283-91.

200. Korach-Andre M, Archer A, Barros RP, Parini P, Gustafsson JA. Both liver-X receptor (LXR) isoforms control energy expenditure by regulating brown adipose tissue activity. Proc Natl Acad Sci U S A. 2011 Jan 4;108(1):403-8.

201. Laffitte BA, Chao LC, Li J, Walczak R, Hummasti S, Joseph SB, et al. Activation of liver X receptor improves glucose tolerance through coordinate regulation of glucose metabolism in liver and adipose tissue. Proc Natl Acad Sci U S A. 2003 Apr 29;100(9):5419-24.

202. Mitro N, Mak PA, Vargas L, Godio C, Hampton E, Molteni V, et al. The nuclear receptor LXR is a glucose sensor. Nature. 2007 Jan 11;445(7124):219-23.

203. Osborne TF, Espenshade PJ. Evolutionary conservation and adaptation in the mechanism that regulates SREBP action: what a long, strange tRIP it's been. Genes Dev. 2009 Nov 15;23(22):2578-91.

204. McMahon AP, Ingham PW, Tabin CJ. Developmental roles and clinical significance of hedgehog signaling. Curr Top Dev Biol. 2003;53:1-114.

205. Riobo NA, Manning DR. Pathways of signal transduction employed by vertebrate Hedgehogs. Biochem J. 2007 May 1;403(3):369-79.

206. Wang Y, McMahon AP, Allen BL. Shifting paradigms in Hedgehog signaling. Curr Opin Cell Biol. 2007 Apr;19(2):159-65.

207. Rohatgi R, Milenkovic L, Scott MP. Patched1 regulates hedgehog signaling at the primary cilium. Science. 2007 Jul 20;317(5836):372-6.

208. Satir P, Pedersen LB, Christensen ST. The primary cilium at a glance. J Cell Sci. 2010 Feb 15;123(Pt 4):499-503.

209. Huangfu D, Liu A, Rakeman AS, Murcia NS, Niswander L, Anderson KV. Hedgehog signalling in the mouse requires intraflagellar transport proteins. Nature. 2003 Nov 6;426(6962):83-7.

210. Simpson F, Kerr MC, Wicking C. Trafficking, development and hedgehog. Mech Dev. 2009 May-Jun;126(5-6):279-88.

211. Pepinsky RB, Zeng C, Wen D, Rayhorn P, Baker DP, Williams KP, et al. Identification of a palmitic acid-modified form of human Sonic hedgehog. J Biol Chem. 1998 May 29;273(22):14037-45.

212. Porter JA, Ekker SC, Park WJ, von Kessler DP, Young KE, Chen CH, et al. Hedgehog patterning activity: role of a lipophilic modification mediated by the carboxy-terminal autoprocessing domain. Cell. 1996 Jul 12;86(1):21-34.

213. Cooper MK, Wassif CA, Krakowiak PA, Taipale J, Gong R, Kelley RI, et al. A defective response to Hedgehog signaling in disorders of cholesterol biosynthesis. Nat Genet. 2003 Apr;33(4):508-13.

214. Corcoran RB, Scott MP. Oxysterols stimulate Sonic hedgehog signal transduction and proliferation of medulloblastoma cells. Proc Natl Acad Sci U S A. 2006 May 30;103(22):8408-13.

215. Dwyer JR, Sever N, Carlson M, Nelson SF, Beachy PA, Parhami F. Oxysterols are novel activators of the hedgehog signaling pathway in pluripotent mesenchymal cells. J Biol Chem. 2007 Mar 23;282(12):8959-68.

216. Nachtergaele S, Mydock LK, Krishnan K, Rammohan J, Schlesinger PH, Covey DF, et al. Oxysterols are allosteric activators of the oncoprotein Smoothened. Nat Chem Biol. 2012 Feb;8(2):211-20.

217. Benned-Jensen T, Norn C, Laurent S, Madsen CM, Larsen HM, Arfelt KN, et al. Molecular characterization of oxysterol binding to the Epstein-Barr virus-induced gene 2 (GPR183). J Biol Chem. 2012 Oct 12;287(42):35470-83.

218. Rosenkilde MM, Benned-Jensen T, Andersen H, Holst PJ, Kledal TN, Luttichau HR, et al. Molecular pharmacological phenotyping of EBI2. An orphan seven-transmembrane receptor with constitutive activity. J Biol Chem. 2006 May 12;281(19):13199-208.

219. Gatto D, Paus D, Basten A, Mackay CR, Brink R. Guidance of B cells by the orphan G protein-coupled receptor EBI2 shapes humoral immune responses. Immunity. 2009 Aug 21;31(2):259-69.

220. Pereira JP, Kelly LM, Xu Y, Cyster JG. EBI2 mediates B cell segregation between the outer and centre follicle. Nature. 2009 Aug 27;460(7259):1122-6.

221. Pereira JP, Kelly LM, Cyster JG. Finding the right niche: B-cell migration in the early phases of T-dependent antibody responses. Int Immunol. 2010 Jun;22(6):413-9.

222. Hannedouche S, Zhang J, Yi T, Shen W, Nguyen D, Pereira JP, et al. Oxysterols direct immune cell migration via EBI2. Nature. 2011 Jul 28;475(7357):524-7.

223. Liu C, Yang XV, Wu J, Kuei C, Mani NS, Zhang L, et al. Oxysterols direct B-cell migration through EBI2. Nature. 2011 Jul 28;475(7357):519-23.

224. Gatto D, Wood K, Caminschi I, Murphy-Durland D, Schofield P, Christ D, et al. The chemotactic receptor EBI2 regulates the homeostasis, localization and immunological function of splenic dendritic cells. Nat Immunol. 2013 May;14(5):446-53.

225. Barroso R, Martinez Munoz L, Barrondo S, Vega B, Holgado BL, Lucas P, et al. EBI2 regulates CXCL13-mediated responses by heterodimerization with CXCR5. FASEB J. 2012 Dec;26(12):4841-54.

226. Villablanca EJ, Raccosta L, Zhou D, Fontana R, Maggioni D, Negro A, et al. Tumor-mediated liver X receptor-alpha activation inhibits CC chemokine receptor-7 expression on dendritic cells and dampens antitumor responses. Nat Med. 2010 Jan;16(1):98-105.

227. Traversari C, Russo V. Control of the immune system by oxysterols and cancer development. Curr Opin Pharmacol. 2012 Dec;12(6):729-35.

228. Guo D, Reinitz F, Youssef M, Hong C, Nathanson D, Akhavan D, et al. An LXR agonist promotes glioblastoma cell death through inhibition of an EGFR/AKT/SREBP-1/LDLR-dependent pathway. Cancer Discov. 2011 Oct;1(5):442-56.

229. Guo D, Hildebrandt IJ, Prins RM, Soto H, Mazzotta MM, Dang J, et al. The AMPK agonist AICAR inhibits the growth of EGFRvIII-expressing glioblastomas by inhibiting lipogenesis. Proc Natl Acad Sci U S A. 2009 Aug 4;106(31):12932-7.

230. Bauman DR, Bitmansour AD, McDonald JG, Thompson BM, Liang G, Russell DW. 25-Hydroxycholesterol secreted by macrophages in response to Toll-like receptor activation suppresses immunoglobulin A production. Proc Natl Acad Sci U S A. 2009 Sep 29;106(39):16764-9.

231. Liu Y, Hulten LM, Wiklund O. Macrophages isolated from human atherosclerotic plaques produce IL-8, and oxysterols may have a regulatory function for IL-8 production. Arterioscler Thromb Vasc Biol. 1997 Feb;17(2):317-23.

232. Rydberg EK, Salomonsson L, Hulten LM, Noren K, Bondjers G, Wiklund O, et al. Hypoxia increases 25-hydroxycholesterol-induced interleukin-8 protein secretion in human macrophages. Atherosclerosis. 2003 Oct;170(2):245-52.

233. Chuu CP, Lin HP. Antiproliferative effect of LXR agonists T0901317 and 22(R)-hydroxycholesterol on multiple human cancer cell lines. Anticancer Res. 2010 Sep;30(9):3643-8.

234. Fukuchi J, Kokontis JM, Hiipakka RA, Chuu CP, Liao S. Antiproliferative effect of liver X receptor agonists on LNCaP human prostate cancer cells. Cancer Res. 2004 Nov 1;64(21):7686-9.

235. Chuu CP, Hiipakka RA, Kokontis JM, Fukuchi J, Chen RY, Liao S. Inhibition of tumor growth and progression of LNCaP prostate cancer cells in athymic mice by androgen and liver X receptor agonist. Cancer Res. 2006 Jul 1;66(13):6482-6.

236. Chuu CP. Modulation of liver X receptor signaling as a prevention and therapy for colon cancer. Med Hypotheses. 2011 May;76(5):697-9.

237. Sallusto F, Lanzavecchia A. Understanding dendritic cell and T-lymphocyte traffic through the analysis of chemokine receptor expression. Immunol Rev. 2000 Oct;177:134-40.

238. Ohl L, Mohaupt M, Czeloth N, Hintzen G, Kiafard Z, Zwirner J, et al. CCR7 governs skin dendritic cell migration under inflammatory and steady-state conditions. Immunity. 2004 Aug;21(2):279-88.

239. Randolph GJ, Ochando J, Partida-Sanchez S. Migration of dendritic cell subsets and their precursors. Annu Rev Immunol. 2008;26:293-316.

240. Xu L, Shen S, Ma Y, Kim JK, Rodriguez-Agudo D, Heuman DM, et al. 25-Hydroxycholesterol-3-sulfate attenuates inflammatory response via PPARgamma signaling in human THP-1 macrophages. Am J Physiol Endocrinol Metab. 2012 Apr 1;302(7):E788-99.

241. Russo V. Metabolism, LXR/LXR ligands, and tumor immune escape. J Leukoc Biol. 2011 Oct;90(4):673-9.

242. Yeung YT, Bryce NS, Adams S, Braidy N, Konayagi M, McDonald KL, et al. p38 MAPK inhibitors attenuate pro-inflammatory cytokine production and the invasiveness of human U251 glioblastoma cells. J Neurooncol. 2012 Aug;109(1):35-44.

243. Sharma V, Dixit D, Koul N, Mehta VS, Sen E. Ras regulates interleukin-1beta-induced HIF-1alpha transcriptional activity in glioblastoma. J Mol Med (Berl). 2011 Feb;89(2):123-36.

244. Zhu VF, Yang J, Lebrun DG, Li M. Understanding the role of cytokines in Glioblastoma Multiforme pathogenesis. Cancer Lett. 2012 Mar 28;316(2):139-50.

245. Ye XZ, Xu SL, Xin YH, Yu SC, Ping YF, Chen L, et al. Tumor-associated microglia/macrophages enhance the invasion of glioma stem-like cells via TGF-beta1 signaling pathway. J Immunol. 2012 Jul 1;189(1):444-53.

246. Wang Y, Zhu S, Cloughesy TF, Liau LM, Mischel PS. p53 disruption profoundly alters the response of human glioblastoma cells to DNA topoisomerase I inhibition. Oncogene. 2004 Feb 12;23(6):1283-90.

247. Pfaffl MW. A new mathematical model for relative quantification in real-time RT-PCR. Nucleic Acids Res. 2001 May 1;29(9):e45.

248. Folch J, Lees M, Sloane Stanley GH. A simple method for the isolation and purification of total lipides from animal tissues. J Biol Chem. 1957 May;226(1):497-509.

249. Yamanaka K, Saito Y, Yamamori T, Urano Y, Noguchi N. 24(S)-hydroxycholesterol induces neuronal cell death through necroptosis, a form of programmed necrosis. J Biol Chem. 2011 Jul 15;286(28):24666-73.

250. McQuibban GA, Gong JH, Wong JP, Wallace JL, Clark-Lewis I, Overall CM. Matrix metalloproteinase processing of monocyte chemoattractant proteins generates CC chemokine receptor antagonists with anti-inflammatory properties in vivo. Blood. 2002 Aug 15;100(4):1160-7.

251. McClelland S, Cox C, O'Connor R, de Gaetano M, McCarthy C, Cryan L, et al. Conjugated linoleic acid suppresses the migratory and inflammatory phenotype of the monocyte/macrophage cell. Atherosclerosis. 2010 Jul;211(1):96-102.

252. Heinig M, Petretto E, Wallace C, Bottolo L, Rotival M, Lu H, et al. A trans-acting locus regulates an anti-viral expression network and type 1 diabetes risk. Nature. 2010 Sep 23;467(7314):460-4.

253. Bahador M, Cross AS. From therapy to experimental model: a hundred years of endotoxin administration to human subjects. J Endotoxin Res. 2007;13(5):251-79.

254. Miller RJ, Jung H, Bhangoo SK, White FA. Cytokine and chemokine regulation of sensory neuron function. Handb Exp Pharmacol. 2009(194):417-49.

255. Watkins LR, Maier SF. Immune regulation of central nervous system functions: from sickness responses to pathological pain. J Intern Med. 2005 Feb;257(2):139-55.

256. Akira S, Takeda K. Toll-like receptor signalling. Nat Rev Immunol. 2004 Jul;4(7):499-511.

257. Chicoine MR, Zahner M, Won EK, Kalra RR, Kitamura T, Perry A, et al. The in vivo antitumoral effects of lipopolysaccharide against glioblastoma multiforme are mediated in part by Toll-like receptor 4. Neurosurgery. 2007 Feb;60(2):372-80; discussion 81.

258. Ullen A, Singewald E, Konya V, Fauler G, Reicher H, Nusshold C, et al. Myeloperoxidase-derived oxidants induce blood-brain barrier dysfunction in vitro and in vivo. PLoS One. 2013;8(5):e64034.

259. Choi JJ, Choi YJ, Chen L, Zhang B, Eum SY, Abreu MT, et al. Lipopolysaccharide potentiates polychlorinated biphenyl-induced disruption of the blood-brain barrier via TLR4/IRF-3 signaling. Toxicology. 2012 Dec 16;302(2-3):212-20.

260. Jaworowicz DJ, Jr., Korytko PJ, Singh Lakhman S, Boje KM. Nitric oxide and prostaglandin E2 formation parallels blood-brain barrier disruption in an experimental rat model of bacterial meningitis. Brain Res Bull. 1998 Aug;46(6):541-6.

261. Sakaguchi O, Sakaguchi S. Alterations of lipid metabolism in mice injected with endotoxin. Microbiol Immunol. 1979;23(2):71-85.

262. Gaal D, Kremmer T, Balint Z, Holczinger L, Bertok L, Nowotny A. Effects of bacterial endotoxins and their detoxified derivatives on serum and liver lipids in mice. Toxicol Appl Pharmacol. 1984 Sep 30;75(3):437-43.

263. Feingold KR, Staprans I, Memon RA, Moser AH, Shigenaga JK, Doerrler W, et al. Endotoxin rapidly induces changes in lipid metabolism that produce hypertriglyceridemia: low doses stimulate hepatic triglyceride production while high doses inhibit clearance. J Lipid Res. 1992 Dec;33(12):1765-76.

264. Nonogaki K, Moser AH, Pan XM, Staprans I, Grunfeld C, Feingold KR. Lipoteichoic acid stimulates lipolysis and hepatic triglyceride secretion in rats in vivo. J Lipid Res. 1995 Sep;36(9):1987-95.

265. Feingold KR, Hardardottir I, Memon R, Krul EJ, Moser AH, Taylor JM, et al. Effect of endotoxin on cholesterol biosynthesis and distribution in serum lipoproteins in Syrian hamsters. J Lipid Res. 1993 Dec;34(12):2147-58.

266. Feingold KR, Pollock AS, Moser AH, Shigenaga JK, Grunfeld C. Discordant regulation of proteins of cholesterol metabolism during the acute phase response. J Lipid Res. 1995 Jul;36(7):1474-82.

267. Massey JB. Membrane and protein interactions of oxysterols. Curr Opin Lipidol. 2006 Jun;17(3):296-301.

268. Javitt NB. Oxysterols: novel biologic roles for the 21st century. Steroids. 2008 Feb;73(2):149-57.

269. Liu SY, Aliyari R, Chikere K, Li G, Marsden MD, Smith JK, et al. Interferon-inducible cholesterol-25-hydroxylase broadly inhibits viral entry by production of 25-hydroxycholesterol. Immunity. 2013 Jan 24;38(1):92-105.

270. Blanc M, Hsieh WY, Robertson KA, Kropp KA, Forster T, Shui G, et al. The transcription factor STAT-1 couples macrophage synthesis of 25-hydroxycholesterol to the interferon antiviral response. Immunity. 2013 Jan 24;38(1):106-18.

271. Shackleford G, Makoukji J, Grenier J, Liere P, Meffre D, Massaad C. Differential regulation of Wnt/beta-catenin signaling by Liver X Receptors in Schwann cells and oligodendrocytes. Biochem Pharmacol. 2013 Jul 1;86(1):106-14.

272. Guo D, Dunbar JD, Yang CH, Pfeffer LM, Donner DB. Induction of Jak/STAT signaling by activation of the type 1 TNF receptor. J Immunol. 1998 Mar 15;160(6):2742-50.

273. Lee SH, Nishino M, Mazumdar T, Garcia GE, Galfione M, Lee FL, et al. 16-kDa prolactin down-regulates inducible nitric oxide synthase expression through inhibition of the signal transducer and activator of transcription 1/IFN regulatory factor-1 pathway. Cancer Res. 2005 Sep 1;65(17):7984-92.

274. Tsukada J, Waterman WR, Koyama Y, Webb AC, Auron PE. A novel STAT-like factor mediates lipopolysaccharide, interleukin 1 (IL-1), and IL-6 signaling and recognizes a gamma interferon activation site-like element in the IL1B gene. Mol Cell Biol. 1996 May;16(5):2183-94.

275. Theunissen JJ, Jackson RL, Kempen HJ, Demel RA. Membrane properties of oxysterols. Interfacial orientation, influence on membrane permeability and redistribution between membranes. Biochim Biophys Acta. 1986 Aug 7;860(1):66-74.

276. Babiker A, Diczfalusy U. Transport of side-chain oxidized oxysterols in the human circulation. Biochim Biophys Acta. 1998 Jun 15;1392(2-3):333-9.

277. Van Brocklyn J, Letterle C, Snyder P, Prior T. Sphingosine-1-phosphate stimulates human glioma cell proliferation through Gi-coupled receptors: role of ERK MAP kinase and phosphatidylinositol 3-kinase beta. Cancer Lett. 2002 Jul 26;181(2):195-204.

278. Malchinkhuu E, Sato K, Muraki T, Ishikawa K, Kuwabara A, Okajima F. Assessment of the role of sphingosine 1-phosphate and its receptors in high-density lipoprotein-induced stimulation of astroglial cell function. Biochem J. 2003 Mar 15;370(Pt 3):817-27.

279. Costet P, Luo Y, Wang N, Tall AR. Sterol-dependent transactivation of the ABC1 promoter by the liver X receptor/retinoid X receptor. J Biol Chem. 2000 Sep 8;275(36):28240-5.

280. Sato K, Malchinkhuu E, Horiuchi Y, Mogi C, Tomura H, Tosaka M, et al. Critical role of ABCA1 transporter in sphingosine 1-phosphate release from astrocytes. J Neurochem. 2007 Dec;103(6):2610-9.

281. Liu X, Xiong SL, Yi GH. ABCA1, ABCG1, and SR-BI: Transit of HDL-associated sphingosine-1-phosphate. Clin Chim Acta. 2012 Feb 18;413(3-4):384-90.

282. Pyne NJ, Tonelli F, Lim KG, Long JS, Edwards J, Pyne S. Sphingosine 1-phosphate signalling in cancer. Biochem Soc Trans. 2012 Feb;40(1):94-100.

283. Velazquez E, Santos A, Montes A, Blazquez E, Ruiz-Albusac JM. 25-Hydroxycholesterol has a dual effect on the proliferation of cultured rat astrocytes. Neuropharmacology. 2006 Aug;51(2):229-37.

284. Pommier AJ, Dufour J, Alves G, Viennois E, De Boussac H, Trousson A, et al. Liver x receptors protect from development of prostatic intra-epithelial neoplasia in mice. PLoS Genet. 2013 May;9(5):e1003483.

285. Dufour J, Pommier A, Alves G, De Boussac H, Lours-Calet C, Volle DH, et al. Lack of liver X receptors leads to cell proliferation in a model of mouse dorsal prostate epithelial cell. PLoS One. 2013;8(3):e58876.

286. Farwell WR, Scranton RE, Lawler EV, Lew RA, Brophy MT, Fiore LD, et al. The association between statins and cancer incidence in a veterans population. J Natl Cancer Inst. 2008 Jan 16;100(2):134-9.

287. Nedelcu D, Liu J, Xu Y, Jao C, Salic A. Oxysterol binding to the extracellular domain of Smoothened in Hedgehog signaling. Nat Chem Biol. 2013 Sep;9(9):557-64.

288. Yi T, Wang X, Kelly LM, An J, Xu Y, Sailer AW, et al. Oxysterol gradient generation by lymphoid stromal cells guides activated B cell movement during humoral responses. Immunity. 2012 Sep 21;37(3):535-48.

289. Zhang L, Shih AY, Yang XV, Kuei C, Wu J, Deng X, et al. Identification of structural motifs critical for epstein-barr virus-induced molecule 2 function and homology modeling of the ligand docking site. Mol Pharmacol. 2012 Dec;82(6):1094-103.

290. Bursill CA, Castro ML, Beattie DT, Nakhla S, van der Vorst E, Heather AK, et al. High-density lipoproteins suppress chemokines and chemokine receptors in vitro and in vivo. Arterioscler Thromb Vasc Biol. 2010 Sep;30(9):1773-8.

291. Silva J, Beckedorf A, Bieberich E. Osteoblast-derived oxysterol is a migration-inducing factor for human breast cancer cells. J Biol Chem. 2003 Jul 11;278(28):25376-85.

292. Ivaska J, Pallari HM, Nevo J, Eriksson JE. Novel functions of vimentin in cell adhesion, migration, and signaling. Exp Cell Res. 2007 Jun 10;313(10):2050-62.

293. Nieminen M, Henttinen T, Merinen M, Marttila-Ichihara F, Eriksson JE, Jalkanen S. Vimentin function in lymphocyte adhesion and transcellular migration. Nat Cell Biol. 2006 Feb;8(2):156-62.

294. Schmid MC, Varner JA. Myeloid cells in tumor inflammation. Vasc Cell. 2012;4(1):14.

295. Parney IF, Waldron JS, Parsa AT. Flow cytometry and in vitro analysis of human glioma-associated macrophages. Laboratory investigation. J Neurosurg. 2009 Mar;110(3):572-82.

296. Rittirsch D, Hoesel LM, Ward PA. The disconnect between animal models of sepsis and human sepsis. J Leukoc Biol. 2007 Jan;81(1):137-43.

297. Heverin M, Meaney S, Lutjohann D, Diczfalusy U, Wahren J, Bjorkhem I. Crossing the barrier: net flux of 27-hydroxycholesterol into the human brain. J Lipid Res. 2005 May;46(5):1047-52.

298. Gamba P, Leonarduzzi G, Tamagno E, Guglielmotto M, Testa G, Sottero B, et al. Interaction between 24-hydroxycholesterol, oxidative stress, and amyloid-beta in amplifying neuronal damage in Alzheimer's disease: three partners in crime. Aging Cell. 2011 Jun;10(3):403-17.

299. Brown J, 3rd, Theisler C, Silberman S, Magnuson D, Gottardi-Littell N, Lee JM, et al. Differential expression of cholesterol hydroxylases in Alzheimer's disease. J Biol Chem. 2004 Aug 13;279(33):34674-81.

300. Memon RA, Staprans I, Noor M, Holleran WM, Uchida Y, Moser AH, et al. Infection and inflammation induce LDL oxidation in vivo. Arterioscler Thromb Vasc Biol. 2000 Jun;20(6):1536-42.

301. Poli G, Sottero B, Gargiulo S, Leonarduzzi G. Cholesterol oxidation products in the vascular remodeling due to atherosclerosis. Mol Aspects Med. 2009 Jun;30(3):180-9.

302. Lemaire S, Lizard G, Monier S, Miguet C, Gueldry S, Volot F, et al. Different patterns of IL-1beta secretion, adhesion molecule expression and apoptosis induction in human endothelial cells treated with 7alpha-, 7beta-hydroxycholesterol, or 7-ketocholesterol. FEBS Lett. 1998 Dec 4;440(3):434-9.

303. Hayden JM, Brachova L, Higgins K, Obermiller L, Sevanian A, Khandrika S, et al. Induction of monocyte differentiation and foam cell formation in vitro by 7-ketocholesterol. J Lipid Res. 2002 Jan;43(1):26-35.

304. Gallin JI, Kaye D, O'Leary WM. Serum lipids in infection. N Engl J Med. 1969 Nov 13;281(20):1081-6.

305. Sammalkorpi K, Valtonen V, Kerttula Y, Nikkila E, Taskinen MR. Changes in serum lipoprotein pattern induced by acute infections. Metabolism. 1988 Sep;37(9):859-65.

306. Grunfeld C, Pang M, Doerrler W, Shigenaga JK, Jensen P, Feingold KR. Lipids, lipoproteins, triglyceride clearance, and cytokines in human immunodeficiency virus infection and the acquired immunodeficiency syndrome. J Clin Endocrinol Metab. 1992 May;74(5):1045-52.

307. Auerbach BJ, Parks JS. Lipoprotein abnormalities associated with lipopolysaccharide-induced lecithin: cholesterol acyltransferase and lipase deficiency. J Biol Chem. 1989 Jun 15;264(17):10264-70.

308. Ettinger WH, Miller LD, Albers JJ, Smith TK, Parks JS. Lipopolysaccharide and tumor necrosis factor cause a fall in plasma concentration of lecithin: cholesterol acyltransferase in cynomolgus monkeys. J Lipid Res. 1990 Jun;31(6):1099-107.

309. Sprecher H. Biochemistry of essential fatty acids. Prog Lipid Res. 1981;20:13-22.

310. Halushka PV, Mais DE, Mayeux PR, Morinelli TA. Thromboxane, prostaglandin and leukotriene receptors. Annu Rev Pharmacol Toxicol. 1989;29:213-39.

311. Gargiulo S, Sottero B, Gamba P, Chiarpotto E, Poli G, Leonarduzzi G. Plaque oxysterols induce unbalanced up-regulation of matrix metalloproteinase-9 in macrophagic cells through redox-sensitive signaling pathways: Implications regarding the vulnerability of atherosclerotic lesions. Free Radic Biol Med. 2011 Aug 15;51(4):844-55.

7 Figures